TURUN YLIOPISTON JULKAISUJA
ANNALES UNIVERSITATIS TURKUENSIS

SARJA - SER. D OSA - TOM. 946

MEDICA - ODONTOLOGICA

IMAGING OF DOPAMINE AND SEROTONIN TRANSPORTERS

Pre-Clinical Studies with Radiotracers for Positron Emission Tomography

by

Päivi Marjamäki

TURUN YLIOPISTO
UNIVERSITY OF TURKU
Turku 2011

From

Turku PET Centre and Department of Clinical Physiology and Nuclear Medicine
University of Turku, Turku, Finland

Supervised by

Professor Olof Solin, PhD
Turku PET Centre and Department of Chemistry
University of Turku
Turku, Finland

and

Docent Merja Haaparanta-Solin, PhD
Turku PET Centre
University of Turku
Turku, Finland

Reviewed by

Professor Jesper Ekelund, MD, PhD
Department of Psychiatry
Helsinki University Hospital
Helsinki, Finland

and

Anu Airaksinen, PhD
Laboratory of Radiochemistry
Department of Chemistry
University of Helsinki
Helsinki, Finland

Dissertation opponent

Docent Kim Bergström, PhD
Centre for Drug Research
Faculty of Pharmacy
University of Helsinki
Helsinki, Finland

ISBN 978-951-29-4518-4 (PRINT)
ISBN 978-951-29-4519-1 (PDF)
ISSN 0355-9483
Painosalama Oy – Turku, Finland 2011

to Henri, Henna and Jalo

ABSTRACT

Päivi Marjamäki

IMAGING OF DOPAMINE AND SEROTONIN TRANSPORTERS
Pre-Clinical Studies with Radiotracers for Positron Emission Tomography

Turku PET Centre and Department of Clinical Physiology and Nuclear Medicine
University of Turku, Turku, Finland
Annales Universitatis Turkuensis
Painosalama OY, Turku, Finland 2011

The action of the neurotransmitters dopamine (DA) and serotonin (5-HT) at synapses is terminated by their rapid reuptake into presynaptic nerve endings via plasma membrane dopamine (DAT) and serotonin (SERT) transporters. Alterations in the function of these transporters have been suggested as a feature of several neurological and neuropsychiatric diseases, such as Parkinson's disease (PD), depression, and anxiety. A suitable clinical method for studying these transporters non-invasively *in vivo* is positron emission tomography (PET) utilizing radiopharmaceuticals (tracers) labelled with short-lived positron-emitting radionuclides.

The aim of this study was to evaluate in rats two novel radiotracers, [^{18}F]*β*-CFT-FP and [^{18}F]FMe-McN, for imaging DAT and SERT, respectively, using *in vitro*, *ex vivo* and *in vivo* methods. Substituting an *N*-methyl in [^{18}F]*β*-CFT, a well known DAT tracer, with a [^{18}F]fluoropropyl group significantly changed the properties of the tracer. [^{18}F]*β*-CFT showed slow kinetics and metabolism, and a high specific uptake in the striatum, whereas [^{18}F]*β*-CFT-FP showed fast kinetics and metabolism, and a moderate specific uptake in the striatum. [^{18}F]*β*-CFT-FP was selective for DAT; but [^{18}F]*β*-CFT also bound to the noradrenaline transporter. [^{18}F]*β*-CFT-FP may be a suitable PET tracer for imaging the striatal DAT sites, but a tracer with a higher affinity is needed for imaging extrastriatal DAT sites.

In rats, [^{18}F]FMe-McN showed high target-to-non-target ratios, specificity and selectivity for SERT, but slow kinetics. However, [^{18}F]FMe-McN reveals potential for imaging SERT, at least in pre-clinical studies. In addition, the sensitivities of [^{18}F]*β*-CFT and [^{18}F]FDOPA (a precursor of DA) for detecting mild nigrostriatal hypofunction were compared in an animal model of PD. The uptake of [^{18}F]FDOPA was significantly affected by compensatory effects in dopaminergic cells, whereas [^{18}F]*β*-CFT was more sensitive and therefore more suitable for PET studies of mild dopaminergic symptoms.

In conclusion, both novel tracers, [^{18}F]*β*-CFT-FP and [^{18}F]FMe-McN, have potential, but are not optimal PET tracers for DAT and SERT imaging in rats, respectively. [^{18}F]*β*-CFT is superior to [^{18}F]FDOPA for imaging mild nigral lesions in rat brains.

Keywords: [^{18}F]FDOPA, [^{18}F]*β*-CFT, [^{18}F]*β*-CFT-FP, [^{18}F]FMe-McN, DAT, SERT, PET, rat

TIIVISTELMÄ

Päivi Marjamäki

DOPAMIINI- JA SEROTONIINITRANSPORTTERIN KUVANTAMINEN
Prekliinisiä tutkimuksia positronisäteilevillä radiomerkkiaineilla

Valtakunnallinen PET-keskus, Kliinisen fysiologian ja isotooppilääketieteen oppiaine, Kliininen laitos, Turun yliopisto
Annales Universitatis Turkuensis
Painosalama OY, Turku 2011

Hermovälittäjäaineiden, dopamiinin ja serotoniinin, vaikutus synapseissa päättyy solukalvon spesifisten takaisinottokohtien, ns. transporttereiden siirtäessä välittäjäaineet nopeasti takaisin presynaptiseen hermopäätteeseen. Dopamiini- ja serotoniinitransportterin (DAT ja SERT) toiminnan on osoitettu muuttuneen monissa neurologisissa ja psykiatrisissa sairauksissa, kuten Parkinsonin taudissa (PD), masennuksessa ja ahdistustiloissa. Potilailla näiden transporttereiden toimintaa voidaan kajoamattomasti tutkia positroniemissiotomografialla (PET), jossa käytetään lyhytikäisillä, positronisäteilevillä radioisotoopeilla leimattuja merkkiaineita.

Tämän väitöskirjatyön tarkoituksena oli tutkia kahden uuden PET-merkkiaineen, [^{18}F]β-CFT-FP:n ja [^{18}F]FMe-McN:n, ominaisuuksia ja arvioida niiden soveltuvuutta DAT:n ja SERT:n kuvantamiseen *in vitro*-, *ex vivo*- *ja in vivo*-menetelmin rotalla. Aiemmin kehitetyn [^{18}F]β-CFT:n *N*-metyyliryhmän korvaaminen [^{18}F]fluoripropyyli-ryhmällä vaikutti merkittävästi yhdisteen biologiseen käyttäytymiseen. [^{18}F]β-CFT sitoutui voimakkaasti rotan aivojen tyvitumakkeiden DAT:iin, ja sen kinetiikka ja metaboloituminen olivat hitaita, sen sijaan [^{18}F]β-CFT-FP:n kinetiikka ja metabolia olivat nopeita ja sen spesifinen sitoutuminen tyvitumakkeiden DAT:iin oli vähäisempää. [^{18}F]β-CFT-FP oli selektiivinen DAT:lle, mutta [^{18}F]β-CFT sitoutui myös noradrenaliinitransportteriin. [^{18}F]β-CFT-FP saattaa olla käyttökelpoinen tyvitumakkeiden DAT:n kuvantamisessa, muilla aivoalueilla tarvitaan suuremman affiniteetin omaavaa merkkiainetta. [^{18}F]FMe-McN sitoutui spesifisesti ja selektiivisesti SERT:iin, mutta sen kinetiikka oli hidas. [^{18}F]FMe-McN:ä voidaan kuitenkin pitää käyttökelpoisena PET-merkkiaineena ainakin koe-eläintutkimuksissa. Lisäksi verrattiin [^{18}F]β-CFT:n ja [^{18}F]FDOPA:n (dopamiinin esiaste) kykyä osoittaa dopaminergisen järjestelmän vaurioita PD:n eläinmallissa. Kompensatoriset tekijät hermosoluissa vaikuttivat merkittävästi [^{18}F]FDOPA:n sitoutumiseen, sen sijaan [^{18}F]β-CFT osoitti herkemmin dopaminergisen järjestelmän lievät vauriot rotan aivoissa.

Yhteenvetona todetaan, että [^{18}F]β-CFT-FP ja [^{18}F]FMe-McN ovat käyttökelpoisia, mutta eivät optimaalisia PET-merkkiaineita DAT:n ja SERT:n kuvantamiseen rotassa, ja että [^{18}F]β-CFT soveltuu [^{18}F]FDOPA:a paremmin lievien dopaminergisten vaurioiden kuvantamiseen rotan aivoissa.

Avainsanat: [^{18}F]FDOPA, [^{18}F]β-CFT, [^{18}F]β-CFT-FP, [^{18}F]FMe-McN, DAT, SERT, PET, rotta

TABLE OF CONTENTS

ABBREVIATIONS

(*S,S*)-[^{18}F]FMeNER	(*S,S*)-2-[α-(2-[^{18}F]methoxyphenoxy)benzyl]morpholine
(*S,S*)-reboxetine	2-[α-(2-ethoxyphenoxy)phenylmethyl]morpholine
[^{11}C]altropane	*N*-(1-iodoprop-1-en-3-yl)-2β-[^{11}C]carbomethoxy-3β-(4-fluorophenyl)nortropane
[^{11}C]DASB	*N,N*-[^{11}C]dimethyl-2-(2-amino-4-cyanophenylthio)benzylamine
[^{11}C]LBT-999	(*E*)-*N*-(4-fluorobut-2-enyl)-2β-[^{11}C]carbomethoxy-3β-(4-tolyl)-nortropane
[^{11}C]PE2I	*N*-(3-iodoprop-2*E*-enyl)-2β-[^{11}C]carbomethoxy-3β-(4-methylphenyl)nortropane
[^{11}C]RTI-31	2β-[^{11}C]carbomethoxy-3β-(4-chlorophenyl)tropane
[^{11}C]RTI-32	2β-[^{11}C]carbomethoxy-3β-(4-methylphenyl)tropane
[^{11}C]RTI-357	[methyl-^{11}C]-2β-carbomethoxy-3β-(4-isopropenylphenyl)nortropane
[^{11}C]β-CFT	*N*-([^{11}C]methyl)-2β-carbomethoxy-3β-(4-fluorophenyl)nortropane
[^{11}C]β-CFT-FP	*N*-(3-fluoropropyl)-2β-[^{11}C]carbomethoxy-3β-(4-fluorophenyl)-nortropane
[^{11}C]β-CIT	*N*-([^{11}C]methyl)-2β-carbomethoxy-3β-(4-iodophenyl)nortropane
[^{11}C]β-CIT-FE	*N*-(2-fluoroethyl)-2β-[^{11}C]carbomethoxy-3β-(4-iodophenyl)-nortropane
[^{11}C]β-CIT-FP	*N*-(2-fluoropropyl)-2β-[^{11}C]carbomethoxy-3β-(4-iodophenyl)-nortropane
[^{18}F](+)FCT	(+)-*N*-(4-[^{18}F]fluorobenzyl)-2β-propanoyl-3β-(4-chlorophenyl)-tropane
[^{18}F](+)FTT	(+)-*N*-(4-[^{18}F]fluorobenzyl)-2β-propanoyl-3β-(4-tolyl)tropane
[^{18}F](*R/S*)FIPCT	2β-(*R/S*)-carbo-1-[^{18}F]fluoro-2-propoxy-3β-(4-chlorophenyl)-tropane
[^{18}F]FDA	6-[^{18}F]fluorodopamine
[^{18}F]FDOPA	6-[^{18}F]fluoro-*L*-DOPA
[^{18}F]FE@CIT	2β-carbo-2'-[^{18}F]fluoroethoxy-3β-(4-iodophenyl)tropane
[^{18}F]FECNT	*N*-(2-[^{18}F]fluoroethyl)-2β-carbomethoxy-3β-(4-chlorophenyl)-nortropane
[^{18}F]FECT	2β-carbo-2'-[^{18}F]fluoroethoxy-3β-(4-chlorophenyl)tropane
[^{18}F]FETT	2β-carbo-2'-[^{18}F]fluoroethoxy-3β-(4-methylphenyl)tropane
[^{18}F]FMe-McN	1,2,3,5,6,10β-hexahydro-6-[4([^{18}F]fluoromethylthio)phenyl]-pyrrolo[2,1-a]isoquinoline
[^{18}F]FPCT	*N*-(3-[^{18}F]fluoropropyl)-2β-carbomethoxy-3β-(4-chlorophenyl)-nortropane
[^{18}F]LBT-999	(*E*)-*N*-(4-[^{18}F]fluorobut-2-enyl)-2β-carbomethoxy-3β-(4-tolyl)-nortropane
[^{18}F]MCL-3222	2β-carbo-2'-[^{18}F]fluoroethoxy-3β-(4-bromophenyl)tropane

[^{18}F]*p*-FWIN	2*β*-carbomethoxy-3*β*-(4-[^{18}F]fluoromethylphenyl)tropane
[^{18}F]*β*-CFT	2*β*-carbomethoxy-3*β*-(4-[^{18}F]fluorophenyl)tropane
[^{18}F]*β*-CFT-FE	*N*-(2-[^{18}F]fluoroethyl)-2*β*-carbomethoxy-3*β*-(4-fluorophenyl)-nortropane
[^{18}F]*β*-CFT-FP	*N*-(3-[^{18}F]fluoropropyl)2*β*-carbomethoxy-3*β*-(4-fluorophenyl)-nortropane
[^{18}F]*β*-CIT-FP	*N*-(3-[^{18}F]fluoropropyl)-2*β*-carbomethoxy-3*β*-(4-iodophenyl)-nortropane
3-MT	3-methoxytyramine
4-[^{18}F]ADAM	[^{18}F]AFA, *N,N*-dimethyl-2-(2-amino-4-[^{18}F]fluorophenylthio)-benzylamine
5-HIAA	5-hydroxyindolacetic acid
5-HT	serotonin, 5-hydroxytryptamine
5-HTP	*L*-5-hydroxytryptophan
6-OHDA	6-hydroxydopamine
AAAD	DOPA decarboxylase or aromatic *L*-amino acid decarboxylase
ACF	2-(2-amino-4-chloro-5-fluorophenyl)thio-*N,N*-dimethylbenzene-methanamine
ADAM	2-[2-(dimethylaminomethylphenylthio)]-5-iodophenylamine
ADHD	attention deficit hyperactivity disorder
AFM	2-[2-(dimethylaminomethylphenylthio)]-5-fluoromethylphenyl-amine
amino-MPTP	1-methyl-4-(2-aminophenyl)-1,2,3,6-tetrahydropyridine
AMPH	amphetamine
AMY	amygdalae
APO	apomorphine
BBB	blood-brain barrier
CaMK	Ca^{2+}/calmodulin-dependent protein kinase
CE	cerebellum
cis-DDPI	*cis*-*N,N*-dimethyl-3-(2,4-dichlorophenyl)indanamine
CNS	central nervous system
COMT	catechol-*O*-methyl-transferase
CT	computed tomography
CX	frontal cortex
DA	dopamine
DAT	dopamine transporter
DOPAC	3,4-dihydroxyphenylacetic acid
DR	dorsal raphe
EOB	end of bombardment
EOS	end of synthesis
FE*m*ZIENT	2*β*-carbo-(2-fluoroethoxy)-3*β*-(3-((*Z*)-2-iodoethenyl)phenyl)-nortropane
FENET	(2*S*,3*S*)-2-[*α*-(2-(2-fluoroethyl)phenoxy)phenylmethyl]morpholine

FPNET	(2*S*,3*S*)-2-[*α*-(2-(3-fluoropropyl)phenoxy)phenylmethyl]morpholine
GABA	γ-aminobutyric acid
GBR 12909	1-[2-[bis(4-fluorophenyl)methoxy]ethyl]-4-(3-phenylpropyl)-piperazine
HPLC	high-performance liquid chromatography
HPTLC	high-performance thin layer chromatography
HRRT	high resolution research tomograph
HVA	homovanillic acid
HY	hypothalamus
i.p.	intraperitoneal
i.v.	intravenous
ID	injected dose
LC	locus coeruleus
L-DOPA	3,4-dihydroxy-*L*-phenylalanine (levodopa)
log P	n-octanol/water partition coefficient
m	*meta*
MADAM	*N,N*-dimethyl-2-(2-amino-4-methylphenylthio)benzylamine
MAO	monoamine oxidase
McN5652	1,2,3,5,6,10*β*-hexahydro-6-[4-(methylthio)phenyl]pyrrolo[2,1-a]-isoquinoline
MD	microdialysis
MDMA	ecstasy or 3,4-methylenedioxymethamphetamine
MENET	(2*S*,3*S*)-2-[*α*-(2-methylphenoxy)phenylmethyl]morpholine
MESNET	(2*S*,3*S*)-2-[*α*-(2-methylphenylthio)phenylmethyl]morpholine
MHPG	3-methoxy-4-hydroxyphenylethylene glycol
MPP^+	1-methyl-4-phenylpyridium ion
MPTP	1-methyl-4-phenyl-1,2,3,6-tetrahydropyridine
MRI	magnetic resonance imaging
MW	molecular weight
NA	noradrenaline (norepinephrine)
NDRI	NA and DA reuptake inhibitor
NET	noradrenaline (norepinephrine) transporter
NSS	neurotransmitter: sodium symporter
OCD	obsessive-compulsive disorder
o	*ortho*
p	*para*
p.i.	post injection
PD	Parkinson's disease
PET	positron emission tomography
PKA	cAMP-dependent protein kinase
PKC	protein kinase C
PKG	cGMP-dependent protein kinase
PSL	photo-stimulated luminescence

RTI-336	2β-[3-(4-methylphenyl)isoxazol-5-yl]-3β-(4-chlorophenyl)tropane
s.c.	subcutaneous
SA	specific radioactivity
SD	standard deviation
SERT	serotonin transporter
SN	substantia nigra
SNP	single nucleotide polymorphisms
SNRI	5-HT and NA reuptake inhibitor
SSRI	selective serotonin reuptake inhibitor
STR	striatum
$t_{½}$	physical half-life
TAC	time activity curve
TCA	tricyclic antidepressant
TH	tyrosine hydroxylase
THA	thalamus
TLC	thin layer (planar) chromatography
TMD	transmembrane domain
TPH	tryptophan hydroxylase
VMA	3,4-dihydroxymandelic acid
VMAT2	vesicular monoamine transporter
VNTR	variable number of tandem repeat polymorphism
VTA	ventral tegmental area

LIST OF ORIGINAL PUBLICATIONS

This thesis is based on the following original publications, which are referred to in the text by their Roman numerals.

I. Forsback S, Niemi R, Marjamäki P, Eskola O, Bergman J, Grönroos T, Haaparanta M, Haapalinna A, Rinne J, Solin O. Uptake of 6-[^{18}F]fluoro-*L*-dopa and [^{18}F]*β*-CFT reflect nigral neuronal loss in a rat model of Parkinson's disease. Synapse 51:119–127, 2004.

II. Koivula T *, Marjamäki P *, Haaparanta M, Fagerholm V, Grönroos T, Lipponen T, Perhola O, Vepsäläinen J, Solin O. *Ex vivo* evaluation of *N*-(3-[^{18}F]fluoropropyl)-2*β*-carbomethoxy-3*β*-(4-fluorophenyl)nortropane in rats. Nucl Med Biol 35:177–183, 2008.

III. Marjamäki P, Haaparanta M, Forsback S, Fagerholm V, Eskola O, Grönroos T, Koivula T, Solin O. Comparison of 2*β*-carbomethoxy-3*β*-(4-[^{18}F]fluorophenyl)-tropane and *N*-(3-[^{18}F]fluoropropyl)-2*β*-carbomethoxy-3*β*-(4-fluorophenyl)nor-tropane, tracers for imaging dopamine transporter in rat. Mol Imaging Biol 12:269–277, 2010.

IV. Marjamäki P, Zessin J, Eskola O, Grönroos T, Haaparanta M, Bergman J, Lehikoinen P, Forsback S, Brust P, Steinbach J, Solin O. *S*-[^{18}F]fluoromethyl-(+)-McN5652, a PET tracer for the serotonin transporter: evaluation in rats. Synapse 47:45–53, 2003.

V. Marjamäki P, Haaparanta M, Eskola O, Fagerholm V, Grönroos T, Forsback S, Bergman J, Solin O. Effect of gender in the binding of *S*-[^{18}F]Fluoromethyl-(+)-McN5652 to the serotonin transporter in intact rats. *Manuscript.*

*Equal contribution

1. INTRODUCTION

The dopaminergic, noradrenergic and serotonergic neurons, located in the midbrain of rats, spread throughout the brain as an extensive network that allows a widely distributed release of the monoamine neurotransmitters dopamine (DA), noradrenaline (NA), and serotonin (5-hydroxytryptamine, 5-HT). These neurotransmitters are important mediators for numerous vital functions in the central nervous system (CNS) and peripheral organs.

Intracellular communication in the CNS is driven by a controlled release and reuptake of neurotransmitters. In response to an action potential, neurons release neurotransmitters into the synaptic cleft to be bound to specific receptors. The action of monoamines at the synapses is predominantly terminated by a rapid reuptake of monoamines into presynaptic nerve endings via neurotransmitter-specific membrane reuptake sites, monoamine transporters for DA (DAT), NA (NET) and 5-HT (SERT). These transporters share genetic, structural, and functional homologies presumed to reflect a common substrate translocation mechanism. However, they are distinguished by their substrate specificity. They are also important targets for a wide spectrum of transport antagonists, such as clinically effective antidepressants, and for abused substances like cocaine and amphetamines. Alterations in the functions of DAT, NET or SERT have been suggested as a feature of several common neuropsychiatric and neurological diseases such as attention deficit hyperactivity disorder (ADHD), depression, anxiety, obsessive-compulsive disorder (OCD) and Parkinson's disease (PD).

Positron emission tomography (PET) is a non-invasive method for the *in vivo* imaging of biological and physiological processes, such as the function of monoamine transporters in neuropsychiatric and neurological disorders and their drug treatments. The PET method utilises radiopharmaceuticals (tracers) that are labelled with short-lived positron-emitting radionuclides. A pharmaceutical with a high affinity for a transporter, such as drugs in clinical use, may not, however, have optimal properties for use as a PET tracer. Therefore, radiolabelled tracer candidates must be pre-clinically evaluated for their binding characteristics, including specificity, selectivity and biodistribution, as well as their metabolic and kinetic behaviour.

In this study, four different ^{18}F-labelled tracers were studied in rats using *in vivo*, *ex vivo* and *in vitro* methods. Two widely used PET tracers, [^{18}F]FDOPA and [^{18}F]β-CFT, were compared in terms of their sensitivity for detecting nigrostriatal hypofunction in an animal model of PD. In addition, the properties of two novel radiotracers, [^{18}F]β-CFT-FP and [^{18}F]FMe-McN, were evaluated to discover their usefulness as PET tracers for DAT and SERT in rats, respectively.

2. REVIEW OF THE LITERATURE

2.1. Dopaminergic, noradrenergic and serotonergic neuronal systems in rat brains

The monoamine neurotransmitters DA, NA, and 5-HT, are important mediators for numerous vital functions both in the CNS and peripheral organs. In the brain, these transmitters are synthesized by specific neurons that mediate their effects through widely distributed neuronal networks.

In rat brains, dopaminergic neurons are located in several clusters of cells in the brain stem (A8-A15) and most of the cell bodies are in the substantia nigra (SN, A9) and ventral tegmental area (VTA, A10) (Figure 2.1.). The projections of the dopaminergic system can be separated into four behaviourally relevant parts: nigrostriatal, mesolimbic, mesocortical, and tuberoinfundibular pathways. The SN neurons predominantly project to the caudatus-putamen and dorsal striatum (STR) forming the nigrostriatal pathway, which is responsible for controlling the initiation of movements, resting muscle tone and targeted movements. The mesolimbic dopaminergic pathway is formed of neurons that project from the VTA to the ventral STR, which comprises the nucleus accumbens, olfactory tubercle and limbic regions, like the amygdalae (AMY), hippocampus and septum. The VTA also sends axons to the cortical areas, such as the medial, prefrontal, entorhinal and cingulate cortices, a system known as the mesocortical dopaminergic pathway. Mesolimbic and mesocortical pathways are important in the initiation and maintenance of goal-directed and reward-mediated behaviours, including mood and cognitive functions. The tuberoinfundibular tract regulates some hypothalamic and pituitary peptides, such as prolactin (Bannon et al. 1995, Bannon 2005, Hoffman et al. 1998, Lorang et al. 1994).

Anatomically speaking, noradrenergic cells are located bilaterally in seven clusters of cells (A1-A7) in the rat brain stem (Figure 2.1.). The locus coeruleus (LC, A6), the largest noradrenergic nucleus and the primary source of noradrenergic fibres, spreads anteriorly throughout the cerebral cortex and the limbic system, *e.g.* neocortex, cingulate cyrus, cingulum, olfactory bulb, hypothalamus (HY), thalamus (THA), AMY and hippocampus, as well as to the cerebellum (CE) and spinal cord as an extensive network, which allows a widely distributed release of NA. The lateral tegmental noradrenergic neurons send projections to the basal forebrain, HY and brain stem. The noradrenergic system contributes to the collection and processing of environmental and sensory stimuli related to alertness, arousal, attention and vigilance. It also controls the autonomic (sympathetic) nervous system by releasing NA from postganglionic neurons (Berridge and Waterhouse 2003, Lorang et al. 1994, Kuhar et al. 1999, Tejani-Butt 1992).

The adult serotonergic system in rats is organized into two subsystems: the superior and inferior raphe nuclei, including nine discrete serotonergic cell groups (B1-B9) in

the brain stem (Figure 2.1.). The majority of serotonergic soma are found in the dorsal raphe (DR, B6 and B7), about 50% of 5-HT neurons in the rat CNS, and in the median raphe (MnR, B5 and B8) nuclei. The superior group, including the DR and MnR, innervates the midbrain and forebrain with countless branches and thousands of varicosities and terminals. The DR predominantly innervates the STR, nucleus accumbens, SN, motor cortex, and AMY, while the MnR projects heavily into the cingulate cortex, septal nuclei, hippocampus and HY. A dense serotonergic innervation is also seen in the LC, the suprachiasmatic nucleus (rhythm centre), and in several cortical areas. The caudal inferior cell groups (B1-B4) innervate the CE, pons, medulla and spinal cord (Duncan et al. 1992, Jacobs and Azmitia 1992, Piñeyro and Blier 1999). The cortical projection areas are innervated by two morphologically distinct classes of serotonergic axon terminals; fine axons with small varicosities from the DR, and beaded axons with large spherical varicosities from the MnR. These two types of axons have different regional distributions and they are sensitive to the neurotoxic effects of amphetamines (AMPHs) in different ways; the fine axons are degenerated, but the beaded axons are spared (Mamounas et al. 1991). 5-HT has a general effect on behaviour by modulating the tone of nervous system activity, thereby integrating and regulating many functions, such as sleep, circadian rhythm, emotional, motor, feeding, cognitive and reproductive behaviours (Hoffman et al. 1998, Frazer and Hensler 1999).

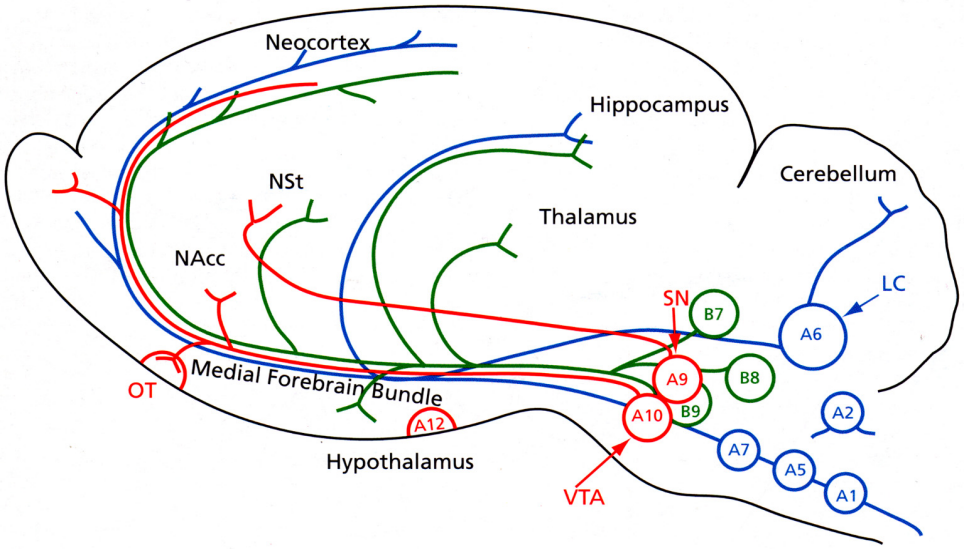

Figure 2.1. Schematic representation of the main dopaminergic (A9, A10, A12; red), noradrenergic (A1, A2, A5, A6, A7; blue) and serotonergic (B7, B8, B9; green) cell groups and their projections in rat brains. Nacc, nucleus accumbens; NSt, neostriatum; OT, olfactory tubercle; LC (A6), locus coeruleus; SN (A9), substantia nigra; VTA (A10), ventral tegmental area (Sigma, RBI; catalogue: Neuropsychiatric Disorders).

2.2. Monoamine neurotransmitters: DA, NA and 5-HT

The catecholamines DA and NA, are synthesized (Figure 2.2.A.) from an aromatic amino acid, *L*-tyrosine in the cytoplasm of dopaminergic and noradrenergic neurons, respectively. *L*-tyrosine is converted to 3, 4-dihydroxy-*L*-phenylalanine (levodopa, *L*-DOPA) by tyrosine hydroxylase (TH), and then to DA by the aromatic *L*-amino acid decarboxylase (AAAD or DOPA decarboxylase). The synthesis rate of the DA is dependent on the activity of the TH, which is under the control of complex end-product inhibition mechanisms, the neuron firing rate, and autoreceptors in the nerve-endings (Kuhar et al. 1999). Inside dopaminergic cells, DA is mainly metabolized by monoamine oxidase (MAO) to an aldehyde, and further to 3, 4-dihydroxyphenylacetic acid (DOPAC). Outside cells, DOPAC can be either conjugated to glucuronides or transformed to homovanillic acid (HVA) by catechol-O-methyltransferase (COMT). A fraction of DA is first methylated to 3-methoxytyramine (3-MT) by COMT, and then oxidized to HVA (Eisenhofer et al. 2004). The actions of DA are mediated via DA receptors, which are divided into two major classes: D_1- and D_2-like metabotropic receptors, which transmit signals through G-proteins. The subtypes D_2, D_3 and D_4 belong to D_2-receptors, and subtypes D_1 and D_5 belong to D_1-receptors (Kuhar et al. 1999).

In noradrenergic cells, DA is converted to NA by dopamine-β-hydroxylase. NA is metabolized by MAO and COMT to normetanephrine, 3, 4-dihydroxymandelic acid (VMA), 3-methoxy-4-hydroxyphenylethylene glycol (MHPG), and adrenaline (Eisenhofer et al. 2004). NA performs its actions on the target cell by binding to α_1-, α_2- or β-adrenoceptors, all of which have three subtypes (α_{1A}, α_{1B}, α_{1D}; α_{2A}, α_{2B}, α_{2C}; β_1, β_2, β_3) (Kuhar et al. 1999).

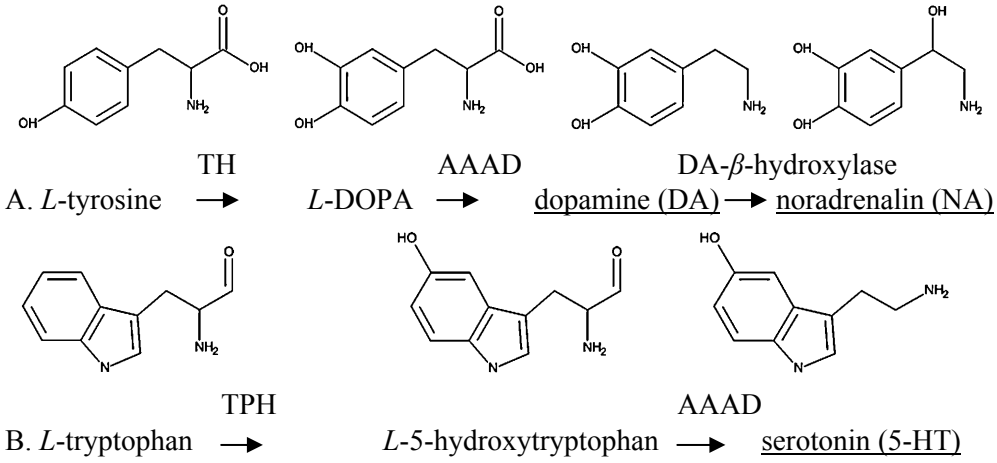

Figure 2.2. Structures and synthesis routes of (A) dopamine, noradrenalin and (B) serotonin.

An indolamine, 5-HT, one of the transmitters that has been known about for longest, is synthesized (Figure 2.2.B.) in serotonergic neurons. Tryptophan hydroxylase (TPH) converts *L*-tryptophan, an amino acid, to *L*-5-hydroxytryptophan (5-HTP) and then AAAD to 5-HT. *L*-tryptophan availability is the rate limiting step for 5-HT synthesis. 5-HT primarily metabolizes through MAO to an aldehyde and then to 5-hydroxyindolacetic acid (5-HIAA). 5-HT content in the CNS constitutes only 1 – 2% of the whole pool of this monoamine in the organism. 5-HT acts via its receptors, which are classified into seven subclasses (5-HT_{1-7}) and at least 17 different subtypes based on structural, biochemical and pharmacological differences. A majority of these receptors belong to the family of metabotropic receptors, except for 5-HT_3, which is an ionotropic receptor (Frazer and Hensler 1999, Hansson et al. 1998).

2.3. Transporters for DA, NA and 5-HT

Intracellular communication in the dopaminergic, noradrenergic and serotonergic neuronal systems is driven by a controlled release and reuptake of the monoamine neurotransmitters DA, NA and 5-HT, which are first synthesized and packaged into synaptic vesicles by vesicular monoamine transporters (VMAT2). In response to an action potential (depolarization), Ca^{2+}-channels open and the subsequent intracellular Ca^{2+} increase promotes the fusion of synaptic vesicles with the plasma membrane. This exocytosis mechanism releases neurotransmitters into the synaptic cleft to be bound to specific receptors present on both postsynaptic and presynaptic neurons. Finally, DA, NA and 5-HT are removed from the synaptic cleft into the presynaptic cell through neurotransmitter-specific transporters (Hoffman et al. 1998).

2.3.1. Localization of the monoamine transporters

The biogenic monoamine neurotransmitters (DA, NA and 5-HT) are rapidly cleared from the synaptic cleft by the specific presynaptic plasma membrane transporters DAT, NET and SERT, which belong to a large SLC6 family of high-affinity Na^+/Cl^--coupled transporters (the neurotransmitter: sodium symporters, NSS) as well as transporters for γ-aminobutyric acid (GABA), glycine, and proline.

In the CNS, DAT gene expression is restricted to dopaminergic neurons; therefore DAT is an excellent neurochemical marker for the density and structural integrity of DA neurons and their projections. In rodents, DAT mRNA is found in great abundance within the dopaminergic neurons of the SN, and in lesser amounts in the VTA, in the olfactory bulb and within the HY (Lorang et al. 1994). In dopaminergic neurons, the DAT protein is localized primarily on extrasynaptic plasma membranes of axonal terminals near aggregates of synaptic vesicles, or in somatodendritic regions and cell bodies. The highest DAT protein levels are found in the caudate-putamen, nucleus accumbens, SN, VTA, and the olfactory tubercle, with lower levels of DAT sites in the globus pallidus, cingulate cortex, HY, some thalamic nuclei, and AMY (Nirenberg et al. 1996, 1997a, b).

The NET mRNA is localized to the noradrenergic cell groups A1, A2 and A4-A7 (Hoffman et al. 1998). The highest densities of NET proteins have been demonstrated in the LC and THA. Several regions in the limbic system, such as the bed nucleus of the stria terminalis, AMY and hippocampus, as well as some nuclei in the HY, raphe nuclei and CE contain intermediate levels of NET sites, while the occipital cortex and STR only have low levels of NET sites (Lorang et al. 1994, Tejani-Butt 1992).

In the adult rat brain, SERT mRNA closely parallels the distribution of TPH in serotonergic cell bodies in the raphe nuclei, although low levels of SERT mRNA were also found in the frontal cortex, hippocampus, and STR, associated with the ascending 5-HT pathways (Lesch et al. 1993). The SERT protein has a widespread and heterogeneous distribution, with the highest densities in the raphe nuclei, AMY, SN, LC, THA, and to a lesser extent in the STR, hippocampus and superior colliculus. The CE only receives a sparse serotonergic innervation (Blakely et al. 1994, D´Amato et al. 1987, Hansson et al. 1998, Hrdina et al. 1990, Burchett and Bannon 1997). The SERT protein expression is preferentially sorted into axons, where it appears to be concentrated at varicosities and terminal boutons, and into dendritic arbors in close proximity to serotonergic cell bodies in the midbrain and brain stem raphe nuclei, and also into serotonergic cell bodies (Sur et al. 1996, Zahniser and Doolen 2001, Zhou et al. 1998). Expression of the SERT gene in the brain seems to be mostly neuronal, but SERT mRNA is found in the non-neuronal cells of peripheral tissues *e.g.* in the endothelium of the lungs, adrenal glands, kidneys, gut, stomach, spleen, uterus, placenta, lymphoblasts, and platelets (Blakely et al. 1998, Kitayama and Dohi 1996, Schroeter et al. 1997).

2.3.2. Molecular structure of DAT, NET and SERT

DAT, a protein with 619 amino acids, and the closely related NET and SERT (617 and 630 amino acids, respectively), are all encoded by a single gene, although differential post-transcriptional or post-translational modifications, *e.g*. alternative mRNA splicing, glycosylations and phosphorylations of transporter proteins, apparently occur (Blakely et al. 1991, 1994, Ramamoorthy et al. 1993). The DAT, NET, and SERT genes and proteins, share structural organization, high sequence identity, and functional homologies, *e.g.* SERT exhibits ~ 50% absolute sequence homology with DAT and NET. The transporters have also remained remarkably stable across phylogeny, *e.g.* human and monkey transporters are over 90% homologous to mouse and rat sequences at the amino acid level (Miller et al. 2001).

Monoamine transporters are proteins with twelve hydrophobic transmembrane domains (TMDs), intracellular amino and carboxyl termini, and a large glycosylated second extracellular loop (Figure 2.3.). In general, the glycosylation of membrane proteins contributes to their folding, stability, trafficking and ligand recognition. Within the TMDs, the DAT, NET and SERT proteins show considerable sequence homology,

presumed to reflect a common mechanism for substrate translocation, whereas the connecting loops and cytoplasmic tails are more divergent and may represent sites for unique protein functions (Torres et al. 2003). The amino and carboxyl terminal tails and intracellular loops contain numerous serine, threonine, and tyrosine residues that could serve as sites for phosphorylation, and many of these residues are present within consensus sequences for kinases, including protein kinase C (PKC), as well as cAMP-dependent (PKA), cGMP-dependent (PKG), and Ca^{2+}/calmodulin-dependent (CaMK) protein kinases (Amara and Kuhar 1993, Blakely et al. 1991, 1994, Hoffman et al. 1991, Lorang et al. 1994, White et al. 2005, Zahniser and Doolen 2001). Quaternary structure evidence suggests that SERT and DAT molecules operate as homodimeric or homotetrameric quaternary forms (Chang et al. 1998, Gether et al. 2006, Kocabas et al. 2003).

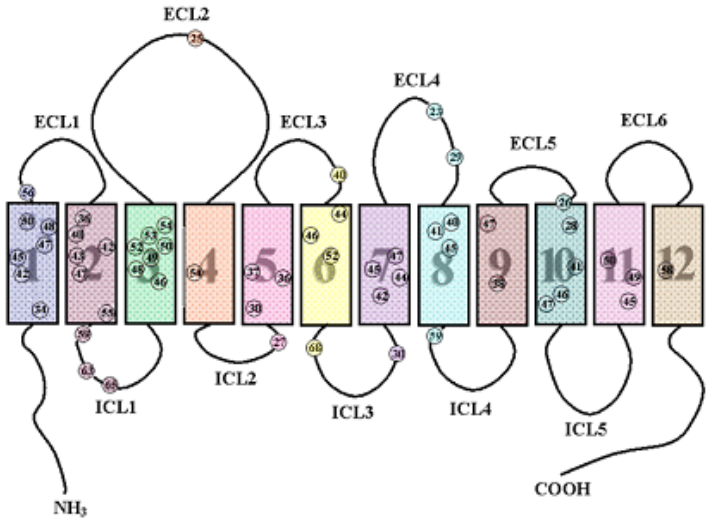

Figure 2.3. Schematic representation of a monoamine transporter with twelve TMDs. Numbers inscribed in circles indicate specific mutagenesis targets; ECL, extracellular loop; ICL, intracellular loop (from Surratt et al. 2005).

2.3.3. Transport mechanisms and acute regulation

There are several advantages of clearing monoamine neurotransmitters from the synaptic cleft with transporters: 1. Fast transmitter reuptake by DAT, NET or SERT allows an improved temporal discrimination of consecutive release events as compared to the simple diffusion of transmitters. 2. The effects of released transmitters are restricted to a smaller area, permitting the dense packing of chemically identical, but functionally distinct synapses. 3. Translocating the neurotransmitters from the extracellular space back into synaptic vesicles allows transmitters to be recycled for another round of releases. 4. Increasing and decreasing amounts of transporter activities provide mechanisms for fine-tuning and controlling the spatial and temporal dynamics of neurotransmission (Hoffman et al. 1998, Masson et al. 1999).

Transport of 5-HT across the cell membrane is driven by a Na^+-concentration gradient, maintained by Na^+-K^+-ATPases. The SERT is thought to operate primarily by means of an alternating access mechanism, in which a single multifunctional binding site, accessible from the cell exterior, binds Na^+, $Cl^–$, and protonated 5-HT simultaneously to form a quaternary complex. When the binding site is full, a conformational change is triggered that closes the site's access to the external medium and opens access to the cytoplasmic surface of the membrane. After the dissociation of 5-HT, Na^+ and $Cl^–$ into the cytoplasm, K^+ associates with SERT to promote the reorientation of the unloaded transporter for another transport cycle. The cotransport of $Cl^–$ is required for all these transporters; SERT also transports K^+, but in an antiport fashion. The overall stoichiometry of the 5-HT uptake cycle is: 1 5-HT: 1 Na^+: 1 $Cl^–$: 1 K^+. The transport function of DAT exhibits ion dependence distinct from that of NET and SERT, with an apparent transport stoichiometry of 1 DA: 2 Na^+: 1 $Cl^–$ (Murphy et al. 2004, Rudnick and Clark 1993, Schwartz et al. 2003). NET also regulates extracellular DA concentrations by transporting DA in several brain regions, especially in the prefrontal cortex where DAT density is low. In a similar way, NA is an endogenous substrate for DAT (Gether et al. 2006, Morón et al. 2002).

Neurotransmitters and a wide variety of second messengers, protein kinases and phosphatases can rapidly modify the transport activity, trafficking and surface expression of transporters, *e.g.* the substrate occupancy and transport activity of SERT promotes its retention on the cell surface. Extracellular 5-HT stabilizes the SERT-protein-phosphatase 2A complex, leading to increased phosphatase activity, thereby preventing SERT phosphorylation by protein kinases (PKC) and the subsequent internalization of the transporters, *i.e.* the activation of PKC down-regulates transporter-mediated neurotransmitter reuptake through a rapid internalization of the transporters from the cell surface to intracellular compartments (Blakely et al. 1998, Blakely and Bauman 2000, Hahn and Blakely 2002, White et al. 2005). The PKC-stimulated down-regulation of transport activity and endocytosis of the transporter have also been demonstrated for DAT and NET. DAT also undergoes other modifications, such as ubiquitinylation, which have been considered as signals for internalization (Mortensen et al. 2008). The phosphorylation of transporter proteins decreases their transport activity, and might also change their turnover rate, or interactions with numerous other proteins like syntaxin 1A, a plasma membrane docking site for synaptic vesicles. Syntaxin 1A also promotes the presence and activity of SERT at the cell surface (Vaughan 2004). Another presynaptic protein, α-synuclein, interacts with DAT in a similar manner (Torres et al. 2003). Acute regulation of neurotransmitter transport could also occur indirectly, *e.g.* by the phosphorylation of Na^+K^+-ATPases, phosphatases or proteins affecting ion gradients. Thus, monoamine transporters are dynamically controlled via intracellular and extracellular regulation of the phosphorylation state by numerous protein kinases, phosphatases and other proteins (Blakely et al. 1998, Jayanthi and Ramamoorthy 2005, Zahniser and Doolen 2001).

In most cases, the activation of presynaptic autoreceptors (*e.g.* D_2 and 5-HT_1, Figure 2.4.) by released neurotransmitters results in the inhibition of neuronal firing, neurotransmitter synthesis and release, thereby mediating inhibitory feedback control and providing another mechanism for neurotransmitter regulation (Zahniser and Doolen 2001).

2.3.4. Drug interactions with monoamine transporters

Drugs that interact with monoamine transporters can be divided into two classes based on their action mechanisms: reuptake inhibitors and substrate-type releasers. Reuptake inhibitors, such as selective 5-HT reuptake inhibitors (SSRIs) and cocaine (Figure 2.4.), bind to transporters, but are not transported themselves, resulting in increased extracellular neurotransmitter concentrations due to the blocked transporter-mediated reuptake, and subsequently to the phosphorylation and internalization of the transporter (Murphy et al. 2004). Although DAT, NET and SERT share a high degree of structural homology, they can be distinguished by their monoamine substrate specificity and by their differing sensitivities to a wide spectrum of transport antagonists (Bannon et al. 1995). NET and SERT are targets for several clinically effective classes of antidepressants, including tricyclic antidepressants (TCAs), SSRIs, selective NA reuptake inhibitors (SNRIs), like nisoxetine and reboxetine, and NA/DA reuptake inhibitors (NDRIs). SSRIs, including fluoxetine, fluvoxamine, paroxetine, sertraline, and citalopram are potent inhibitors of SERT (K_i ~1 nM) (Murphy et al. 2004). NET and SERT are both sensitive to TCAs, but tertiary amines (imipramine and chlomipramine) have a more potent effect on SERT, and secondary amines (desipramine, nortriptyline) on NET. Some drugs, like imipramine and amitriptyline, are metabolized to desipramine and nortriptyline with altered selectivity (Iversen 2006). Most SERT and NET selective antidepressants have some affinity for both transporters. In addition to inhibiting and internalizing SERT, citalopram was also able to induce trafficking of SERT proteins from neural extensions into the cell bodies of the neurons (Lau et al. 2008). Antidepressants did not acutely alter SERT mRNA expression, but the chronic treatment of rats with a variety of antidepressants, including several TCAs and SSRIs, decreased SERT mRNA expression significantly, by 30 - 40% (Lesch et al. 1993, Piñeyro and Blier 1999).

Under certain circumstances, monoamine transporters release neurotransmitters by a non-Ca^{2+}-dependent, non-exocytose mechanism that is Na^+-dependent and induced by substrate-type releasers, such as amphetamine (AMPH), a phenylisopropylamine (Figure 2.4.). Substrate-type releasers bind to the transporter and are subsequently transported into the cytoplasm of nerve terminals. In the neuron, AMPH increases the influx of extracellular Na^+, and the subsequent increase in the intracellular Na^+ concentration triggers rapid bursts of neurotransmitter efflux through a channel-like mode of the transporter, a process that is different from the slow exchange-like transport mechanism. DAT phosphorylation is suggested to be a key point in the

interaction of AMPH and DAT, which promotes an intrinsic protein conformation favourable for reverse transport (Vaughan 2004, Gether et al. 2006). Similarly, AMPH induces NA and 5-HT releases by the reversed operation of NET and SERT. The efflux of transmitters caused by transporter-mediated reversed exchange increases transmitter concentrations in the synaptic cleft, thereby heightening the responses of postsynaptic neurons. This type of neurotransmitter release, which has a non-vesicular origin, is not regulated via presynaptic receptors, and the exact contribution of this kind of channel-like activity to cell physiology is unclear (Blakely et al. 2005, Robertson et al. 2009, Torres et al. 2003).

Substrate-type releasers are also able to disrupt the storage of neurotransmitters in vesicles by interacting with VMAT2 and by inducing dissipation of the H^+-gradient across synaptic vesicles. This mechanism increases cytoplasmic neurotransmitter concentrations, thereby further promoting reverse transport. DAT is supposed to be the major target for psychostimulants, like AMPH, 3,4-methylenedioxymethamphetamine (MDMA or ecstasy), methamphetamine, and cocaine (Figure 2.4.) because their activity appears to be specific to the brain regions implicated in reward (Rudnick and Clark 1993, Sulzer et al. 1995). Monoamine transporters also function as gateways for the cell-specific entry of neurotoxins and environmental chemicals, resulting in neurodegenerative changes in target cells and selective neuronal death. The neurotoxins 6-hydroxydopamine (6-OHDA) and 1-methyl-4-phenyl-1,2,3,6-tetrahydropyridine (MPTP or MPP^+), enter neurons via DAT, while 1-methyl-4-(2-aminophenyl)-1,2,3,6-tetrahydropyridine (amino-MPTP) enters neurons via SERT (Murphy et al. 2004) (Figure 2.4.).

The binding of a substrate to the transporter depends on specific residues in the transporter molecule that interact with substrates, such as the molecular determinants in the SERT TMD XII for the binding of TCAs (White et al. 2005), or a single amino acid, tyrosine 95 (Tyr95) in SERT TMD1 that determines the selectivity of *S*-citalopram for SERT over DAT or NET. The hydroxyl group of Tyr95 and the nitril group of *S*-citalopram form a dipole-dipole interaction that could not be formed in DAT or NET, where the corresponding amino acid is a phenylalanine. The 30-fold lower affinity of the other isomer, *R*-citalopram, is caused by sterical hindrance at the binding site. The tropane ring of cocaine interacts with both Tyr95 in SERT and the phenylalanines in DAT and NET, which is in accordance with its high affinity for all three transporters, although its effects on behaviour mostly result from its binding to DAT (Uhl et al. 2002, Ravna et al. 2003).

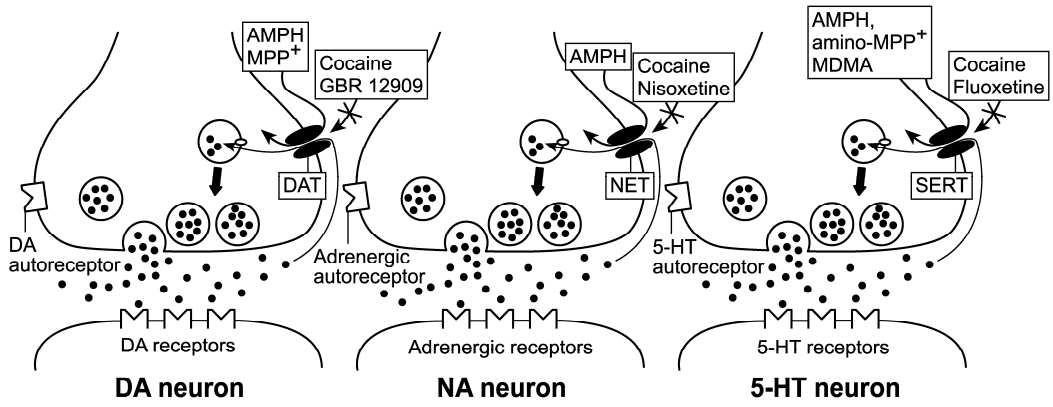

Figure 2.4. Schematic representation of dopaminergic, noradrenergic and serotonergic synaptic terminals with DAT, NET and SERT sites. Reuptake inhibitors (GBR 12909, nisoxetine, fluoxetine, cocaine), psychostimulants (AMPH, MDMA) and neurotoxins (MPP^+, amino-MPP^+) act at monoamine transporters (Timo Kattelus).

2.3.5. Clinical significance of monoamine transporters

Alterations in DAT levels have been demonstrated to be a feature of attention deficit hyperactivity disorder (ADHD), Wilson and Lesch-Nyhan diseases, and drug abuse, whereas altered LC and NET functions have been associated with orthostatic hypotension, affective and anxiety disorders, drug addiction, autonomic arousal and sleep disturbances. It has been suggested that SERT makes genetic contributions to a long list of neuropsychiatric disorders, including ADHD, obsessive-compulsive disorder (OCD), Tourette's syndrome, Asperger's syndrome, impulsive aggressive behaviour, autism, social phobia, anorexia nervosa, major depression, migraines, and alcohol abuse (Hahn and Blakely 2002, Murphy et al. 2004, Torres et al. 2003).

Several regulatory domains such as alternate promoters and polyadenylation sites, together with differential splicing resulting in multiple mRNA species, control the expression of the transporter genes. Genetic variability in these regulatory domains contributes to individual differences in the transporter activity and disease susceptibility. Studies on mutations and polymorphisms in monoamine transporter genes support linkage and association of genetic variation to psychiatric and other disorders, as well as to responses to pharmacotherapies. The theory that the dysregulation of transporter genes contributes to disease states is supported by the discovery of a single coding mutation (the A457P variant) in the human NET gene, associated with orthostatic intolerance syndrome, characterized by a diminished expression of NET and a reduced affinity for NA (Hahn and Blakely 2002, Hahn et al. 2003). Another missence mutation in the TMD8 region of the SERT gene, resulting in I425V substitution, was found in two families with several neuropsychiatric disorders including OCD, Asperger's syndrome, anorexia nervosa, depression and alcohol abuse (Ozaki et al. 2003).

In general, single nucleotide polymorphisms (SNPs), like the A457P variant, that substitute one amino acid for another could alter the expression levels and functions of transporters in a variety of ways, *e.g.* by producing an unstable protein conformation or by displacing a specific amino acid that participates in substrate binding. Polymorphisms that do not alter the amino acid sequence of transporters, including *e.g.* noncoding SNPs, variable 44-base insertion/deletion and a variable number of tandem repeat (VNTR) regions, have no effect on protein function, but they could, through the modulation of transcriptional or translational efficiency, alter transporter expression levels. For example, the transcriptional activity of the human SERT gene is modulated by a variable 44-base insertion/deletion polymorphism in the promoter region (termed 5HTTLPR). This SERT gene-linked polymorphic region, present only in humans and primates, is usually composed of either fourteen (short or S allele) or sixteen (long or L allele) repeated elements, although alleles with up to twenty repeats occasionally occur, as do variants with single-base insertions, deletions, or substitutions within individual repeat elements. The S and L variants modulate the transcriptional activity of the SERT promoter, yielding differences in SERT mRNA and protein concentrations. The L allele, especially the homozygous LL genotype, which exhibits higher SERT activity, appears to be more vulnerable to depression and ADHD (Murphy et al. 2004), while the S promoter polymorphism was reported to be associated with lower SERT activity and an increased risk of the early onset of alcoholism (Hallikainen et al. 1999). Allelic variants of SERT VNTR exhibit different transporter activities in quantitative and qualitative terms, and they have been associated with susceptivity to a variety of anxiety-related disorders (Bannon et al. 2001).

Several coding and non-coding polymorphic variants of the DAT and NET genes have also been found, such as ten different alleles containing between 3 and 13 copies of a tandem repeat in an untranslated region of the DAT gene. This 3'-untranslated region of the human DAT cDNA is longer than in rats, and unlike the rat, it contains a polymorphic repetitive element with a 40 nucleotide consensus sequence (VNTR polymorphism). Since the VNTR region is localized to the noncoding gene region, allelic variants cannot result in structural or functional differences in the DAT protein, but they have been shown to have a modulatory influence on *in vivo* DAT density (VanNess et al. 2005). DAT polymorphisms are reported to be more closely linked to hyperactivity than to attention deficits in ADHD (Uhl et al. 2002). Many other polymorphisms scattered throughout monoamine transporter genes have been identified, but no clear associations between these genes and neuropsychiatric disorders have been verified. However, it has been suggested that monoamine transporters, as components of polygenic processes, contribute to diseases or disorders (Bannon et al. 2001).

The classic monoamine hypothesis for depression proposes that its biological basis is a dysfunction of central noradrenergic and/or serotonergic systems. However, this hypothesis does not provide a complete explanation for the actions of antidepressants, and the pathophysiology of depression itself remains unclear, although the hypothesis has evolved to include adaptive changes in several receptors. Other hypotheses suggested for depression are the cytokine and the hypothalamic-pituitary-thyroid hypotheses and the role of the brain-derived neurotrophic factor in the etiology of depression (Hirschfeld 2000, White et al. 2005).

2.4. Positron-emitting radiopharmaceuticals for imaging DAT, NET and SERT

2.4.1. Positron-emitting radionuclides

In a nuclear reaction, the atoms of a stable element are bombarded by a particle, such as a proton (H^+, p), and the nucleus of the stable atom absorbs this particle. The resulting nucleus (with a higher atomic number) is unstable and decomposes quickly, emitting radiation (photons and/or particles). When positively charged particles, such as a H^+, deuteron ($^2H^+$) or helium nucleus ($^4He^{2+}$) are used as the bombarding particles, neutron deficient (or H^+-rich) radioisotopes are produced, which decay and stabilize through electron capture or positron (β^+) emission. In this process, a proton in the nucleus is converted to a neutron (n) by the emission of a β^+, along with a neutrino (ν): $p \rightarrow n + \beta^+ + \nu$ (Figure 2.5.). Positively charged particles are accelerated by a cyclotron along a circular path to generate a high energy intensity beam for the bombardment of the target material (gas, liquid or solid) that undergoes a nuclear transformation to H^+-rich, β^+-emitting radionuclides.

PET radiopharmaceuticals (tracers) are labelled with short-lived radionuclides; the most commonly used isotopes are ^{15}O, ^{13}N, ^{11}C, ^{68}Ga and ^{18}F with physical half-lives ($t_{1/2}$) of 2.05, 10.0, 20.4, 68.3 and 109.6 min, respectively. Replacing a carbon-12 atom with carbon-11 gives a compound that is physiologically indistinguishable from the unlabelled compound. Fluorine does not generally occur in biomolecules in living organisms, but it commonly replaces a hydrogen atom or a hydroxyl group in medicinal chemistry. [^{18}F]Fluorine is currently the most utilized PET radiohalogen, due to the fact that it is relatively easy to produce in large quantities, its convenient half-life, and its nearly optimal decay properties. Fluorine is the most electronegative of all the elements, and it can react with both organic and inorganic compounds as a positively charged electrophile or as a negatively charged nucleophile. Efficient incorporation of the ^{18}F-radiolabel into radiopharmaceuticals is possible using either nucleophilic routes with a high specific radioactivity (SA) [^{18}F]fluoride, or electrophilic routes with a lower SA [^{18}F]fluorine. Two types of methods are used to produce these two different chemical forms of fluorine: a liquid target for the production of nucleophilic fluoride ions ([^{18}F]F^-) and a gas target for the production of electrophilic fluorine gas ([^{18}F]F_2).

The most common nuclear reaction used to produce [^{18}F]F$^-$ is based on the proton bombardment of ^{18}O atoms in highly enriched [^{18}O]water as the target material (Ruth and Wolf 1979). Because [^{18}F]fluoride can be produced with a high SA, nucleophilic fluorination reactions are suitable for preparing radiotracers with a high SA (Bergman et al. 2001). [^{18}F]F_2 can be produced by the proton bombardment of [^{18}O]oxygen gas (Nickels et al. 1983). Since [^{18}F]F_2 is always diluted with carrier fluorine gas, the SA of the electrophilic [^{18}F]F_2 is low. In order to increase the SA of ^{18}F-radiolabelled tracers based on electrophilic reactions, a multi-step method has been developed to generate [^{18}F]F_2 with a high SA, in which [^{18}F]F$^-$ is first converted to [^{18}F]methylfluoride, before [^{18}F]F_2 with a high SA is generated in a discharge chamber. In general, electrophilic reactions involve the "carrier added" [^{18}F]F_2 gas with a low SA, while nucleophilic reactions involve the "no carrier added" [^{18}F]F$^-$ ion with a high SA (Kilbourn 1990, Bergman et al. 1994, 1997, Bergman and Solin 1997). The theoretical maximum SA for [^{18}F] is 63,300 GBq/μmol.

2.4.2. Pre-clinical imaging with positron-emitting radiopharmaceuticals

Pre-clinical imaging of biological processes using positron-emitting tracers in animals *in vivo* is performed with PET scanners, and on *ex vivo* or *in vitro* tissue sections using autoradiography. The basic principle of PET imaging techniques is based on the coincident detection of the two 511-keV annihilation gamma (γ) quanta produced by the interaction of a positron with an electron (Figure 2.5.). Storage phosphor imaging, also known as radioluminography or photo-stimulated luminescence (PSL) autoradiography, is based on using phosphor crystals to absorb and store energy deposited from radioactivity decay (*e.g.* BaFBrI:Eu^{2+} or $CaSO_4$:Dy^{3+}), coated on a plastic imaging plate. After exposure to a radioactive source, the imaging plate is excited with a laser beam to release luminescence light from the energy stored by the crystals. The light signal is amplified by a photomultiplier tube and analyzed by a computer (Knol et al. 2008, Fuji Photo Film Co., Ltd., Japan).

One of the factors limiting the ultimate spatial resolution attainable by PET imaging or PSL autoradiography is the "positron range", the distance from the positron emission site to its annihilation site. The energy of the annihilation γ quantum is 511 keV for all quanta, but the positrons emitted by different radionuclides have different β^+-decay energies ($E_{\beta+}$), and, as a result, the distance travelled by a positron through tissue to its annihilation site (*i.e.* positron range) is proportional to the kinetic energy of the positron. In the case of ^{68}Ga, for example, the maximal $E_{\beta+}$-energy is 1900 keV and the maximal positron range in water is 8.2 mm, while for ^{18}F, the figures are 634 keV and 2.4 mm, respectively, meaning that the imaging resolution is better with ^{18}F-labelled tracers.

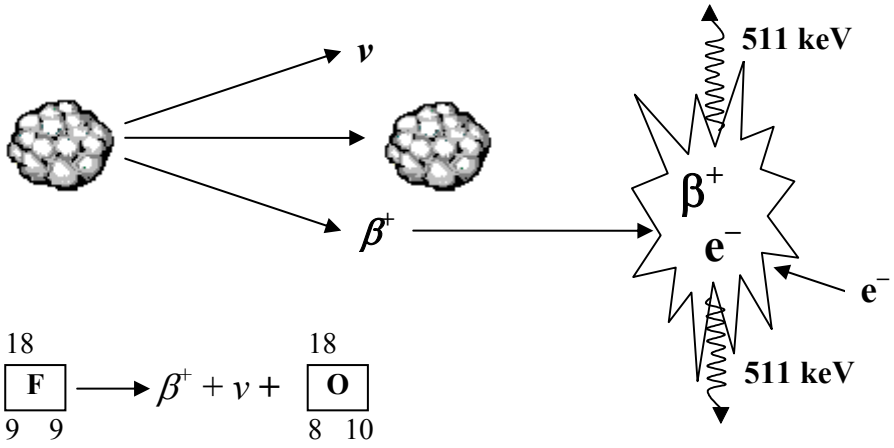

Figure 2.5. Schematic illustration of the decay of fluorine-18 to oxygen-18 with subsequent annihilation of a positron and an electron. Two 511 keV gamma (γ) quanta are produced and emitted in opposite directions.

2.4.3. Affinity and selectivity of positron-emitting radiopharmaceuticals

The binding of a ligand to its receptor depends on the affinity (K_d or K_i) of the ligand to the receptor and the number of receptors (B_{max}) available for binding. The radioligand affinity is the ratio of the dissociation (k_{off}) and association (k_{on}) rate constants ($K_d = k_{off}/k_{on}$), where the k_{on} depends largely on diffusion of ligands and is therefore similar for many compounds. Like many antidepressants, ligand may have a high affinity for a target, but may not, however, possess optimal properties as a PET tracer. The affinity of an ideal PET tracer represents a compromise between high affinity binding to targets with a high signal-to-noise ratio and reaching the binding equilibrium within a reasonable period of time. The optimal affinity of a radioligand also depends on the density of its binding sites; the number of binding sites should exceed the K_d of the ligand; *i.e.* high affinity radioligands are suitable for binding sites that are expressed at low densities (Halldin et al. 2001).

Very high affinity ($K_d < 0.1$ nM) radioligands tend to accumulate in an irreversible manner and fail to approach equilibrium binding conditions, at least within an appropriate scanning time. As a result their binding to the target will depend strongly on their rate of delivery and transport via the blood stream, which may be affected by pharmacological interventions or pathological conditions. The irreversible-like binding results in a low k_{off} and slow kinetics (Farde et al. 1989, Gifford et al. 1998). In PET studies, it may be an advantage to employ radiotracers with lower affinities ($K_i > 0.1$), because these provide a pseudo-equilibrium state within a reasonable PET scanning time, as they have higher rates of dissociation from the target sites. To be sensitive to changes in target concentrations, the tracer-target association phase should be

sufficiently fast, binding to the target should be reversible and the tracer should be rapidly cleared from tissue to blood to allow the binding equilibrium. Since reversible type tracers have the potential to compete with neurotransmitters, they may be more optimal for the measurement of quantitative parameters such as K_d, B_{max} and binding potential. Low affinity tracers usually show too low signal-to-noise ratios and a rapid washout from the target (Seeman et al. 1989, Endres and Carson 1998, Carson et al. 1997, Laruelle et al. 2003). Because agonists are usually more quickly inactivated or metabolized, PET tracers are generally developed using antagonists or inhibitors.

High selectivity is another important characteristic of a good tracer. For an ideal PET tracer, its selectivity should be more than one order of magnitude higher for the binding site of interest than for other sites. However, the distinct anatomical distribution of the binding site of interest allows the use of less selective ligands (Halldin et al. 2001); *e.g.* [^{18}F]*β*-CFT can be used to measure striatal DAT sites despite the fact that it also binds to NET sites, since NET is virtually absent in the STR.

2.4.4. Structure-activity relationship of cocaine analogues

Currently, the majority of radiotracers for monoamine transporters, especially for DAT, are cocaine analogues, like phenyltropanes (Figure 2.6.). Structural modifications can change the biological properties of phenyltropanes, in which the 3*β*-benzoyl group of cocaine is replaced by a 3*β*-(4-substituted phenyl) group to get a series of 2*β*-carbomethoxy-3*β*-(4-substituted phenyl)tropanes (Wong 1993, Xing 2000). Of particular interest are substituents attached at the carbon-2 (*C*2), carbon-3 (*C*3), or nitrogen (*N*) positions of the phenyltropanes.

A substituent, such as a 2*β*-carbomethoxy ester, at the *C*2 position of a phenyltropane is required for high DAT affinity, although a range of other esters, heterocycles, amides, and vinyl or alkyl groups can replace carbomethoxy esters without a loss of DAT affinity. An isopropyl ester at the *C*2 position, for example, significantly enhanced DAT selectivity with only minor effects on DAT affinity, while replacing the carbomethoxy ester at the *C*2 position with either a hydrogen or a carboxyl group decreased the potency of phenyltropanes (Bennett et al. 1995, Xing et al. 2000). Bulky groups at the *C*2 position decrease SERT and NET affinity, leading to increased DAT selectivity, as shown by the 2*β*-isoxazole analogues like 2*β*-[3-(4-methylphenyl)isoxazol-5-yl]-3*β*-(4-chlorophenyl)tropane (RTI-336, Figure 2.6.) (Carroll et al. 1992, Bennett et al. 1995, Emond et al. 1997). However, some of the compounds with bulky *C*2-groups are nonselective and inhibit both DAT and SERT, like 2*β*-carboxylic acid-2-(3-iodo-4-aminophenyl)ethylester-3*β*-(4-methoxyphenyl)-tropane, developed for the treatment of cocaine abuse (Jin et al. 2008a, b).

Stereochemistry at the *C*2 position is an important factor; epimerization from *β* to *α* decreases the biological activity of cocaine-like compounds (Carroll et al. 1992).

Natural cocaine has a 2*β*,3*β*-configuration; tropanes with other configurations have little or no biological activity (Drewes et al. 2007). Generally, the *R*-configuration of the tropane ring is required for the potent activity of phenyltropanes; only the *R*-isomer of cocaine obtained from natural sources is addictive. In some cases, however, the *S*-enantiomers are more potent, *e.g.* 2*β*-(*S*)-carbo-1-[^{18}F]fluoro-2-propoxy-3*β*-(4-chlorophenyl)tropane, [^{18}F](*S*)-FIPCT, exhibited higher DAT affinity (K_i 0.67 nM) than the (*R*)-isomer (K_i 3.2 nM) (Singh 2000, Xing et al. 2000).

Removing the ester link of cocaine at the *C*3 position, and the nature of the substituent on the aromatic ring directly attached at the 3*β*-position, strongly influence DAT site recognition. A methyl group or a halogen substituent at the 3' and/or 4' position (but not at the 2' position) of the aromatic ring increase the potency and selectivity of phenyltropanes for DAT when compared with cocaine, as shown by 2*β*-carbomethoxy-3*β*-(4-fluorophenyl)tropane (*β*-CFT or WIN-35,428) and its 4'-iodophenyl analogue (*β*-CIT) (Meltzer et al. 1993, Emond et al. 1997, Stout et al. 1999). Substituting the *para*-fluorine in *β*-CFT with larger groups yields compounds with increased DAT affinity and selectivity, such as its 4'-fluoromethyl analogue (*p*-FWIN), while the *ortho* isomer (2'-fluoromethyl) (*o*-FWIN) has a low affinity for DAT (Stout et al., 1999). In the phenyltropanes, increased electron density around both the aromatic ring and the 4′-substituent correlates with high DAT affinity, *i.e.* 4′-substituted analogues have a higher affinity for DAT than the unsubstituted derivatives. However, replacing the 4'-methoxy group with a larger ethoxy group increased SERT affinity, and decreased DAT affinity, indicating that SERT is more tolerant to steric substituents on the *para*-position of the ring. The addition of one *ortho* halogen atom to the 4'-methoxy analogue increased NET affinity, but diiodo or dibromo additions resulted in a 5-fold loss of NET affinity (Jin et al. 2008b).

The *N*-substituent at the amino group of phenyltropanes is important for their level of DAT and SERT selectivity. The demethylation of the bridgehead *N* improves SERT selectivity, while *N*-substitutions with alkenyl, alkynyl, or benzyl groups yield compounds with high selectivity and affinity for DAT. This is demonstrated by the *N*-substituted derivatives of *β*-CFT and *β*-CIT, which all have weak SERT affinities, especially the *N*-fluoropropyl derivative of *β*-CIT (*β*-CIT-FP), which has the highest DAT affinity among tropanes (Chaly et al. 1996). Nitrogen can also be replaced with oxygen or carbon without a loss of potency. However, replacing the *N*-methyl group with an acetyl group to create an amide, or adding a methyl group to create a quaternary salt reduces DAT affinity (Bennett et al. 1995, Carroll et al. 1992, Emond et al. 1997, Meltzer et al. 1993).

2.4.5. Radiotracers for DAT

Most successful DAT tracers are 3*β*-phenyltropanes, cocaine analogues (Figure 2.6., Table 2.1.). Among radiolabelled *β*-CFT analogues (Clarke et al. 1973), the kinetics of

N-([^{11}C]methyl)-2*β*-carbomethoxy-3*β*-(4-fluorophenyl)nortropane ([^{11}C]WIN-35,428, [^{11}C]*β*-CFT) was too slow in human PET studies compared to the short half-life of ^{11}C (Wong et al. 1993), whereas the longer half-life of ^{18}F allows the use of [^{18}F]*β*-CFT in human PET studies (Laakso et al 1998, Rinne et al. 1999a, b). In the rat brain, the maximum STR-to-CE ratio was 9.6 at ~ 2 h *p.i.* for [^{18}F]*β*-CFT (Haaparanta et al. 1996). *N*-(2-[^{18}F]fluoroethyl)-2*β*-carbomethoxy-3*β*-(4-fluorophenyl)nortropane ([^{18}F]*β*-CFT-FE) showed faster kinetics and adequate selectivity for DAT over SERT in rats (Firnau et al. 1995) and in monkeys, but a lower DAT affinity (*β*-CFT: K_i 26 nM, *β*-CFT-FE: K_i 71 nM, Harada et al. 2004). This was also shown by its 3-[^{18}F]fluoropropyl analogue, [^{18}F]*β*-CFT-FP in a preliminary evaluation in rats (Firnau et al. 1995, K_i 48 nM, Harada et al. 2004). Its ^{11}C-labelled analogue, *N*-(3-fluoropropyl)-2*β*-[^{11}C]carbomethoxy-3*β*-(4-fluorophenyl)nortropane ([^{11}C]*β*-CFT-FP) was DAT selective in *post mortem* human brain sections (Kämäräinen et al. 2000a, b). All these *β*-CFT derivatives exhibited reduced affinities for DAT, NET and SERT, but improved DAT selectivity, with lower STR-to-CE ratios when compared to [^{18}F]*β*-CFT.

β-CIT (RTI-55), a 4'-iodophenyl analogue of *β*-CFT, has a high DAT affinity (K_i 0.54 nM), but its SERT affinity is equal (K_i 0.50 nM) (Okada et al. 1998, Harada et al. 2004), so it is not selective. To a large extent, [^{11}C]*β*-CIT binding in the thalamus represents specific binding to NET and SERT sites (Müller et al. 1993, Farde et al. 1994). In humans, *N*-(2-fluoroethyl)-2*β*-[^{11}C]carbomethoxy-3*β*-(4-iodophenyl)-nortropane ([^{11}C]*β*-CIT-FE) obtained a high STR-to-CE ratio of 9 within 60 min (Halldin et al. 1996), but it was not sufficiently DAT selective. In monkeys, *N*-(3-[^{18}F]fluoropropyl)-2*β*-carbomethoxy-3*β*-(4-iodophenyl)nortropane ([^{18}F]*β*-CIT-FP) showed higher *in vivo* selectivity, a STR-to-CE ratio of ~ 5 (Lundkvist et al. 1997), and a STR-to-occipital cortex ratio of 3.5 in humans (Chaly et al. 1996, Kazumata et al. 1998). [^{18}F]*β*-CIT-FP metabolized quickly to its radiolabelled free carboxylic acid form, and to the unlabelled nor-*β*-CIT. Contrary to [^{18}F]*β*-CIT-FP, [*O*-methyl-^{11}C]*β*-CIT-FP ([^{11}C]*β*-CIT-FP) metabolized more slowly to a lipophilic, radiolabelled [^{11}C]nor-*β*-CIT, which had a high SERT affinity and was capable of entering the brain. Therefore, it was suggested that [^{18}F]*β*-CIT-FP was superior to [^{11}C]*β*-CIT-FP as a DAT tracer (Lundkvist et al. 1997), although [^{11}C]*β*-CIT-FP binding in the STR reached equilibrium and a high STR-to-CE ratio of 8 within 70 min (Lundkvist et al. 1995). The fluoroethyl and fluoropropyl analogues of *β*-CIT exhibited reduced affinity for both DAT and SERT, like the *β*-CFT analogues.

In rats, the potential DAT tracers, 2*β*-[^{11}C]carbomethoxy-3*β*-(4-methylphenyl)tropane ([^{11}C]RTI-32) and 2*β*-carbo-2'-[^{18}F]fluoroethoxy-3*β*-(4-methylphenyl)tropane ([^{18}F]FETT), labelled at the 2*β*-carboxy position, exhibited very high STR-to-CE ratios of 27 and 21 at 90 min and 120 min *p.i.* respectively (Wilson et al. 1996a). In their 4'-chlorophenyl analogues, [^{11}C]RTI-31 and

[^{18}F]FECT, the chlorine substituent resulted in a higher accumulation of the tracers in the STR, as well as a slower washout of non-specific binding with a pseudo equilibrium at 3 h *p.i.*. Therefore, [^{11}C]RTI-31 and [^{18}F]FECT were less suitable as PET tracers. [^{11}C]RTI-32 and [^{11}C]RTI-31 metabolized quickly, but radioactive metabolites did not enter the brain, while the [^{18}F]fluoroethyl ester at the *C*2-position in both [^{18}F]FETT and [^{18}F]FECT was more stable against cleavage by esterases (Chitneni et al. 2008). In rats, 2*β*-carbo-2'-[^{18}F]fluoroethoxy-3*β*-(4-iodophenyl)tropane ([^{18}F]FE@CIT) showed a STR-to-CE ratio of 3.7 at 60 min *p.i.*, increased DAT selectivity when compared to [^{123}I]*β*-CIT, and good [^{18}F]fluoroethyl ester stability against cleavage (Ettlinger et al. 2008, Mitterhauser et al. 2005). [^{18}F]MCL-322, a derivative of RTI-51 (*i.e.* *β*-CBT, a bromine containing CFT analogue) showed a high DAT affinity (K_i 2.3 nM) and selectivity and a STR-to-CE ratio of 2.8 at 115 min *p.i.* in a PET study of rats (Wuest et al. 2005). Replacing the methyl ester of RTI-31 with a ^{18}F-fluoroisopropyl ester gives [^{18}F](*R/S*)-FIPCT, which showed reduced SERT and NET affinities. [^{18}F](*S*)-FIPCT exhibited higher DAT affinity and longer retention in the brain than its *R*-isomer, which achieved a transient equilibrium within 90 min and was therefore more suitable for quantitation of the striatal DAT sites. [^{18}F](*S*)-FIPCT may be a potential tracer for mapping extrastriatal DAT sites due to its prolonged retention in the brain, which will afford higher signal-to-noise ratios at later points in time. In rats, the *R*- and *S*-isomers had STR-to-CE ratios of 6.0 and 11.8 at 60 min *p.i.,* respectively (Xing et al. 2000).

In monkeys, *N*-(2-[^{18}F]fluoroethyl)-2*β*-carbomethoxy-3*β*-(4-chlorophenyl)nortropane ([^{18}F]FECNT) was highly DAT selective with a high affinity (K_i 1.5 nM), and a maximum putamen-to-CE ratio of 12.7 at ~ 2 h *p.i.* (Goodman et al. 1997, 2000). In human PET studies, [^{18}F]FECNT showed a high specific brain uptake and favourable, reversible DAT binding kinetics, which attained equilibrium within 90 min (Davis et al. 2003). [^{18}F]FECNT metabolized rapidly; the radiolabelled metabolites were polar and were identified as either [^{18}F]fluoroethanol, [^{18}F]fluoroacetaldehyde, or [^{18}F]fluoroacetic acid. However, these ^{18}F-labelled two-carbon residues were able to enter the brain and were uniformly distributed across brain regions (Zoghbi et al. 2006). PET studies on monkeys using the *N*-3-[^{18}F]fluoropropyl analogue ([^{18}F]FPCT) showed a putamen-to-CE ratio of 3.4 at ~ 2 h *p.i.,* and the uptake in the STR remained nearly constant, indicating irreversible-like binding to DAT sites (Goodman et al. 1997). It was suggested that [^{18}F]FECNT is superior to [^{11}C]*β*-CFT, [^{11}C]*β*-CIT/RTI-55, [^{18}F]*β*-CIT-FP, and [^{18}F]FPCT for human brain PET studies. An undesired feature of using several ^{11}C-labelled tracers for DAT imaging is the prolonged time they require to reach DAT binding equilibrium compared to the short half-life of ^{11}C, which limits their usefulness in PET studies.

N-(3-iodoprop-2*E*-enyl)-2*β*-[^{11}C]carbomethoxy-3*β*-(4-methylphenyl)nortropane ([^{11}C]-PE2I) bound with high affinity, specificity and selectivity to DAT sites, with a STR-to-

CE ratio of ~ 10, reaching a peak binding equilibrium within 1 h in human and monkey brains (Emond et al. 1997, Halldin et al. 2003). The measurement of DAT binding, even in small brain regions, including the SN, was reproducible and reliable. Therefore, [^{11}C]PE2I was suitable for the quantitation of both striatal and extrastriatal DAT sites in humans (Hirvonen et al. 2008). The combination of nitrogen and phenyl substitutions resulted in a PET tracer with high DAT affinity and selectivity. However, the aryl methyl group of [^{11}C]PE2I underwent a rapid hydroxylation to polar and radioactive 4'-hydroxymethyl and 4'-carboxyl derivatives that accumulated in the brain, presumably by binding to DAT, which may limit the utility of [^{11}C]PE2I for measuring DAT sites (Shetty et al. 2007).

Substituting the *para* fluorine of the phenyl ring in *β*-CFT with larger groups (*e.g.* methyl, chlorine, bromine or iodine) increases DAT affinity and selectivity, as shown by 2*β*-carbomethoxy-3*β*-(4-[^{18}F]fluoromethylphenyl)tropane ([^{18}F]*p*-FWIN) (Stout et al. 1999). In a monkey PET study, *N*-(1-iodoprop-1-en-3-yl)-2*β*-[^{11}C]carbomethoxy-3*β*-(4-fluorophenyl)nortropane ([^{127}I,^{11}C]altropane), a *N*-3-iodoallyl derivative of [^{11}C]*β*-CFT, showed fast and specific striatal uptake, high DAT selectivity, reversible binding kinetics and slow metabolism to polar metabolites, and was proposed as a suitable PET tracer (Fischman et al. 2001). Different variations on the tropane structure are the *N*-benzyl-2*β*-ethyl ketones, (+)-*N*-(4-[^{18}F]fluorobenzyl)-2*β*-propanoyl-3*β*-(4-tolyl)tropane ([^{18}F](+)FTT) and its 4'-chlorophenyl analogue ([^{18}F](+)FCT) that showed reversible kinetics in a monkey PET study. [^{18}F](+)FCT was the more suitable of the two tracers with a STR-to-CE ratio of 2.6 (Mach et al. 2000).

A new generation of highly selective DAT ligands, the *N*-(*E*)-fluorobutenyl tropanes FBFNT, FBClNT, FBBrNT, FBINT and LBT-999, which have either a F, Cl, Br, I atom or a methyl substituent at the 4'-position of the 3*β*-phenyl ring, are derivatives of *β*-CFT, *β*-CCT (RTI-31), *β*-CBT (RTI-51), *β*-CIT (RTI-55) and RTI-32, respectively. The DAT affinities (K_i) of these compounds were high, ranging from 0.17 to 2.54 nM, the SERT affinities (K_i) ranged from 0.21 to 86 nM, but the NET affinities were low. FBFNT and FBClNT showed 10- and 50-fold selectivity for DAT over SERT, respectively; FBBrNT and FBINT were less selective. All these *N*-(*E*)-fluorobutenyl tropanes were labelled with ^{18}F, however they all exhibited ^{18}F-radioactivity accumulation in the bone, indicating a significant defluorination of the [^{18}F]fluorobutenyl group (Dollé et al. 2005, Stehouwer and Goodman 2009). The ^{11}C-labelled (*E*)-*N*-(4-fluorobut-2-enyl)-2*β*-[^{11}C]carbomethoxy-3*β*-(4-tolyl)nortropane ([^{11}C]LBT-999) showed high affinity (K_i 9 nM), fast reversible binding kinetics, and high selective DAT binding, with a STR-to-CE ratio of 25 at 60 min *p.i.* in rat brains (Chalon et al. 2006), and a STR-to-CE ratio of 30 at 110 min *p.i.* in a PET study of baboons (Saba et al. 2007) reflecting properties of a promising PET tracer for DAT.

2.4.6. Radiotracers for NET

The development of an ideal radiotracer for NET has been challenging due to the low density and widespread distribution of NET binding sites in the brain. Several potent NET inhibitors, including [^{11}C]desipramine (Van Dort et al. 1997, Schou et al. 2006), (*R/S*)-[^{11}C]nisoxetine (Haka and Kilbourn 1989), (*R*)-[^{11}C]nisoxetine, [^{11}C]oxaprotiline, [^{11}C]lortalamine (Ding et al. 2005), [^{11}C]talopram and [^{11}C]talsupram (Schou et al. 2006) have been radiolabelled for *in vivo* NET imaging, but they were not suitable due to slow kinetics, poor selectivity or high non-specific binding.

The *S,S*-isomer of 2-[α-(2-ethoxyphenoxy)phenylmethyl]morpholine, (*S,S*)-reboxetine, is a potent NET inhibitor with a high affinity (K_i 1.0 nM) and selectivity. Reboxetine has also been approved for the clinical treatment of depression in humans. However, its [^{18}F]fluoroethyl and [^{18}F]fluoromethyl ether derivatives and their deuterated analogues, (*S,S*)-[^{18}F]fluororeboxetine ((*S,S*)-[^{18}F]FRB, Ding et al. 2005), (*S,S*)-2-[α-(2-[^{18}F]methoxyphenoxy)benzyl]morpholine ((*S,S*)-[^{18}F]FMeNER, Schou et al. 2004), (*S,S*)-[^{18}F]FRB-D_4 (Ding et al. 2005), and (*S,S*)-[^{18}F]FMeNER-D_2 (Schou et al. 2004) had undesirable properties as PET tracers, such as high defluorination, slow kinetics and poor specific-to-non-specific ratios. The deuteration of the molecules reduced defluorination, but did not totally inhibit it. (*S,S*)-[^{18}F]FMeNER-D_2 was the most suitable of these tracers; in monkey PET studies its uptake in the THA achieved peak equilibrium within 30 min *p.i.* and a THA-to-caudate ratio of 1.5 (Takano et al. 2009).

The ^{11}C-labelled reboxetine analogues [^{11}C]*O*-methylreboxetine ((*S,S*)-[^{11}C]MRB or (*S,S*)-[^{11}C]MeNER), and (*S,S*)-3-Cl-[^{11}C]MRB, a more potent but less selective tracer than reboxetine, have been suggested as potential tracers for NET (Ding et al. 2005). (*S,S*)-[^{11}C]MeNER (K_d 0.95 nM) was the most promising, due to its faster clearance and a HY-to-STR uptake ratio of 2.5 at 60 min *p.i.* in rats, although it did not reach binding equilibrium during a 90 min PET study (Schou et al. 2003, 2004, Wilson et al. 2003). Recently, (*S,S*)-[^{11}C]MeNER was shown to be suitable in NET studies on humans (Ding et al. 2010). Reboxetine undergoes extensive oxidative metabolism through three major metabolic pathways: the hydroxylation of the ethoxy-bearing aryl ring, *O*-de-ethylation, and the oxidation of the morpholinyl moiety. A similar biotransformation was also expected for (*S,S*)-[^{11}C]MeNER due to its close structural similarity. The major metabolite in the rat brain was an unlabelled, hydrophilic, *O*-demethylated MeNER. In humans, (*S,S*)-[^{11}C]MeNER metabolized slowly to a polar metabolite and a transient lipophilic metabolite. However, the kinetics of the lipophilic metabolite was favourable for PET imaging, as it was rapidly cleared from plasma (Schou et al. 2009).

Replacing the phenyl alkyl ether (2-ethoxyphenoxy) in reboxetine with different alkyl groups yielded (2*S*,3*S*)-2-[α-(2-methylphenoxy)phenylmethyl]morpholine (MENET), its 2-fluoroethyl (FENET), and 3-fluoropropyl analogues (FPNET). MENET showed

high NET affinity (K_i 1.0 nM) and selectivity, while the fluoroethyl and fluoropropyl derivatives showed lower NET affinity and a similar affinity to SERT sites. The target-to-non-target uptake ratios for [^{18}F]FENET and [^{18}F]FPNET were ~ 1.1, reflecting the poor NET imaging properties of these tracers. Replacing the oxygen atom with a sulphur atom as the linker of the three rings in MENET yielded a 2'-methylphenylthio derivative (MESNET) that was three times more potent (K_i 0.3 nM) for NET than MENET, but with decreased NET selectivity. This indicates that replacing the benzyl phenyl ether oxygen atom with a sulphur atom enhanced both NET and SERT affinity. However, this oxygen atom was necessary for low SERT affinity, as indicated by the enhanced SERT affinity of MESNET (K_i 15 nM) as compared to MENET (K_i 93 nM). [^{11}C]MESNET showed slower binding kinetics than [^{11}C]MENET, and target-to-non-target ratios from 1.3 to 1.5 at 90 min *p.i.* in monkeys, similar to the ratios for [^{11}C]MENET (Zeng et al. 2009), and (*S,S*)-[^{11}C]MeNER (Schou et al. 2003). [^{11}C]MENET was suggested as the most promising NET imaging tracer due to its kinetic behaviour (Zeng et al. 2009) (see Figure 2.6. and Table 2.1.).

2.4.7. Radiotracers for SERT

In the past, a number of SSRIs, including fluoxetine (Das and Mukherjee 1993, Kilbourn et al. 1989), sertraline (Lasne et al. 1989), citalopram (Hume et al. 1991), cyanoimipramine (Takano et al. 2002), and paroxetine derivatives (Dannals et al. 1989, Suehiro et al. 1991) as well as *cis-N,N*-dimethyl-3-(2,4-dichlorophenyl)indanamine (*cis*-DDPI) (Suehiro et al. 1992) have been labelled with ^{11}C or ^{18}F. However, none of these ligands were suitable for PET imaging due to poor kinetics, fast metabolism, nonselectivity or high non-specific binding. Halogenated derivatives of 6-nitroquipazine (6-NQ), one of the most potent (K_i 0.17 nM) and selective SERT inhibitors, showed high SERT affinities in *in vitro* studies (Lee et al. 2003). However, 5-[^{76}Br]bromo-6-NQ accumulated in rat brains with a THA-to-CE ratio of only 2 at 3h *p.i.* (Lundkvist et al. 1999), and 3-(3-[^{18}F]fluoropropyl)-6-NQ ([^{18}F]FPNQ) also showed low signal-to-noise ratios, and remarkable defluorination (Lee et al. 2003). Therefore, 6-NQ derivatives are unsuitable as PET tracers.

Maryanoff et al. (1984) synthesized 1,2,3,5,6α,10β-hexahydro-6-(4-methylthiophenyl)-pyrrolo[2,1-a]isoquinoline, a *cis/trans*-mixture of two diastereomers, and isolated the biologically active *trans*-isomer as a racemic mixture of two enantiomers. One enantiomer, (+)6*S*,10β*R* ((+)McN5652, K_i 0.26 nM), was a highly potent SERT inhibitor, and the other, (-)6*R*,10β*S* was inactive (Shank et al. 1988). Radiolabelling of the active isomer with ^{11}C yielded the first specific and selective PET tracer for SERT, [^{11}C](+)McN5652 (Suehiro et al. 1993a, b), which showed only moderate target-to-non-target ratios due to its high non-specific binding and slow binding kinetics (Szabo et al. 1995a, b). Until now, [^{11}C](+)McN5652 has been one of the most widely used PET tracers for SERT, currently mostly as a reference tracer. The ethyl analogue

[^{18}F]FEt-McN had less favourable properties as a PET tracer, such as poor blood-brain barrier (BBB) penetration and low target-to-non-target ratios (Suehiro et al. 1996).

Numerous phenylthiobenzylamines, such as diphenylsulfide derivatives that are especially modulated on the 4'-position of the phenylthio moiety by a halogen or a fluoroalkyl substituent, have been radiolabelled and evaluated as PET tracers for SERT. In rats, [^{11}C]*N,N*-dimethyl-2-(2-amino-4-cyanophenylthio)benzylamine ([^{11}C]DASB) had a slightly higher target-to-non-target ratio of 9 at 1 h *p.i.* than its 4'-methoxy analogue ([^{11}C]DAPP) (Wilson et al. 2000). [^{11}C]DASB showed high signal-to-noise ratios and fast, reversible binding kinetics suitable for PET imaging also in humans (Houle et al. 2000). ^{11}C-labelled 4'-iodo (ADAM), 4'-bromo (DAPA), and 4'-fluoromethyl (AFM) analogues were compared with [^{11}C]DASB in baboons. [^{11}C]DASB and [^{11}C]AFM were superior: [^{11}C]DASB had fast kinetics, while [^{11}C]AFM showed the highest signal-to-noise ratios, which enables the measurement of SERT in brain regions with low SERT densities (Huang et al. 2002). High SERT selectivity and affinity of both DASB (K_i 1.1 nM) and AFM (K_i 1.0 nM) was also proved in studies using SERT knockout mice (Li et al. 2004). When compared with [^{11}C](+)McN5652, [^{11}C]DASB showed greater uptake ratios due to its higher specific and lower non-specific binding, and was slightly more sensitive in assessing the effects of paroxetine, while [^{11}C](+)McN5652 was better at detecting serotonergic lesions in the brains of baboons. [^{11}C]DASB also represented an improvement over [^{11}C](+)McN5652, as it had higher plasma-free fractions and faster uptake and washout kinetics, resulting in shorter PET scanning periods of baboons (Szabo et al. 2002). However, [^{11}C]DASB plasma clearance was significantly slower in humans, thus the required scanning time with [^{11}C]DASB for healthy humans was similar to that of [^{11}C](+)McN5652 (Frankle et al. 2004).

The 4'-iodo analogue [^{11}C]ADAM was selective and had a high SERT affinity, but its slow *in vivo* kinetics was not appropriate for the short half-life of ^{11}C (Oya et al. 2000, Halldin et al. 2001, Chalon et al. 2003). Substituting the iodine in ADAM for a methyl group yields *N,N*-dimethyl-2-(2-amino-4-methylphenylthio)benzylamine (MADAM) (Emond et al. 2002, Chalon et al. 2003). [^{11}C]MADAM accumulated in monkey brains with a target-to-non-target ratio of 2.5 at 80 min *p.i.* and was rapidly metabolized, as seen with all diphenyl sulphide derivatives, to polar metabolites (Halldin et al. 2005). Improved properties in monkey PET studies were seen with its ^{11}C-labelled 4'-hydroxymethyl analogue ([^{11}C]HOMADAM) that achieved high affinity for SERT (K_i 0.57 nM), higher uptake ratios and faster kinetics than [^{11}C]DASB (Jarkas et al. 2005). Introduction of an unlabelled fluorine atom at the aryl bearing the dimethylaminomethyl group in [^{11}C]HOMADAM (*C*5-position, R3 in Figure 2.6.) resulted in a slight reduction in SERT affinity (K_i 1.26 nM) and increased lipophilicity. This ^{11}C-labelled, fluorinated phenylthiobenzylamine analogue showed reversible

kinetics with a target-to-non-target ratio of 3.4 at 85 min *p.i.*, and may be a viable PET tracer for SERT imaging (Jarkas et al. 2008).

The 4'-methylthio analogue, SMe-ADAM, showed improved affinity for SERT as compared to ADAM. A target-to-non-target ratio of 6.7 at 60 min *p.i.* for [^{11}C]SMe-ADAM in rat brain was similar to those of [^{11}C]DASB and [^{11}C](+)McN5652. Clearance of the non-specific uptake was faster than the washout of [^{11}C](+)McN5652 or [^{11}C]DASB, and the binding equilibrium was reached within 2 h in rats; thus [^{11}C]SMe-ADAM may have potential as a PET tracer for SERT imaging (Zessin et al. 2006). Substitution of the iodine in ADAM with a fluorine atom yields AFA (4-F-ADAM), with a fluoroethyl group AFE, and with a fluoropropyl group AFP. [^{11}C]AFA had a target-to-non-target ratio of 6.4 at 90 min *p.i.* in rats, equal to the ratio of [^{11}C]SMe-ADAM. In monkey brain PET studies, [^{11}C]AFA showed fast kinetics, and a target-to-non-target ratio of 2.5 at 90 min *p.i.*, equal to that of [^{11}C]MADAM (Huang et al. 2004). In human PET studies [^{11}C]AFA did not provide advantages over [^{11}C]DASB or [^{11}C]AFM: it showed fast brain uptake kinetics, but lower uptake levels.

The ^{18}F-labelled diphenylsulphides *N,N*-dimethyl-2-(2-amino-4-[^{18}F]fluorophenylthio)-benzylamine (4-[^{18}F]ADAM, also termed [^{18}F]AFA or [^{18}F]FADAM), [^{18}F]AFM and [^{18}F]AFE were selective and had high SERT affinities. In rat brains *ex vivo*, 4-[^{18}F]ADAM had a target-to-non-target ratio of 12.5 at 2 h *p.i.*, while in PET studies of baboons, the uptake of 4-[^{18}F]ADAM peaked within 1 h with a maximum target-to-non-target ratio of 4.2 at 3 h, which was slightly higher than the ratio of 3.5 for [^{11}C]DASB at 75-95 min *p.i.*. [^{18}F]AFM showed the highest target-to-non-target ratio of ~ 6 at 1 h *p.i.* in baboons, but the slowest kinetics among these ^{18}F-labelled tracers (Shiue et al. 2003). The fluoropropyl analogue ([^{18}F]AFP) showed a slightly reduced SERT affinity and a lower signal-to-noise ratio. Some *in vivo* defluorination of these ^{18}F-labelled tracers was also observed. Moving the fluorine atom from the 4'-position (*para* to the sulphur atom) in 4-F-ADAM to the 5'-position (*meta* to the sulphur atom) in 5-F-ADAM, resulted in reduced affinity, low brain uptake and significant defluorination. A very high SERT affinity (K_i 0.05 nM), selectivity and better resistance against defluorination was exhibited by 2-[(2-amino-4-chloro-5-fluorophenyl)thio]-*N,N*-dimethylbenzenmethanamine (ACF), with both fluorine and chlorine directly attached to the phenyl ring (Table 2.1.). There was a rapid [^{18}F]ACF uptake in rat brains, peaking at 2 min *p.i.*, and the maximum target-to-non-target ratio of 3.6 was reached at 1 h *p.i.*, suggesting potential for [^{18}F]ACF as a PET tracer (Oya et al. 2002).

Replacing one of the *N*-methyl groups of ADAM with a fluoroethyl group resulted in a significant loss of SERT affinity, indicating that functionalizing this position was detrimental to the SERT binding (Emond et al. 2002). However, an evaluation of two *N*-fluorobenzyl derivatives showed that a large *p*-fluorobenzyl group was tolerated (K_i

4 nM), but an additional replacement of the *N*-hydrogen atom with a methyl group completely abolished SERT binding. The addition of the *p*-fluorobenzyl group to the anilino-nitrogen (NH_2-group in Figure 2.6.) resulted in moderate SERT affinity (K_i 10 nM), and its replacement with a *p*-fluorobenzoyl group reduced the affinity (Mavel et al. 2008).

Recently, a novel series of biphenylthiols, fluoroalkyl ether analogues, was developed to achieve easier ^{18}F-radiolabelling and higher radiochemical yields. 2-[2-((dimethylamino)methyl)-4-(3-fluoropropoxy)phenylthio]benzenamine exhibited high SERT affinity (K_i 0.24 nM), but also a moderate affinity for NET (K_i 12.4 nM). This ^{18}F-labelled ligand showed fast clearance and a high target-to-non-target ratio of 9.7 at 3 h *p.i.* in rats. In a rat PET study, favourable *in vivo* kinetics with a target-to-non-target ratio of ~ 4 were seen, suggesting that this tracer has potential for imaging SERT sites (Parhi et al. 2007, Wang et al. 2008).

Among tropanes, *β*-CIT (RTI-55) has a high SERT affinity (K_i 0.50 nM), but a similar affinity for DAT (Farde et al. 1994, Okada et al. 1998, Harada et al. 2004). *N*-desmethylation of the tropane structure increases SERT affinity by ten-fold, but despite this increase, [^{11}C]nor-*β*-CIT still has a considerable affinity for DAT (Bergström et al. 1997). The selectivity for SERT over DAT can be enhanced by incorporating iodine into the 3'-position of the phenyl ring, by introducing an alkyl or alkenyl moiety to the 4'-position of the phenyl ring, or by replacing the *N*-methyl group with hydrogen, as shown by [methyl-^{11}C]-2*β*-carbomethoxy-3*β*-(4-isopropenylphenyl)nortropane ([^{11}C]RTI-357). [^{11}C]RTI-357 accumulated specifically in regions with high densities of SERT sites, with a target-to-non-target ratio of 2.2 and a transient equilibrium at 40 min *p.i.* in monkey PET studies (Helfenbein et al. 1999). Numerous nortropane analogues, such as fluoroethyl ester nortropanes, have been radiolabelled, but their SERT and DAT affinities were in many cases almost equal.

Placing a vinyl halide on the 3*β*-phenyl ring of a nortropane results in vinylhalide fluoroalkyl ester nortropanes, such as the *meta*-isomer 2*β*-carbo-(2-fluoroethoxy)-3*β*-[3-(*Z*-2-iodoethenyl)phenyl]nortropane (FE*m*ZIENT), its bromoethenyl analogue (FE*m*ZBrENT), and their 3-fluoropropoxy analogues, FP*m*ZIENT and FP*m*ZBrENT. All these compounds were SERT selective, with high and nearly equal affinities for SERT ($K_{i's}$ 0.26 – 0.43 nM). As ^{18}F-labelled PET tracers their *in vivo* behaviour was similar, with peak uptakes in SERT-rich regions within 55 min and quasi-equilibrium after ~ 1 h *p.i.* in monkeys (Stehouwer et al. 2008). The *para*-isomer FE*p*ZIENT (Figure 2.6.) had the highest SERT affinity (K_i 0.08 nM), but a lower selectivity. In a monkey PET study, [^{18}F]FE*m*ZIENT provided superior kinetics with a quasi-equilibrium, whereas [^{18}F]FE*p*ZIENT had slower kinetics, but a higher midbrain-to-CE ratio of 4.2 at 225 min, compared to 2.4 for [^{18}F]FE*m*ZIENT. Thus, the position of the vinyl iodine group had a significant effect on the tracer properties. Both isomers, however, are promising candidates for human PET studies; [^{18}F]FE*m*ZIENT being

more suitable for kinetic analyses and [^{18}F]FE*p*ZIENT for SSRI occupancy studies (Plisson et al. 2004).

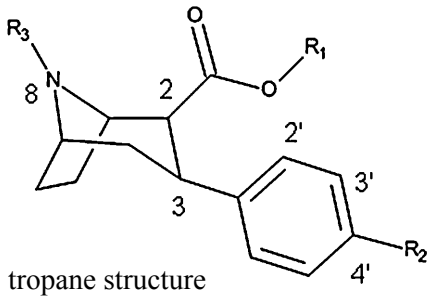

tropane structure

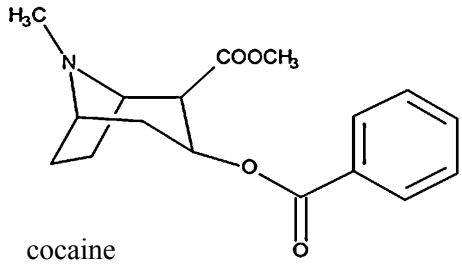

cocaine

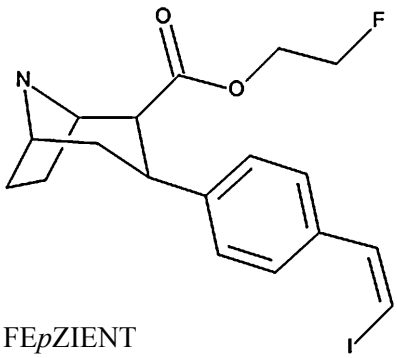

FE*p*ZIENT

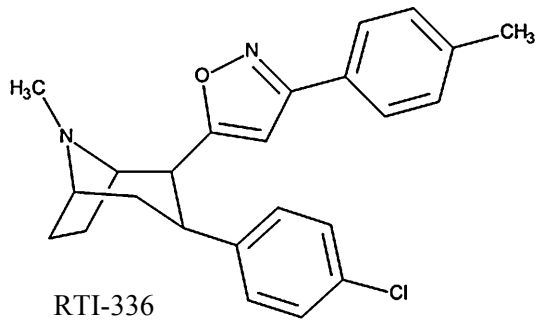

RTI-336

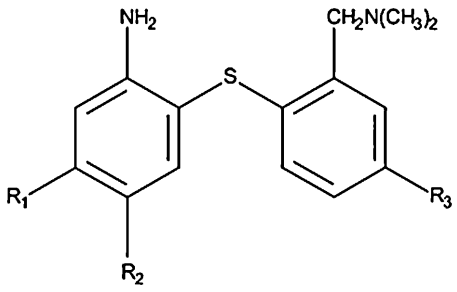

phenylthiobenzylamine structure

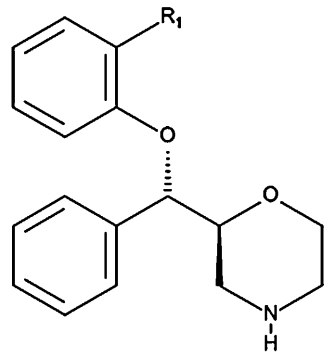

morpholine structure

Figure 2.6. Structures of some DAT, NET and SERT ligands**.**

Table 2.1. Substitutions of some DAT, SERT and NET ligands.

Tropanes	**R1 (*C*2)**	**R2 (*C*4')**	**R3 (*N*)**
β-CFT-FE	CO_2CH_3	H	CH_2CH_2F
β-CIT (RTI-55)	CO_2CH_3	I	CH_3
β-CIT-FP	CO_2CH_3	I	$CH_2CH_2CH_2F$
FIPCT	$CO_2CH(CH_3)CH_2F$	Cl	CH_3
RTI-31	CO_2CH_3	Cl	CH_3
RTI-32	CO_2CH_3	CH_3	CH_3
FETT	$CO_2CH_2CH_2F$	CH_3	CH_3
FECT	$CO_2CH_2CH_2F$	Cl	CH_3
FECNT	CO_2CH_3	Cl	CH_2CH_2F
FPCT	CO_2CH_3	Cl	$CH_2CH_2CH_2F$
MCL-322 (CBT)	$CO_2CH_2CH_2F$	Br	CH_3
MCL-301 (FE@CIT)	$CO_2CH_2CH_2F$	I	CH_3
FTT	$COCH_2CH_3$	CH_3	$CH_2(C_6H_6)F$
(+)FCT	$COCH_2CH_3$	Cl	$CH_2(C_6H_6)F$
FBFNT	CO_2CH_3	F	$CH_2CH{=}CHCH_2F$
LBT-999	CO_2CH_3	CH_3	$CH_2CH{=}CHCH_2F$
Phenylthiobenzylamines	**R1 (C4')**	**R2 (C5')**	**R3 (C5)**
DASB	CN	H	H
DAPP	OCH_3	H	H
DAPA	Br	H	H
ADAM	I	H	H
MADAM	CH_3	H	H
EADAM	CH_2CH_3	H	H
AFM	CH_2F	H	H
4-F-ADAM (AFA)	F	H	H
5-F-ADAM	H	F	H
SMe-ADAM	SCH_3	H	H
HOMADAM	CH_2OH	H	H
ACF	Cl	F	H
F-HOMADAM	CH_2OH	H	F
Morpholines	**R1**		
Reboxetine	OCH_2CH_3		
MeNER	OCH_3		
FMeNER-D_2	OCD_2F		
FRB-D_4	OCD_2CD_2F		
MENET	CH_3		
FENET	CH_2CH_2F		

3. AIMS OF THE STUDY

The purpose of this study was to compare the sensitivity of 2*β*-carbomethoxy-3*β*-(4-[^{18}F]fluorophenyl)tropane ([^{18}F]*β*-CFT) and 6-[^{18}F]fluoro-*L*-DOPA ([^{18}F]FDOPA) for the detection of dopaminergic neuronal hypofunction in an animal model of Parkinson's disease (PD), and to evaluate the properties and suitability of two novel radiotracers, *N*-(3-[^{18}F]fluoropropyl)-2*β*-carbomethoxy-3*β*-(4-fluorophenyl)nortropane ([^{18}F]*β*-CFT-FP) and 1,2,3,5,6,10*β*-hexahydro-6-[4-([^{18}F]fluoromethylthio)phenyl]-pyrrolo[2,1-a]isoquinoline ([^{18}F]FMe-McN), for imaging DAT and SERT sites in rats, respectively.

The specific aims of the experiments were:

1. To evaluate and compare the sensitivity of [^{18}F]*β*-CFT and [^{18}F]FDOPA for the detection of different stages of dopaminergic neuronal lesions in the brain of a rat model of PD.

2. To demonstrate the DAT specificity, biodistribution, kinetics, and metabolism of [^{18}F]*β*-CFT-FP in rats.

3. To compare the properties and suitability of [^{18}F]*β*-CFT-FP and [^{18}F]*β*-CFT as radiotracers for DAT in rats.

4. To demonstrate the SERT specificity, selectivity, biodistribution, kinetics, and metabolism of [^{18}F]FMe-McN in rats.

5. To determine whether there are differences between the genders in the numbers of SERT sites in rat brains that can be assessed *ex vivo* using [^{18}F]FMe-McN.

4. MATERIALS AND METHODS

4.1. General experimental methodology

We performed animal studies *in vivo* to pharmacologically characterize animals of a rat model of PD, and *ex vivo* to compare the sensitivity of two previously developed PET tracers for showing dopaminergic hypofunction in this animal model. In addition, we performed *ex vivo* animal studies and *in vivo* PET imaging to assess the biodistribution and kinetics of two novel PET tracers. The biodistribution of these tracers in rat brains was determined *ex vivo* using PSL autoradiography. The pharmacological properties of the PET tracers were evaluated by pre-treating rats with specific monoamine transporter inhibitors, and determining the changes in the uptake of these tracers by *ex vivo* PSL autoradiography or by *in vitro* binding experiments using rat brain sections. Radiolabelled metabolites in plasma were evaluated by thin layer chromatography (TLC) and PSL autoradiography. The four different radiotracers used in these studies were radiolabelled in house using cyclotron-produced [^{18}F]fluoride.

4.2. Experimental animals

4.2.1. Animals, animal care and ethics

Sprague-Dawley rats (Harlan Sprague-Dawley, Indianapolis, IN, USA) were used in all studies. In study I, the rats (B&K, Sweden) were housed at Orion Pharma (Turku, Finland) and in studies II-V, the rats were bred and housed at the animal facility of the University of Turku (Turku, Finland). The animals were maintained under standard conditions at 22 ± 2 °C, a relative humidity of 50 ± 10% and on a 12 h light/dark cycle with free access to standard food and tap water. Details of the animals and their treatments are shown in Table 4.1. The animal experiments were approved by the Laboratory Animal Care and Use Committee of the University of Turku.

4.2.2. Lesioning of the nigrostriatal dopaminergic pathway (I)

Lesioning the nigrostriatal dopaminergic pathway by injecting 6-hydroxydopamine (6-OHDA) unilaterally into the forebrain of rats is a widely used method to produce an animal model of PD, which reflects the variable hypofunction of dopaminergic neurotransmission known to be characteristic of different stages of PD. In study I, the lesioning of the nigrostriatal dopaminergic pathway and the subsequent pharmacological evaluation of the rats were performed at Orion Pharma (Turku, Finland). In total, 80 male rats were anaesthetised with subcutaneous (*s.c.*) injections of midazolam (Dormicum®, Roche, Palo Alto, CA, USA), fentanyl citrate and fluanisone (Hypnorm®, Janssen, Titusville, NJ, USA), and placed in a stereotaxic frame (Stoelting, USA). 8 µg (2µg/µl) of 6-OHDA (Sigma Chemical Co., St. Louis, MO, USA) were injected unilaterally into the left medial forebrain bundle; sham animals were injected with saline. In order to protect the noradrenergic neurons, rats were

intraperitoneally *(i.p.*) injected with desipramine (10 mg/kg, Sigma Chemical Co. St. Louis, MO, USA) before a 6-OHDA injection.

4.2.3. Pharmacological evaluation for subgroup selection (I)

Lesioned animals were treated with various dopaminergic drugs and their subsequent motor behaviour was recorded to evaluate the stage of their brain lesion. Pharmacological evaluation to select the subgroup started three weeks after surgery. The circling behaviour of the rats was measured using automated rotameters (Ungerstedt and Arbuthnott, 1970) after the administration of apomorphine (APO), a direct DA receptor agonist (50 µg/kg *s.c.,* RBI, Natick, MA, USA), amphetamine (AMPH), an indirect DA receptor agonist (1 mg/kg and 3 mg/kg *s.c.,* Sigma Chemical Co. St. Louis, MO, USA), or *L*-DOPA, a precursor of DA (10 mg/kg *p.o.*). In order to prevent the peripheral metabolism of *L*-DOPA, rats were pre-treated with entacapone (5 mg/kg *p.o.*), a peripheral catechol-*O*-methyl-transferase (COMT) inhibitor, and with carbidopa (10 mg/kg *p.o.*), a peripheral DOPA decarboxylase inhibitor (all from Orion Pharma, Turku, Finland) immediately before *L*-DOPA administration.

Individual responses to the dopaminergic drugs were tested again two months after lesioning. After behavioural tests, the lesioned rats were divided into three groups for each of the two tracers and the group selection was verified for a third time. The selected animals (n = 17) and six sham rats were injected with either saline, APO or AMPH (1 mg/kg) and circling behaviour was monitored for 120 min. The *L*-DOPA response was verified in the animals pre-treated with entacapone and carbidopa, and their circling behaviour was measured for 300 min. The experiment was organised in a crossover manner and the sequence of different treatments was randomised using Latin Square. The washout period between the tests was at least 48 hours.

4.2.4. Estrous cycle phase (V)

Gonadal hormone levels in female rats fluctuate according to the phase of their estrous cycle, and this fluctuation has many effects on the physiology of the animals. Thus, all female rats in study V were studied at the same estrous cycle phase (at the estrous phase). The estrous cycle phase of the female rats was determined at the animal facility of the University of Turku by microscopic examination of vaginal smears, which were obtained daily. The proestrous and estrous receptive phases are characterized by thick vaginal smears, which contain nucleated epithelial cells during the proestrous phase and cornified cells during the estrous phase (Ho et al. 2001).

Table 4.1. Details of the animals and their treatments.

Study	Number of rats		Animal weight (g)	Pre-treatment/ Drugs	Anaesthesia	Radiotracer	Sacrifice time (min *p.i.*)
	Males	Females					
I[#]	1. 80		~250	1. desipramine/6-OHDA	1. midazolam, fentanyl citrate, fluanisone		
	2. 80			2. APO 2. AMPH 2. carbidopa and entacapone/*L*-DOPA			
	3. 11		566 ± 64	3. carbidopa, entacapone	3. diethyl ether	3. [^{18}F]FDOPA	30
	3. 11		580 ± 55	3. -	3. diethyl ether	3. [^{18}F]*β*-CFT	120
II	19		329 ± 19	no treatment or GBR 12909	CO_2/O_2	[^{18}F]*β*-CFT-FP	5, 15, 30, 60, 120
III	20		329 ± 19	no treatment or GBR 12909	CO_2/O_2, urethane for a PET study	[^{18}F]*β*-CFT-FP	5, 15, 30, 60, 120
		16	237 ± 32	no treatment, GBR 12909, fluoxetine or nisoxetine	CO_2/O_2, urethane for a PET study	[^{18}F]*β*-CFT	10, 20, 40, 120
IV	32	8	345 ± 56	no treatment, fluoxetine, GBR 12909 or nisoxetine	diethyl ether	[^{18}F]FMe-McN	30, 60, 120, 240
V	8		430 ± 17		CO_2/O_2	[^{18}F]FMe-McN	120
		12	261 ± 18		CO_2/O_2	[^{18}F]FMe-McN	120

Study I: 1. Lesioning of the rats, 2. Behavioural tests, 3. Radiotracer studies

4.3. Radiotracers

4.3.1. Production of [^{18}F]fluoride

The radiotracers were labelled with fluorine-18, a β^+-emitting radionuclide (^{18}F; $t_{½}$ = 109.8 min). [^{18}F]Fluoride was produced by the nuclear reaction: ^{18}O (p, n) ^{18}F at the Accelerator Laboratory of the Åbo Akademi University (Turku PET Centre, Turku, Finland) (studies I, III – V). ^{18}O-enriched (>94%) water was bombarded with a high-energy proton beam generated by a 20 MeV MGC-20 cyclotron (D.V. Efremov Research Institute, St. Petersburg, Russia). In study II, [^{18}F]fluoride was produced at the Laboratory of Radiochemistry, University of Helsinki (Helsinki, Finland) with a 10 MeV IBA Cyclone 10/5 cyclotron.

4.3.2. Syntheses of [^{18}F]FDOPA, [^{18}F]β-CFT, [^{18}F]β-CFT-FP and [^{18}F]FMe-McN

Four different molecules were radiolabelled and used in studies I-V. The chemical structures of [^{18}F]FDOPA, [^{18}F]β-CFT, [^{18}F]β-CFT-FP and [^{18}F]FMe-McN are shown in Figure 4.1. A summary of the syntheses and injected doses can be found in Table 4.2. [^{18}F]FDOPA, [^{18}F]β-CFT, and [^{18}F]FMe-McN were prepared at the Radiopharmaceutical Chemistry Laboratory of the University of Turku (Turku PET Centre, Turku, Finland), and [^{18}F]β-CFT-FP at the Laboratory of Radiochemistry of the University of Helsinki (Helsinki, Finland).

[^{18}F]FDOPA was synthesized by the electrophilic fluorination of the stannylated precursor, *N*-formyl-3,4-di-*t*-butoxycarbonyloxy-6-(trimethylstannyl)-*L*-phenylalanine ethyl ester (Bergman et al. 1994, Namavari et al. 1992).

[^{18}F]β-CFT ([^{18}F]WIN 35,428) was synthesised by the electrophilic fluorination of 2β-carbomethoxy-3β-(4-trimethylstannylphenyl)tropane (Bergman et al. 1997, Bergman and Solin 1997, Haaparanta et al. 1996).

No-carrier-added [^{18}F]β-CFT-FP was synthesized by the nucleophilic fluorination of 2β-carbomethoxy-3β-(4-fluorophenyl)nortropane (nor-β-CFT) using [^{18}F]fluoropropyl tosylate as a fluoroalkylation reagent (Koivula et al. 2005).

Normethyl-(+)-McN5652 was prepared from the enantiomerically pure thioester analogue of (+)-McN5652 (Zessin et al. 1999). [^{18}F]FMe-McN was synthesized by reacting normethyl-(+)-McN5652 with the fluoromethylation reagent, [^{18}F]bromofluoromethane (Bergman et al. 2001, Eskola et al. 1999, Zessin et al. 2001).

Table 4.2. Characteristics of the radiotracers, values are the mean ± SD.

Radiotracer	SA [GBq/µmol] (EOS)	Radio-chemical purity [%]	Injected radioactivity [MBq]	Injected mass [nmol/kg]
[^{18}F]FDOPA	> 3.7 (I)	> 98 (I)	126 ± 19 (I)	118 ± 36 (I)
[^{18}F]β-CFT	> 9.3 (I) 13 ± 3 (III)	> 98 (I) > 98 (III)	25.6 ± 8.3 (I) 52 ± 20 (III)	3.09 ± 0.80 (I) 23 ± 11 (III)
[^{18}F]β-CFT-FP	36 ± 22 (II, III)	97 ± 3 (II, III)	26.9 ± 8.1 (II, III)	8.0 ± 4.0 (II, III)
[^{18}F]FMe-McN	1107 ± 1017 (IV) 227 ± 158 (V)	> 95 (IV) > 95 (V)	93 ± 36 (IV) 80 ± 11 (V)	1.1 ± 2.3 (IV) 2.1 ± 0.9 (V)

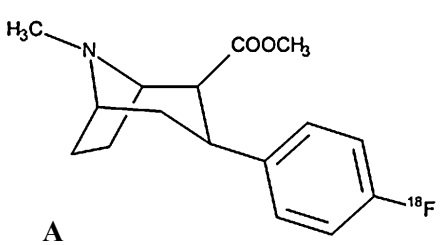

A

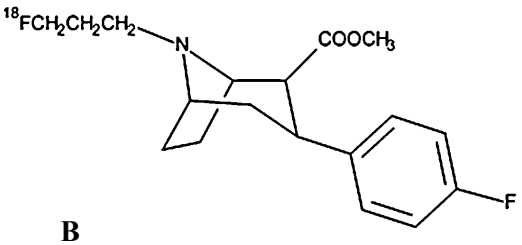

B

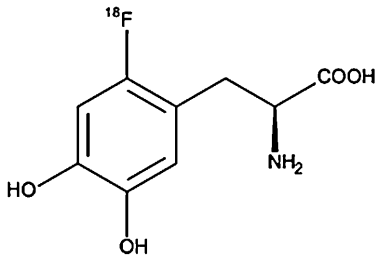

C

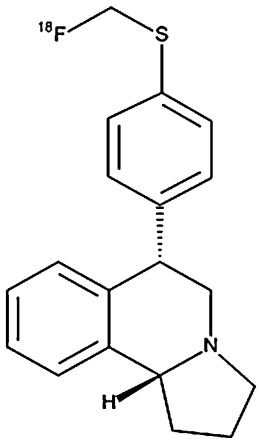

D

Figure 4.1. Structures of [^{18}F]β-CFT (A), [^{18}F]β-CFT-FP (B), [^{18}F]FDOPA (C) and [^{18}F]FMe-McN (D).

4.4. Biodistribution studies

Radiotracers were intravenously (*i.v.*) injected into a tail vein of rats under momentary anaesthesia and allowed to distribute for a specified time (5 - 240 min) before the rats were sacrificed in a carbon dioxide (CO_2) chamber. Arterial blood was collected by cardiac puncture and pieces from tissues and organs were immediately dissected, weighed, and measured for ^{18}F-radioactivity in a well counter (3 × 3 inch, NaI (Tl) crystals, Bicron 3MW3/3P, Bicron Inc., Newbury, OH, USA). All measured data were corrected for background radioactivity and the injected doses and radioactivity of the tissue samples were decay-corrected to the time of the injection. In studies II–IV, the amount of radioactivity accumulated in the tissue samples was expressed as a percentage of the injected dose per gram of tissue (% ID/g). Because the rats in study V were matched according to their age, the body masses of the female rats were significantly lower than the body masses of the male rats. Therefore the ^{18}F-radioactivity uptakes in peripheral organs were normalized to blood radioactivity and expressed as ratios of %ID/g $_{tissue}$ to %ID/g $_{blood}$. The mean values in all studies were calculated from the individual measurements, and expressed to a precision of one standard deviation (mean ± SD).

4.5. Brain autoradiography and image analysis

The regional distribution of the ^{18}F-radioactivity in the rat brain was determined using PSL autoradiography. In study I, the animals were pre-treated with a dose (10 mg/kg, *i.p.*) of entacapone and carbidopa 30 min before being injected with [^{18}F]FDOPA, to prevent the peripheral metabolism of the tracer. The brains were rapidly removed and frozen in isopentane chilled with dry ice. Pieces from the cerebellar cortex of each brain were dissected, weighed and measured for ^{18}F-radioactivity in a well counter. In studies I – IV, the percentages of injected doses per gram of tissue (% ID/g) were used to calibrate the absolute uptake of ^{18}F-radioactivity in autoradiographic images.

Coronal rat brain sections (20 μm) were obtained using a cryomicrotome at -15 °C. The brain sections were thaw-mounted onto microscope slides, air dried and apposed to a phosphoimaging plate (Fuji Imaging Plate BAS-TR2025, Fuji Photo Film Co., Ltd., Japan) for an exposure of 4.0 ± 0.5 h. The imaging plates were scanned with a BAS-5000 Fuji Analyzer (Fuji Photo Film Co., Ltd., Japan). The dynamic linear range of the phosphoimaging method was four decades and the scanning resolution (pixel size) of the imaging plate was 25 μm x 25 μm. The PSL-autoradiographic images were analyzed for count densities (photo-stimulated luminescence per unit area, PSL/mm^2) using an image analysis program (Tina 2.1, Raytest Isotopenmessgeräte, GmbH, Straubenhardt, Germany). Regions of interest were drawn over the brain regions known to contain high densities of DAT, SERT or NET binding sites, such as the STR, DR, SN, VTA, LC, HY, THA, AMY and CX, as well as over the CE, which was used as a reference region for the non-specific uptake of the radiotracers, since it contains

negligible densities of DAT and SERT sites and a low level of NET sites. Brain regions were anatomically identified using a rat brain atlas (Paxinos and Watson 1986). Background count densities were subtracted from the image data, the PSL/mm^2-values were converted into %ID/g-values and expressed as the mean ± SD for each brain region. In study I, the radiotracer uptake in the STR and SN was also expressed as the lesioned side-to-the intact side ratio. In studies II-IV, brain region-to-CE (target-to-non-target) uptake ratios were also calculated and expressed as the mean ± SD. In study V, the results were expressed only as the brain region-to-CE ratios.

4.6. Pharmacological studies

4.6.1. Ex vivo studies (II - IV)

The pharmacological properties of the PET tracers were evaluated by pre-treating rats with specific monoamine transporter inhibitors, and determining the changes in the uptake of these tracers by *ex vivo* PSL autoradiography. In studies II and III, the DAT specificities of the [^{18}F]*β*-CFT-FP and [^{18}F]*β*-CFT bindings were determined in rats from the decreased ^{18}F-radioactivity in brain regions with high densities of DAT sites, after pre-treatment with a selective DAT inhibitor, GBR 12909 (5 mg/kg, Sigma-RBI, St. Louis, MO, USA) (Heikkila and Manzino 1984, Andersen 1989). In study IV, the SERT specificity of the [^{18}F]FMe-McN binding was determined in rats from the decreased [^{18}F]FMe-McN uptake in brain regions with high densities of SERT sites, and in peripheral organs, after pre-treatment with a selective SERT inhibitor, fluoxetine (5 mg/kg, Sigma-RBI, St. Louis, MO, USA) (Wong et al. 1995). The selectivity of [^{18}F]*β*-CFT and [^{18}F]FMe-McN was assessed by pre-treating the rats with a dose (5 mg/kg) of GBR12909, fluoxetine or nisoxetine (RBI, Natick, MA, USA), a selective NET inhibitor (Tejani-Butt et al. 1990, Tejani-Butt 1992) before injections of the tracers.

GBR 12909, fluoxetine and nisoxetine were injected *i.v.* into rats 60 min prior to the injection of the tracer. The animals in the pharmacological studies were sacrificed by CO_2 inhalation 15 min (II), 40 min (III) or 120 min (IV) *p.i.* of the radiotracer. The regional distribution of ^{18}F-radioactivity in the brains of the non-treated and pre-treated rats was determined using PSL-autoradiography, as described in section 4.5. Brain autoradiography and image analysis. Peripheral tissues were handled as described in section 4.4. Biodistribution studies.

4.6.2. In vitro studies (IV)

In study IV, the SERT specificity and selectivity of the [^{18}F]FMe-McN binding was also determined using *in vitro* binding experiments. Coronal rat brain sections (20 μm) were cut at –15°C, thaw-mounted onto microscope slides and stored at –20°C. Before use, the brain sections were warmed to room temperature (RT) and preincubated for 15 min in a 50 mM Tris-HCl (pH 7.4 at 25°C) buffer containing 120 mM NaCl, 5 mM

KCl, 2 mM $CaCl_2$ and 1 mM $MgCl_2$. The brain sections were then incubated for 60 min at RT with 370 kBq (~ 40 pM) of [^{18}F]FMe-McN, along with various concentrations (1 nM - 10 μM) of the displacing drugs fluoxetine, GBR 12909 or nisoxetine. Some sections were incubated without drugs to assess the total binding of [^{18}F]FMe-McN. After incubation the slides were washed in the buffer (3 times for 5 min at 0°C) and dried. Autoradiographic images were generated as described in section 4.5. Brain autoradiography and image analysis. The specific binding of [^{18}F]FMe-McN to SERT sites in a brain region *in vitro* was defined as the difference between the total binding and binding in the presence of 10 μM of drug. The relative displacing potencies of fluoxetine, GBR12909 and nisoxetine were specified and the concentrations of displacing drugs that inhibit 50% of the specifically bound radiotracer (IC_{50}) were graphically approximated.

4.7. Immunohistochemistry (I)

The degree of unilateral lesions in the SN of each animal was confirmed by counting the tyrosine hydroxylase (TH) positive dopaminergic neurons, which were detected by the immunohistochemical ABC-technique (Hsu and Raine, 1981; Hsu et al., 1981).

After fixing the brain sections with ice-cold acetone, endogenous peroxidase activity was blocked using 0.3% hydrogen peroxide (H_2O_2) and non-specific background staining was reduced with normal horse serum (Vectastain ABC Kit, mouse IgG, PK-4002, Vector Laboratories, Inc., Burlingame, CO, USA). Subsequently, the brain sections were incubated overnight at +4°C with the primary antibody, the mouse monoclonal antibody directed against TH (Boehringer Ingelheim Bioproducts Partnership, Heidelberg, Germany) at a dilution of 1:800, and then for 30 min with the biotinylated secondary antibody (Vectastain ABC Kit). The Vectastain A reagent (avidin) and B reagent (biotinylated horseradish peroxidase) were mixed and left to stand to allow the complex to form before incubation with brain sections. Primary antibodies were visualised using diaminobenzidine (DAB) in conjunction with imidazole and H_2O_2 to enhance staining intensity. Upon oxidation, DAB forms a brown end product at the site of the target antigen. Nuclear counterstaining was carried out with haematoxylin. The TH-immunopositive neurons in the SN, from at least four sections from each animal, were counted using a light microscope. The results were calculated for each animal as a ratio of the lesioned to the intact SN for the number of TH-immunopositive neurons. The ratios are expressed as the mean ± SD for each rat group.

4.8. PET Imaging (III)

In study III, dynamic PET scans of two rats were performed for 120 min using a high-resolution PET scanner (ECAT HRRT, Siemens Medical Solutions, Knoxville, TN,

USA). One rat was injected with [^{18}F]β-CFT (53 MBq) and the other with [^{18}F]β-CFT-FP (40 MBq). Results are shown as PET images without quantitation of the data.

4.9. Radiometabolite analyses (III, V)

In studies III and V, the ^{18}F-radioactive metabolites were analysed using planar chromatography (TLC) and PSL autoradiography. Plasma samples were deproteinized by precipitating proteins with acetonitrile (CH_3CN) or methanol (CH_3OH). [^{18}F]β-CFT and its radioactive metabolites were previously analysed from dialysate fractions collected during microdialysis (MD), as reported by Haaparanta et al. (2004). Dialysate fractions were collected at intervals of 15 minutes for 120 minutes. Aliquots from each fraction, deproteinized plasma and parent [^{18}F]β-CFT in deproteinized rat plasma as a standard were applied on a HPTLC RP18-plate (Merck 1.05914, Merck, Darmstadt, Germany) which was developed in a chamber with CH_3CN:0.01 M phosphoric acid (60:40, v/v) as a mobile phase. After migration, the TLC plate was dried, apposed to an imaging plate (Fuji Imaging Plate BAS-TR2025, Fuji Photo Film Co., Ltd., Japan), exposed for 4 h, and scanned with the BAS-1800 Fuji Analyzer (Fuji Photo Film Co., Ltd., Japan) at resolution of 200 μm x 200 μm (pixel size). The autoradiographic images were analyzed for PSL using a Tina 2.1 image analysis program (Raytest Isotopenmessgeräte, GmbH, Straubenhardt, Germany). The proportions of the unmetabolized radioligand and its metabolites were calculated as percentages (%) from the total ^{18}F-radioactivity present in the sample, and expressed as the mean ± SD.

[^{18}F]β-CFT-FP and its radioactive metabolites were analysed from rat plasma at various time points (5 - 120 min). Deproteinized rat plasma samples and standard samples were applied band-wise on HPTLC-RP-18 plates (Merck 1.05914, Darmstadt, Germany) with an automatic TLC sampler (Camag Automatic TLC Sampler III, Camag, Muttenz, Switzerland) and TLC plates were developed with CH_3CN:H_2O (60:40, v/v). After migration the plates were handled as per the analyses of [^{18}F]β-CFT metabolites.

In study V, the unmetabolized [^{18}F]FMe-McN and its radioactive metabolites were analyzed from plasma samples of female and male rats at 120 min *p.i.*. Deproteinized plasma and standard samples were applied on TLC Silica gel 60 RP-18 F_{254} S plates (Merck 1.05559, Darmstadt, Germany) with a Camag TLC sampler and TLC plates were developed with CH_3OH:H_2O:acetic acid (9:1:0.1, v/v/v). After migration the plates were handled as per the analyses of [^{18}F]β-CFT metabolites.

4.10. Statistical analyses (I, III, IV, V)

In study I, behavioural data was analysed using the Kruskal-Wallis analysis of variance, followed by a Mann-Whitney U-test comparison of the groups. The uptakes of ^{18}F-radioactivity in the STR and SN were analysed with repeated measurement

analyses of variance (RM ANOVA) for the design of four parallel groups, with replicated measurements from each side. The statistical model consisted of the fixed effects for each treatment group, side, replicate, and all their interactions. In case of a significant treatment group, treatment-by-side or treatment-by-replicate interaction effect, the analysis was continued with pairwise comparisons using linear contrasts within the same model. The normality of the distributions was tested using the Shapiro-Wilk test for normality. The ratios of the number of TH positive cells in the lesioned side to the intact side were analysed by one way ANOVA, followed by Scheffe F-test as a posthoc analysis. Statistical analyses were conducted using the SAS System for Windows (version 8.01, SAS Institute Inc., Cary, NC, USA). A two-sided *p*-value of less than 0.05 was considered statistically significant. *P*-values reported from multiple comparisons are Tukey-Kramer adjusted.

In studies III and V, statistical analyses were performed using Graph Pad Prism, version 5.01 (Graph Pad Software, San Diego, CA, USA). The effects of the pre-treatment and differences between females and males were tested using unpaired two-tailed Student's t-tests. Mean values were considered statistically different at $p < 0.05$.

In study IV, statistical analyses were performed using the SAS System for Windows (version 8.0). A one-way analysis of variance (ANOVA) was used as a parametric method, and a Kruskal-Wallis test as a nonparametric method for the analyses of effects for pre-treatment. A *p*-value less than 0.05 was considered statistically significant. In all studies, the results were expressed as the mean ± SD.

5. RESULTS

5.1. [^{18}F]FDOPA and [^{18}F]β-CFT as tracers in a rat model of PD (I)

5.1.1. Behavioural tests for subgroup selection

The circling behaviour of the rats as a response to dopaminergic drugs (AMPH, APO, and *L*-DOPA) was measured, and the lesioned rats were divided into three subgroups according to their drug responses. The results of the behavioural tests are presented in Figure 5.1. and show the circling behaviour of each group during a 120 min test period for saline, AMPH and APO treatments, and a 300 min period for a *L*-DOPA treatment. A positive rotation value indicates predominantly contralateral circling to the right, and a negative value denotes predominantly ipsilateral circling to the left. The sham animals (n = 6) did not show a preferred circling behaviour for any of the drugs. Group 1 (n = 5) showed a clear AMPH response, but no other responses. Group 2 (n = 6) showed AMPH and APO responses, but no significant *L*-DOPA response. Group 3 (n = 6) showed responses for all drugs.

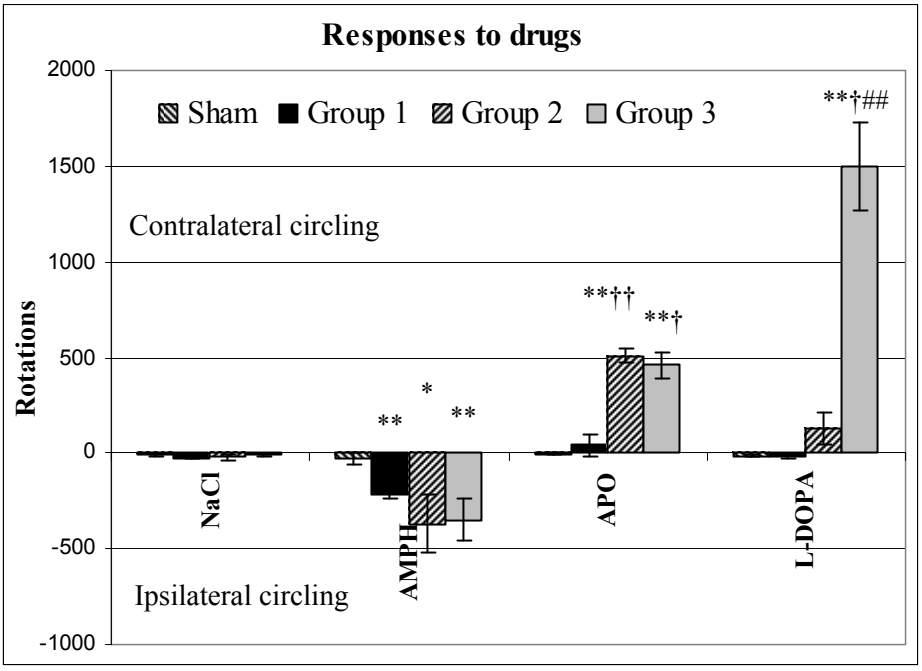

* denotes significant (* $p < 0.05$, ** $p < 0.01$) difference from the sham group
† denotes significant († $p < 0.05$, †† $p < 0.01$) difference as compared with group 1
# denotes significant (## $p < 0.01$) differences between groups 2 and 3

Figure 5.1. The circling behaviour of the sham-operated rat group and lesioned rat groups 1 - 3 (n = 5 - 6 rats/group) as a response to saline (NaCl), AMPH, APO and *L*-DOPA treatments.

5.1.2. Uptake of [^{18}F]FDOPA and [^{18}F]β-CFT in the STR and SN ex vivo

The *ex vivo* uptake of [^{18}F]FDOPA and [^{18}F]*β*-CFT of the left (lesioned) STR and SN was compared with the uptake of the right (intact) STR and SN of the same animal and also with the sham group, and the change in the uptake of the left side was expressed as a % from the uptake of the intact side. The results were also calculated as uptake ratios of the left side to the right side of the STR and SN for both the sham and lesioned rats.

In the group 1 (n = 2) with a mild nigral lesion (only a AMPH response), the striatal uptake of [^{18}F]FDOPA in the lesioned side was reduced by 14.1 ± 2.2%, whereas the group 3 (n = 3) with the most severe nigral lesion (responses for all drugs) showed a 26.3 ± 0.8% decline in the striatal [^{18}F]FDOPA uptake as compared to the intact side of the same animal. The [^{18}F]FDOPA uptakes in the lesioned side decreased slightly more when compared to the sham group (n = 3). The [^{18}F]FDOPA uptake in the SN of the lesioned side decreased in a similar way to that in the STR.

In [^{18}F]FDOPA studies, the lesioned side-to-intact side ratios (Figure 5.2.) were significantly lower in the STR and SN in group 2 animals (0.75 ± 0.07 and 0.86 ± 0.03, respectively, n = 3) and in group 3 (0.74 ± 0.02 and 0.80 ± 0.03, respectively, n = 3) and also in the SN of rat group 1 (0.87 ± 0.01, n = 2), when compared to the sham-operated rats (1.10 ± 0.16 and 1.04 ± 0.03, respectively, n = 3). In the rat group 1, this ratio in the STR (0.86 ± 0.11, n = 2) was slightly, but not significantly, lower than in the sham rats. The differences in [^{18}F]FDOPA uptakes between the lesioned and intact sides were relatively small with ratios ranging from 0.74 to 0.87.

In [^{18}F]*β*-CFT studies, the striatal uptake in the lesioned side was reduced by 56.3 ± 8.1% in group 1 (n = 2) with mild nigral lesion and by 87.2 ± 1.6% in group 3 (n = 3) with the most severe nigral lesion, compared to the intact side of the same animal. The striatal [^{18}F]*β*-CFT uptake in the lesioned side decreased less when it was compared to the sham group (n = 3). The decline in the [^{18}F]*β*-CFT uptake in the lesioned SN in all rat groups was ~ 50% compared to the uptake in the intact side.

With [^{18}F]*β*-CFT, the lesioned side-to-intact side ratio (Figure 5.2.) was significantly decreased in the STR and SN in all lesioned animal groups, 1 (0.38 ± 0.30 and 0.62 ± 0.09, respectively, n = 2), 2 (0.13 ± 0.04 and 0.46 ± 0.06, respectively, n = 3) and 3 (0.13 ± 0.03 and 0.48 ± 0.02, respectively, n = 3), when compared to the sham-operated rats (0.81 ± 0.13 and 0.92 ± 0.06, respectively, n = 3). However, in group 1, the lesioned side-to-intact side ratios decreased less (*i.e.* smaller differences between sides), when compared to groups 2 and 3, which both showed greater differences between sides, with ratios ranging from 0.13 to 0.48.

The sham-operated rats did not show any significant differences in the [^{18}F]FDOPA or [^{18}F]*β*-CFT uptake between the left and right sides. Neither radioligand showed any

significant differences between groups 2 and 3, *i.e*. between animals with or without *L*-DOPA response in addition to AMPH and APO responses (Figure 5.2.).

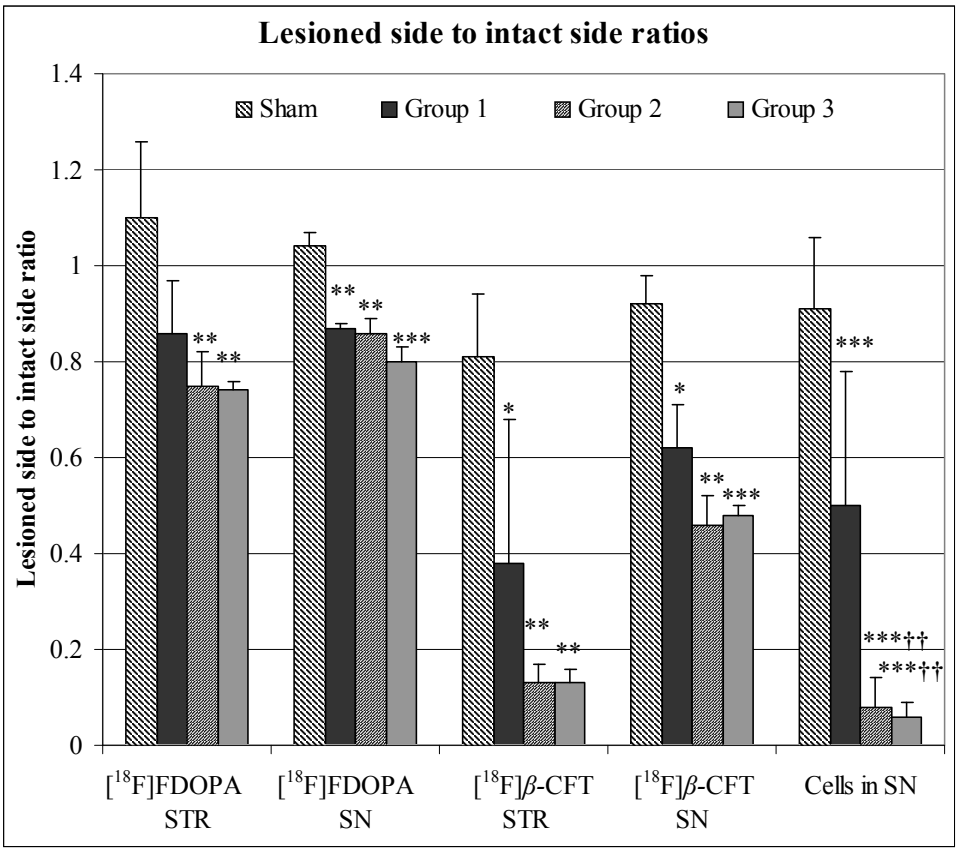

* denotes significant (*$p < 0.05$, **$p < 0.01$, ***$p < 0.001$) difference as compared to the sham group

† denotes significant (††$p < 0.01$) difference as compared with the group 1

Figure 5.2. Lesioned side-to-intact side ratios of [^{18}F]FDOPA and [^{18}F]β-CFT uptakes in the STR (striatum) and SN (substantia nigra) of the sham-operated rats and lesioned rat groups 1 - 3 (n = 2 - 3 rats/group) from *ex vivo* PSL autoradiography. The columns on the far right show the lesioned side-to-intact side ratio for the number of TH-immunopositive cells in the SN (*in vitro* PSL autoradiography, n = 4 - 6 rats/group).

5.1.3. Number of dopaminergic cells in the SN

The degree of unilateral lesion in the SN for each animal was confirmed by counting the number of TH-immunopositive dopaminergic neurons present in the SN from the immunohistochemically-stained brain sections using a microscope. The lesioned side-to-intact side ratio was calculated for each animal, and then the mean ± SD ratio for each animal group was calculated. The ratio of about 1 for the sham-operated rats (n =

6) indicates that there was no significant difference between the left and right sides of the SN. In group 1 (n = 4), there was a decrease of ~ 50% in the number of TH-immunopositive cells in the lesioned side of the SN compared to the intact side, and in the rat groups 2 (n = 6) and 3 (n = 6), the decrease was over 90%. In Figure 5.2., the columns on the far right show the left side-to-right side ratios of the number of the nigral TH-immunopositive cells for the sham-operated and lesioned rat groups.

5.2. Biodistribution studies *ex vivo* (II - V) and PET studies *in vivo* (III)

5.2.1. Biodistribution of [^{18}F]β-CFT-FP ex vivo and in vivo (II, III)

The accumulation of [^{18}F]*β*-CFT-FP in the rat brain CX, STR and CE *ex vivo* was determined by measuring the ^{18}F-radioactivity content of the dissected brain samples in a well counter, and the amount of radioactivity was expressed as %ID/g. [^{18}F]*β*-CFT-FP accumulated rapidly in the brain. The highest uptake value of 2.49 ± 0.72 %ID/g was seen in the STR at 5 min *p.i.* (n = 4), and the cerebellar uptake at 5 min was 0.81 ± 0.27 %ID/g. After that, the radioactivity cleared quickly; after 15 min, ~ 31% (n = 5), and, after 120 min, ~ 4% (n = 3) of the radioactivity was left in the STR. The uptake of [^{18}F]*β*-CFT-FP in the STR and CE as a function of time (time-activity curves, TACs) is shown in Figure 5.3.A. The highest STR-to-CE uptake ratio of 3.13 ± 0.59 was reached at 5 min *p.i.* The time course of the STR-to-CE uptake ratio is shown in Figure 5.3.B.

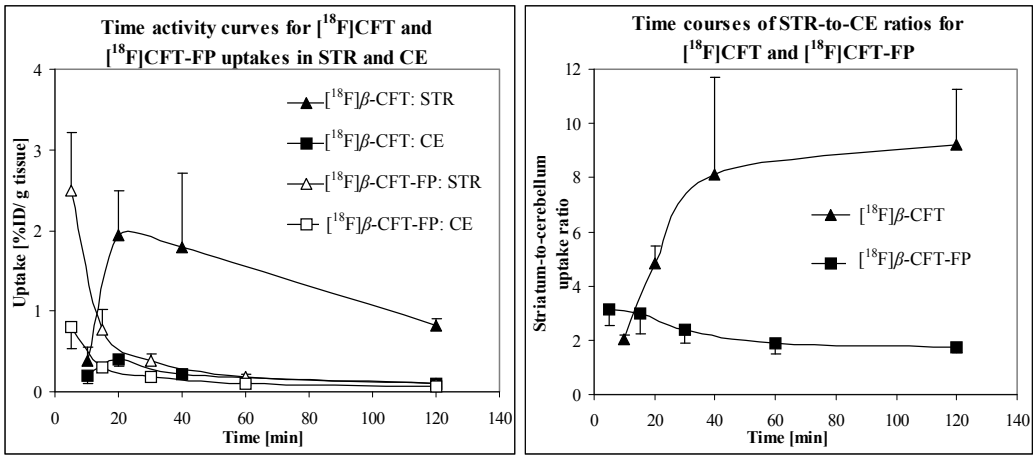

A **B**

Figure 5.3. Time-activity curves in the striatum (STR) and cerebellum (CE) for [^{18}F]*β*-CFT-FP and [^{18}F]*β*-CFT (*ex vivo*) (A). The time courses of the STR-to-CE ratios *ex vivo* for [^{18}F]*β*-CFT-FP and [^{18}F]*β*-CFT (B). In the [^{18}F]*β*-CFT-FP studies, the time points were: 5 min (n = 4), 15 min (n = 5), 30 min (n = 3), 60 min (n = 3), and 120 min (n = 3), and in the [^{18}F]*β*-CFT studies: 10 min (n = 3), 20 min (n = 3), 40 min (n = 5), and 120 min (n = 3).

Contents of [^{18}F]β-CFT-FP-derived radioactivity in peripheral tissues and organs *ex vivo* were measured in a well counter and the amounts of radioactivity were expressed as %ID/g. In peripheral tissues, the highest levels of [^{18}F]β-CFT-FP were measured at 5 min *p.i.* (n = 4) in the intestine, kidneys, liver and pancreas (Figure 5.4.). At later time points, ^{18}F-radioactivity accumulated in bone and subcutaneous fat. *In vivo* biodistribution of the [^{18}F]β-CFT-FP-radioactivity in a whole body PET image (frame 105-120 min) in Figure 5.6.A also shows a high accumulation of ^{18}F-radioactivity in the bone due to defluorination of the tracer.

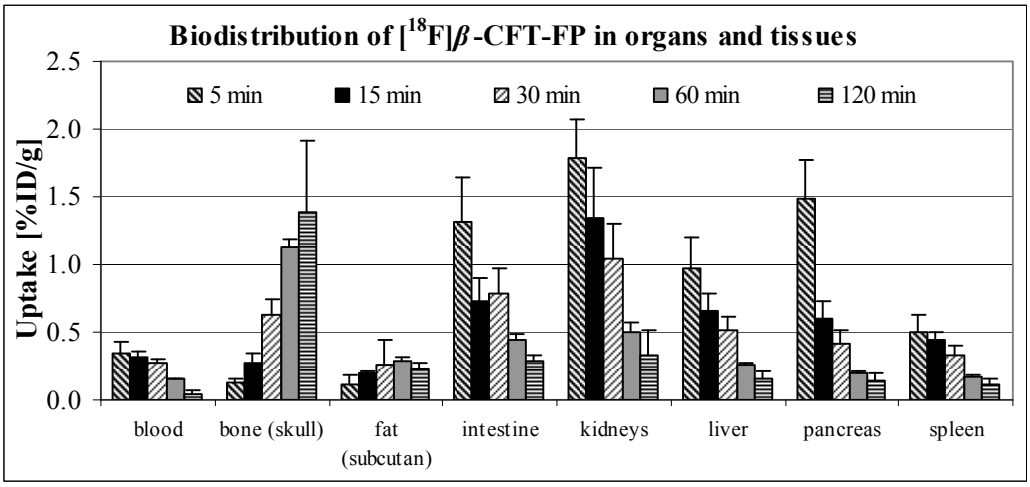

Figure 5.4. Biodistribution of [^{18}F]β-CFT-FP *ex vivo* in rat organs and tissues at 5 min (n = 4), 15 min (n = 5), 30 min (n = 3), 60 min (n = 3), and 120 min *p.i.* (n = 3).

5.2.2. Biodistribution of [^{18}F]β-CFT ex vivo and in vivo (III)

The regional biodistribution of [^{18}F]β-CFT in the rat brain *ex vivo* was determined using PSL autoradiography. Pieces from the CE of each brain were measured for ^{18}F-radioactivity in a well counter, and using these data PSL/mm^2 values were converted to %ID/g values. The [^{18}F]β-CFT uptake peaked at 20 min *p.i.* (n = 3) in all brain regions. The highest uptake of 1.94 ± 0.56 %ID/g was measured in the STR, followed by the VTA, LC and SN with uptake values from 0.99 %ID/g to 0.86 %ID/g. The lowest ^{18}F-radioactivity uptake was seen in the CE (0.40 ± 0.09 %ID/g). The uptake of [^{18}F]β-CFT in the STR and CE *ex vivo* as a function of time is shown in Figure 5.3.A. The maximum STR-to-CE ratio of 9.2 ± 2.0 was reached at 120 min *p.i.* (n = 3). The time course of the STR-to-CE ratio is shown in Figure 5.3.B.

Contents of [^{18}F]β-CFT-derived radioactivity in peripheral tissues and organs *ex vivo* were measured in a well counter and the amount of radioactivity was expressed as %ID/g. In peripheral tissues, the accumulation of [^{18}F]β-CFT peaked at 10 min *p.i.* (n = 3) in most organs. High levels of radioactivity were recorded in the liver, kidneys,

spleen and pancreas (Figure 5.5.). ^{18}F-radioactivity accumulation in the bone increased over time, but was still low at 120 min *p.i.* (n = 3). *In vivo* biodistribution of [^{18}F]β-CFT-radioactivity in a whole body PET image (frame 105-120 min) shows a high accumulation of ^{18}F-radioactivity in the STR and liver (Figure 5.6.B), but not in the bone.

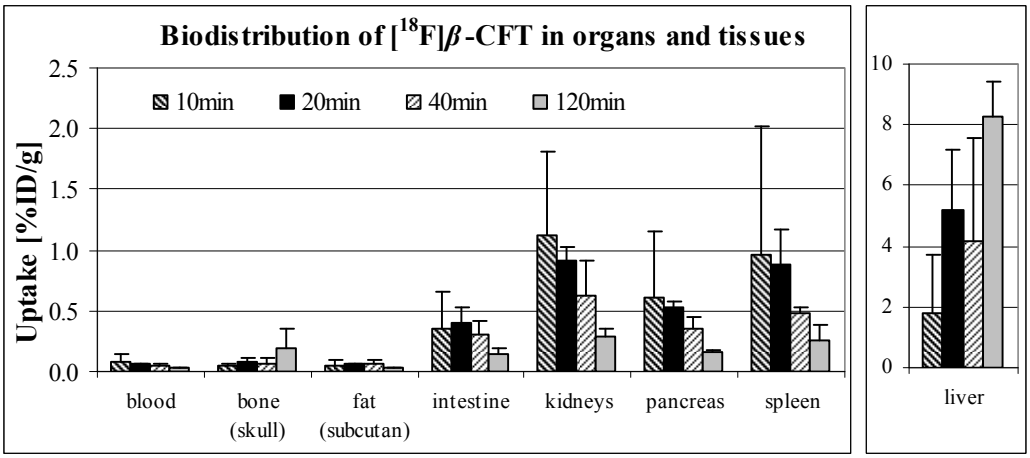

Figure 5.5. Biodistribution of [^{18}F]β-CFT *ex vivo* in rat organs and tissues at 10 min (n = 3), 20 min (n = 3), 40 min (n = 5), and 120 min *p.i.* (n = 3).

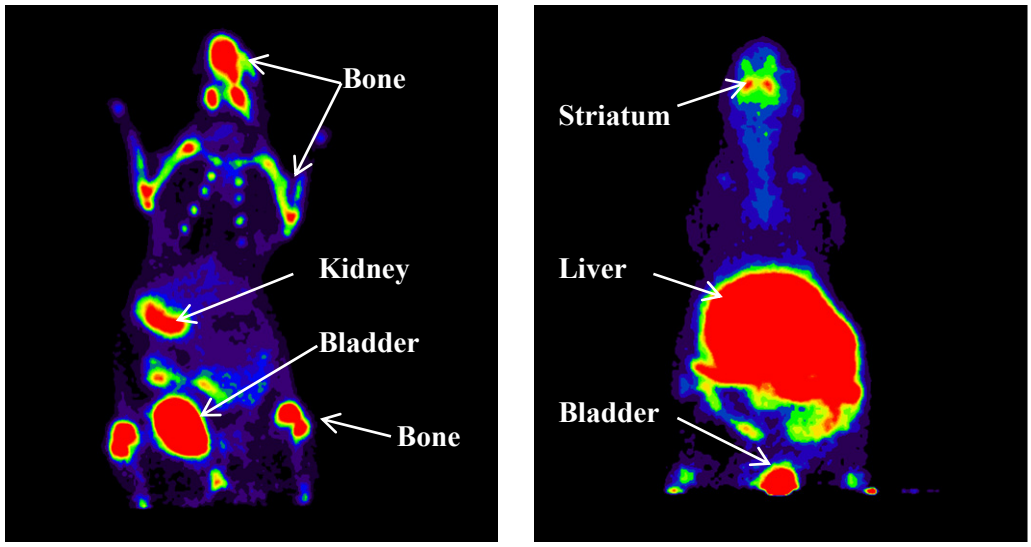

A **B**

Figure 5.6. The *in vivo* biodistribution of [^{18}F]β-CFT-FP (A) and [^{18}F]β-CFT (B) in the whole body PET images of rats (frame 105-120 min).

5.2.3. Biodistribution of [^{18}F]FMe-McN ex vivo (IV,V)

The regional biodistribution of [^{18}F]FMe-McN in the rat brain *ex vivo* was determined using PSL autoradiography. Pieces from the CE of each brain were measured for ^{18}F-radioactivity, and, using these data, PSL/mm^2 values were converted to %ID/g values. In study IV, the [^{18}F]FMe-McN uptake peaked at 30 min *p.i.* in the brain regions with high densities of SERT sites (DR, AMY, HY, LC and THA), with uptake values from 0.73 %ID/g to 0.92 %ID/g (n = 6), and decreased thereafter (Figure 5.7.). The cerebellar uptake at 30 min *p.i.* was significantly lower (0.24 ± 0.07 %ID/g).

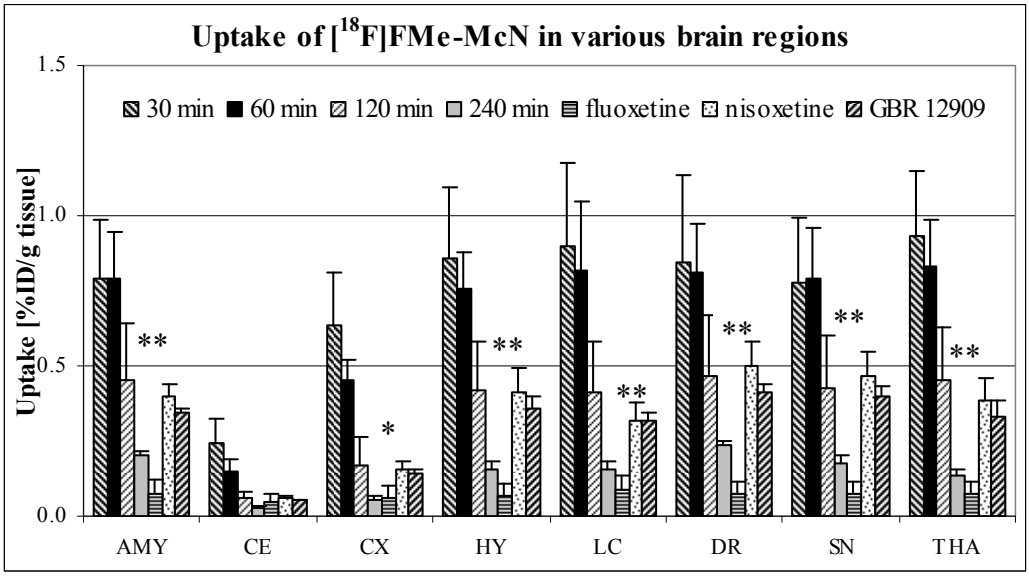

* denotes significant (*$p < 0.05$, **$p < 0.01$) difference between non-treated rats and those pre-treated with fluoxetine at 120 min *p.i.*

Figure 5.7. Biodistribution of [^{18}F]FMe-McN from *ex vivo* PSL autoradiography in rat brain regions at 30 min (n = 6), 60 min (n = 9), 120 min (n = 7) and 240 min (n = 8) *p.i.*, and after a pre-treatment with fluoxetine (n = 4), GBR 12909 (n = 3) or nisoxetine (n = 3) at 120 min *p.i.*, AMY, amygdalae; CE, cerebellum; CX, frontal cortex; HY, hypothalamus; LC, locus coeruleus; DR, dorsal raphe; SN, substantia nigra; THA, thalamus.

The DR-to-CE (target-to-non-target) uptake ratio reached the maximum value of 9.3 within 200 min *p.i.* (Figure 5.8.). In other SERT-rich regions, the maximal region-to-CE ratios were about 8 at 150 min *p.i.*. Figure 5.9. shows a typical autoradiogram of rat brain sections at 120 min *p.i.* of [^{18}F]FMe-McN. In study V, the [^{18}F]FMe-McN uptake ratios of various brain regions to CE for female and male rats at 120 min *p.i.* showed no significant differences between genders.

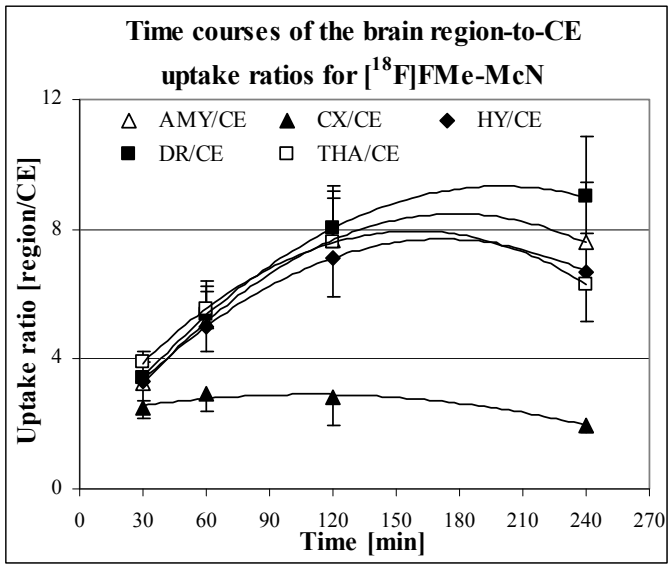

Figure 5.8. The region-to-CE ratios from *ex vivo* PSL autoradiography for [^{18}F]FMe-McN at 30 min (n = 6), 60 min (n = 9), 120 min (n = 7) and 240 min (n = 8). The lines are second-order polynomials fitted to the region-to-CE ratios. AMY, amygdalae; CE, cerebellum; CX, frontal cortex; DR, dorsal raphe; HY, hypothalamus; THA, thalamus.

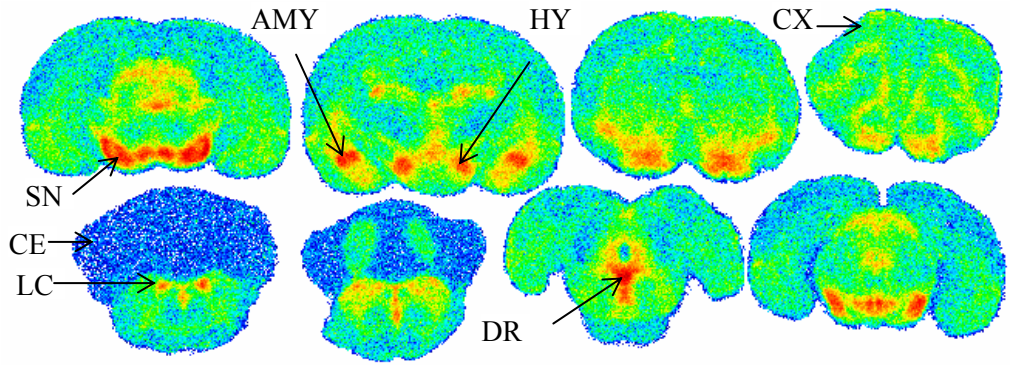

Figure 5.9. A typical *ex vivo* PSL autoradiogram of brain sections showing the regional biodistribution of [^{18}F]FMe-McN (red highest, blue lowest levels, background subtracted) at 120 min *p.i.*. AMY, amygdalae CE, cerebellum; CX, frontal cortex; DR, dorsal raphe; HY, hypothalamus; LC, locus coeruleus; SN, substantia nigra.

In study IV, contents of [^{18}F]FMe-McN-radioactivity in peripheral tissues and organs *ex vivo* were measured in a well counter and the amount of radioactivity was expressed as %ID/g. The highest levels of radioactivity were measured in the adrenal glands,

lungs, liver, spleen, kidneys, intestine, salivary glands, bone marrow and mesenterial fat. The accumulation of radioactivity in bone was low at 30 min *p.i.* but increased later. The biodistribution of [^{18}F]FMe-McN in some organs and peripheral tissues of the rats at different time points *p.i.* and of the rats pre-treated with fluoxetine, nisoxetine or GBR 12909 are shown in Figure 5.10. A significant decrease in the uptake of [^{18}F]FMe-McN was seen in the intestine of rats that were pre-treated with fluoxetine, which reflects specific intestinal binding of [^{18}F]FMe-McN.

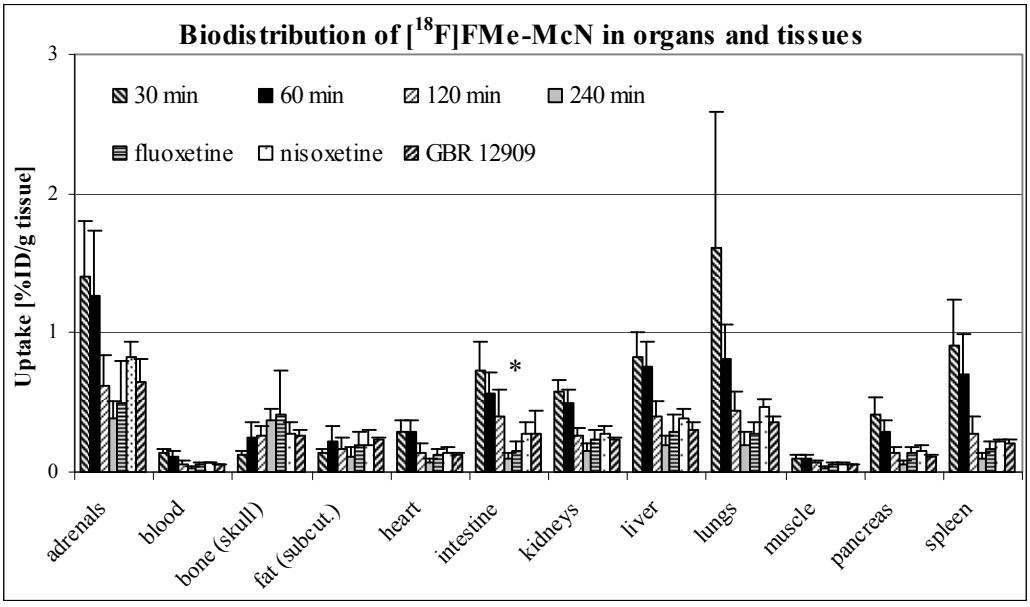

* denotes significant (*$p < 0.05$) difference as compared to the fluoxetine pre-treated rats.

Figure 5.10. Biodistribution of [^{18}F]FMe-McN in organs and tissues *ex vivo* at 30 min (n=6), 60 min (n = 9), 120 min (n = 7) and 240 min (n = 8) *p.i.*, and after a pre-treatment with fluoxetine (n=4), GBR 12909 (n=3) or nisoxetine (n=3) at 120 min *p.i.*.

In study V, the ^{18}F-radioactivity contents of organs were normalized to blood radioactivity and expressed as ratios of %ID/g $_{tissue}$ to %ID/g $_{blood}$, because the body masses of the female rats were significantly lower than the body masses of the males. Male rats had significantly higher organ-to-blood ^{18}F-radioactivity ratios in the adrenal glands, kidneys, lungs and spleen, all of which contain SERT binding sites. Females had significantly higher tissue-to-blood ^{18}F-radioactivity uptake ratios in the heart, liver, muscle and subcutaneous fat, all of which are organs and tissues lacking SERT sites (Figure 5.11.). No differences between genders were seen in the pancreas, stomach, intestine, salivary glands, bone, bone marrow, or mesenterial fat-to-blood ratios.

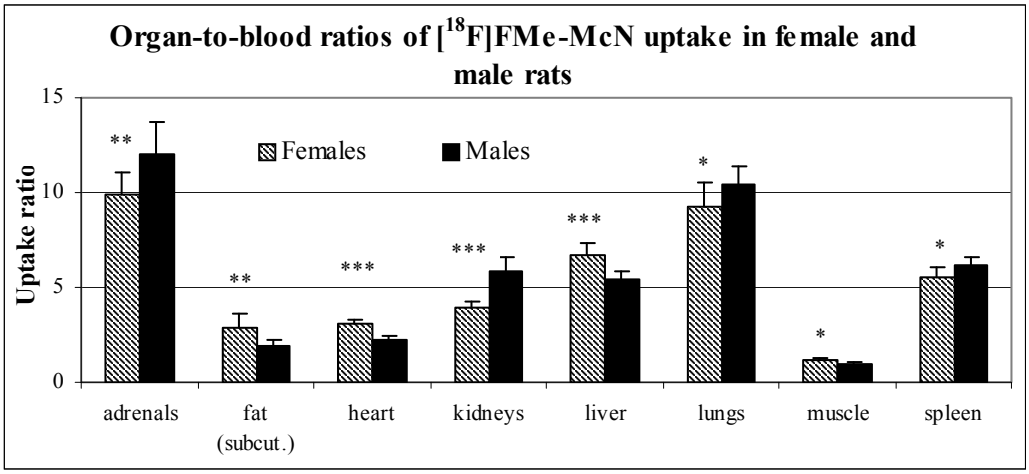

* denotes significant (*$p < 0.05$, **$p < 0.01$, ***$p < 0.001$) difference between genders.

Figure 5.11. Organ-to-blood ratios of [^{18}F]FMe-McN radioactivity biodistribution *ex vivo* in female (n = 12) and male (n = 8) rats.

5.3. Pharmacological studies (II - IV)

5.3.1. Specificity and selectivity of [^{18}F]β-CFT-FP and [^{18}F]β-CFT ex vivo (II, III)

The DAT specificity of [^{18}F]*β*-CFT-FP and [^{18}F]*β*-CFT binding was assessed by pre-treating rats with a highly selective DAT inhibitor GBR 12909. The regional *ex vivo* biodistribution of ^{18}F-radioactivity in the brain regions with high densities of DAT sites in non-treated rats and in rats pre-treated with GBR 12909 was determined using PSL-autoradiography.

In study II, pre-treatment with GBR 12909 reduced the uptake of [^{18}F]*β*-CFT-FP in the STR; the STR-to-CE ratio *ex vivo* at 15 min *p.i.* decreased from 4.7 in a non-treated rat (n = 1) to 2.8 in a rat pre-treated with GBR 12909 (n = 1) indicating specific DAT binding of [^{18}F]*β*-CFT-FP (Figure 5.12.). In extrastriatal brain regions (HY, VTA, and SN) with lower densities of DAT sites, the specific binding of [^{18}F]*β*-CFT-FP was low.

Since [^{18}F]*β*-CFT-FP did not show any significant accumulation in the brain regions with the highest densities of SERT or NET sites, *e.g.* in the DR or LC (Figure 5.12.), no blocking studies with fluoxetine or nisoxetine were performed. Thus, [^{18}F]*β*-CFT-FP binding in the rat brain seemed to be selective for DAT over SERT and NET sites.

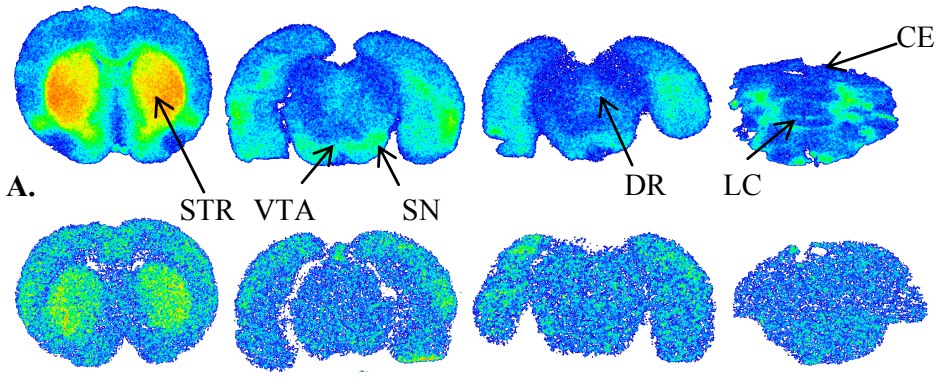

Figure 5.12. *Ex vivo* PSL autoradiograms of brain sections of a non-treated rat (A) and a rat pre-treated with GBR 12909 (B) show the regional brain biodistribution of [^{18}F]*β*-CFT-FP at 15 min *p.i. ex vivo* (red highest, blue lowest levels, background subtracted).

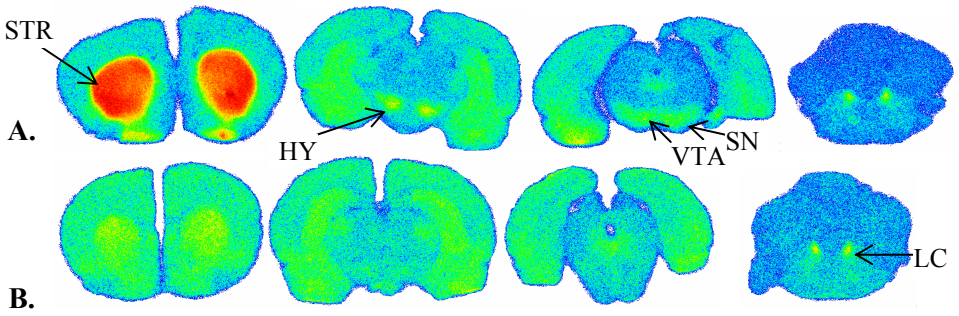

Figure 5.13. *Ex vivo* PSL autoradiograms of brain sections of a non-treated rat (A) and a rat pre-treated with GBR 12909 (B) show the regional brain biodistribution of [^{18}F]*β*-CFT at 40 min *p.i. ex vivo* (red highest, blue lowest levels, background subtracted).

In study III, pre-treatment with GBR 12909 (n = 5) significantly reduced ($p < 0.05$) the uptake of [^{18}F]*β*-CFT in the STR, HY, VTA and SN at 40 min *p.i.* (Figures 5.13. and 5.14.) indicating specific DAT binding both in the STR and extrastriatal DAT sites.

The DAT selectivity of the [^{18}F]*β*-CFT binding was assessed by pre-treating rats with fluoxetine (n = 6) and nisoxetine (n = 6), selective SERT and NET inhibitors, respectively. With the fluoxetine pre-treatment, no significant effects on the ^{18}F-radioactivity uptake were found in any brain region, which reflects the high selectivity of [^{18}F]*β*-CFT for DAT over SERT. In the rats pre-treated with nisoxetine, the ^{18}F-radioactivity uptake decreased significantly in the LC ($p < 0.005$), CX ($p < 0.05$), DR and CE ($p < 0.05$) (Figure 5.14) indicating that [^{18}F]*β*-CFT also specifically binds to NET sites.

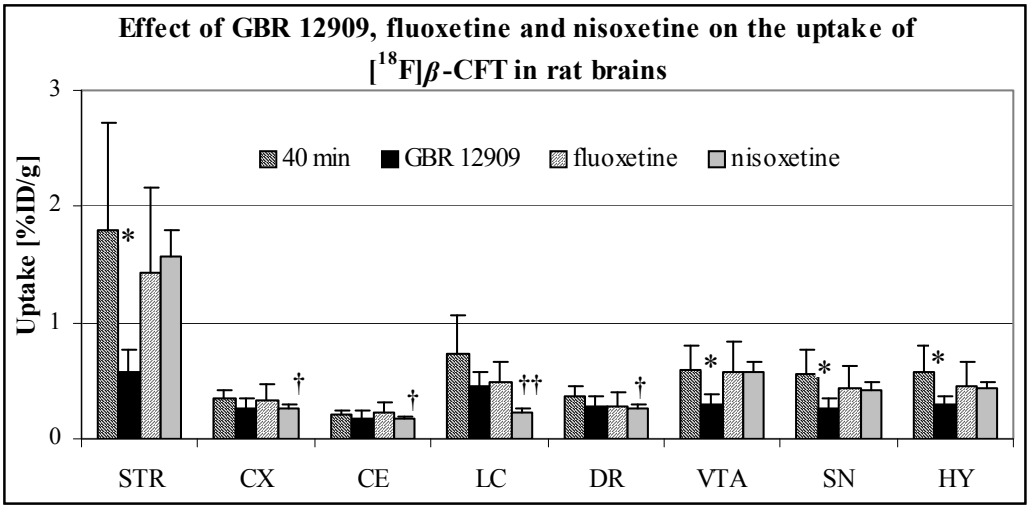

* denotes significant (*$p < 0.05$) difference as compared with the GBR 12909 pre-treated rats
† denotes significant (†$p < 0.05$, ††$p < 0.01$) difference as compared with the nisoxetine pre-treated rats

Figure 5.14. The uptake of [^{18}F]β-CFT from *ex vivo* PSL autoradiography in several brain regions of non-treated rats and of rats pre-treated with GBR 12909 (n = 5), fluoxetine (n = 6) or nisoxetine (n = 6) at 40 min *p.i.*. STR, striatum; CX, frontal cortex; CE, cerebellum; LC, locus coeruleus; DR, dorsal raphe; VTA, ventral tegmental area; SN, substantia nigra; HY, hypothalamus.

5.3.2. Specificity and selectivity of [^{18}F]FMe-McN ex vivo and in vitro (IV)

The specificity of [^{18}F]FMe-McN binding to SERT *ex vivo* was assessed by pre-treating rats with the selective SERT inhibitor fluoxetine (n = 4), and the selectivity by pre-treating the rats with GBR 12909 (n = 3) or nisoxetine (n = 3), selective DAT and NET inhibitors, respectively. The regional *ex vivo* biodistribution of ^{18}F-radioactivity at 120 min *p.i.* in brain regions with high densities of SERT sites of the non-treated rats (n = 7) and rats pre-treated with monoamine inhibitors was determined using PSL-autoradiography. The results were expressed as %ID/g values.

In study IV, pre-treatment of rats with fluoxetine significantly decreased the uptake of [^{18}F]FMe-McN *ex vivo* in the AMY, DR, HY, LC, SN, THA ($p < 0.01$) and in the CX ($p < 0.05$), in rat brain regions with high densities of SERT sites (Figure 5.7.) indicating good specificity of [^{18}F]FMe-McN for SERT sites. When specific binding was defined as the difference in the uptake of [^{18}F]FMe-McN between the brain region and CE, the blockade by fluoxetine corresponded to 91 ± 4% from the specific binding in the DR. In the other regions with high densities of SERT, the blockade of specific binding by fluoxetine ranged from 86 ± 8% to 93 ± 4%. The DR-to-CE uptake ratio decreased from 8.0 ± 1.3 to 1.7 ± 0.2 at 120 min *p.i.* in the fluoxetine pre-treated rats. No significant interactions ($p > 0.05$) between [^{18}F]FMe-McN and GBR 12909 or

nisoxetine were observed *ex vivo* at 120 min *p.i.* in any region studied (Figure 5.7.), which suggests a high selectivity of [^{18}F]FMe-McN binding for SERT over DAT and NET.

The relative displacing potencies of the SERT, DAT and NET inhibitors, fluoxetine, GBR 12909 and nisoxetine, respectively, were also studied *in vitro* by incubating rat brain sections with [^{18}F]FMe-McN along with various concentrations of these drugs. Fluoxetine inhibited the binding of [^{18}F]FMe-McN in the SERT-rich regions at concentrations from 1 nM to 10 μM in a concentration-dependent manner, while nisoxetine and GBR 12909 showed binding inhibition only at higher nM-concentrations. The specific SERT binding *in vitro* in the DR was defined as the difference between the total binding without any drugs and the binding in the presence of 10 μM of fluoxetine. In close concordance with the *ex vivo* results, fluoxetine inhibited [^{18}F]FMe-McN binding *in vitro,* and both GBR12909 and nisoxetine failed to displace [^{18}F]FMe-McN binding from rat brain sections at low nM-concentrations. The concentrations of displacing drugs that inhibit 50% of the specifically bound radiotracer (IC_{50}), as determined graphically for fluoxetine, GBR 12909 and nisoxetine, were ~ 25 nM, ~ 500 nM and ~ 1 μM, respectively. These IC_{50}-values demonstrate that fluoxetine has a 20-fold potency over GBR12909 and a 40-fold potency over nisoxetine as an inhibitor of [^{18}F]FMe-McN binding *in vitro*.

5.4. Radiometabolite analyses (III, V)

In studies III and V, radioactive metabolites were analysed using TLC chromatography and PSL autoradiography. The proportions of unmetabolized tracers and their radiometabolites at various time points were expressed as a % of the total ^{18}F-radioactivity present in the sample. The contents of the total ^{18}F-radioactivity and unmetabolized tracers in plasma (%ID/ml) as a function of time, *i.e.* time activity curves (TACs), were determined for [^{18}F]*β*-CFT and [^{18}F]*β*-CFT-FP. Chemical identities of the metabolites were not determined in this study.

5.4.1. Radiometabolite analyses of [^{18}F]CFT (III)

The proportions of unmetabolized [^{18}F]*β*-CFT and its radiometabolites were analyzed by Haaparanta et al. (2004) from dialysate fractions collected at intervals of 15 min during MD studies (n = 4) for 120 min. Figure 5.15. shows an autoradiogram of a MD fraction (105-120 min). [^{18}F]*β*-CFT metabolized slowly; the amount of unmetabolized [^{18}F]*β*-CFT was ~ 65% from the total ^{18}F-radioactivity during the whole MD study (Figure 5.16.A.). The proportion of unmetabolized [^{18}F]*β*-CFT in the last MD fraction (105-120 min), 63.5 ± 6.3% (n = 4), was equal to the amount of unmetabolized [^{18}F]*β*-CFT in plasma, 63.6 ± 6.4% (n = 3), collected after animal sacrifice at 120 minutes. Three radiolabelled metabolites were found, and they were all more polar than the parent [^{18}F]*β*-CFT. The TAC for the total ^{18}F-radioactivity showed a gradual decrease

from 0.065 %ID/ml in the first MD fraction (0-15 min) to 0.025 %ID/ml in the last MD fraction (105-120 min). The amount of unmetabolized [^{18}F]β-CFT also decreased slowly from 0.040 %ID/ml to 0.015 %ID/ml during MD studies for 120 min (Figure 5.16.B.).

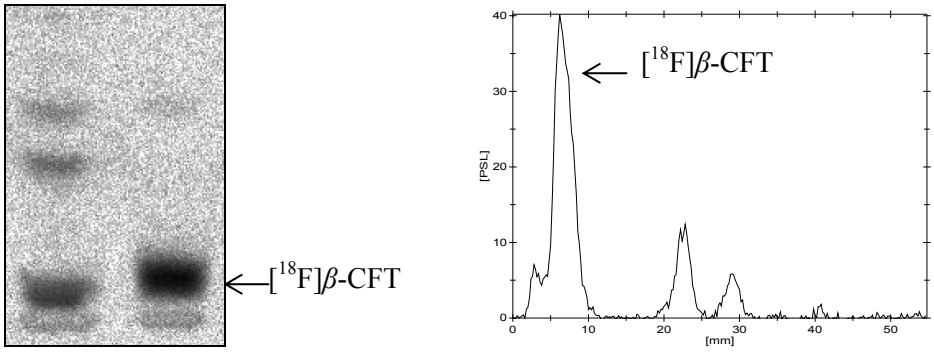

A. B.

Figure 5.15. A PSL autoradiogram of a TLC separation of a MD fraction (105-120 min) (A) and its analysis showing the peaks of [^{18}F]β-CFT and its radiometabolites (B).

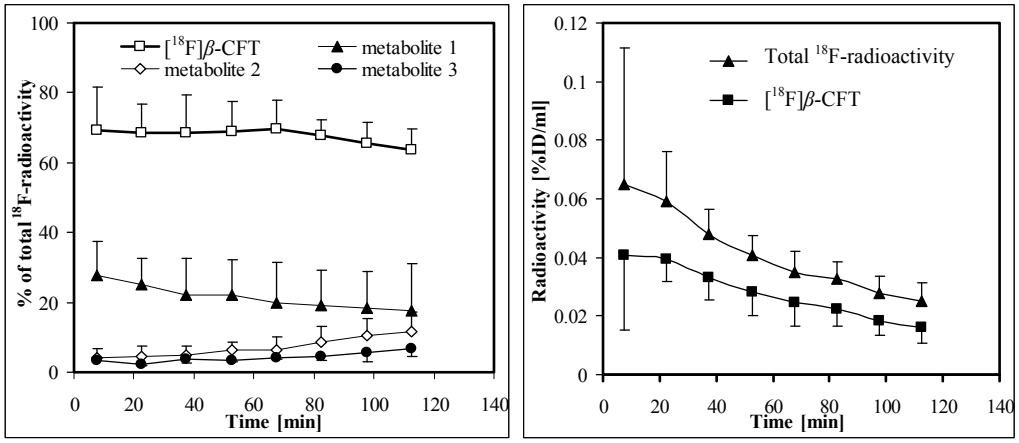

A. B.

Figure 5.16. The proportions (%, mean ± SD) of [^{18}F]β-CFT and its radiometabolites (A) and the TACs for the total ^{18}F-radioactivity and unmetabolized [^{18}F]β-CFT (B), data from TLC analyses and PSL autoradiography (Haaparanta et al. 2004).

5.4.2. Radiometabolite analyses of [^{18}F]CFT-FP (III)

The proportions of [^{18}F]β-CFT-FP and its radiometabolites were analysed from rat plasma at 5 min (n = 4), 15 min (n = 5), 30 min (n = 3), 60 min (n = 3) and 120 min (n = 3) *p.i.*. Figure 5.17. shows an autoradiogram of a plasma sample (15 min). [^{18}F]β-CFT-FP metabolized quickly within 30 min; thereafter the proportion of the

unmetabolized tracer was ~ 20% of the total ^{18}F-radioactivity (Figure 5.18.A.). Three radiolabelled metabolites were found, which were all more polar than the parent tracer.

The TAC showed high total ^{18}F-radioactivity, 0.40 %ID/ml, in plasma at 5 min, and a decrease by 75% to 0.10 %ID/ml at 120 min. The amount of unmetabolized [^{18}F]β-CFT-FP was also high at 5 min, but decreased very quickly, by 75% within 30 min (from 0.20 %ID/ml to 0.050 %ID/ml) and by 93% in 120 min (0.015 %ID/ml) (Figure 5.18.B.).

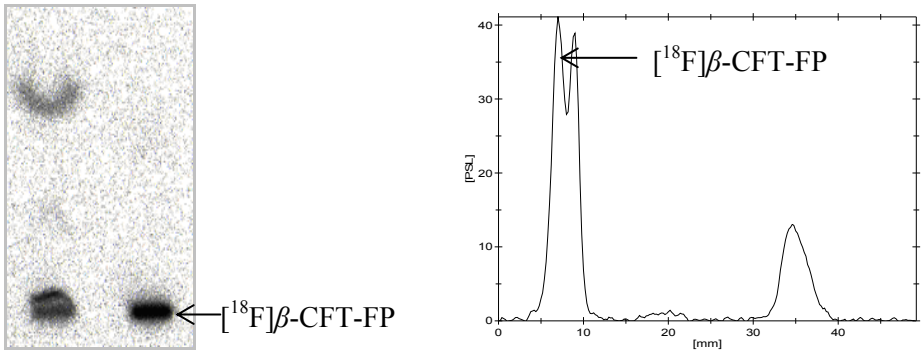

A. B.

Figure 5.17. A PSL autoradiogram of a TLC separation of a plasma sample (A) and its analysis showing the peaks of [^{18}F]β-CFT-FP and its radiometabolites (B) at 15 min *p.i.*.

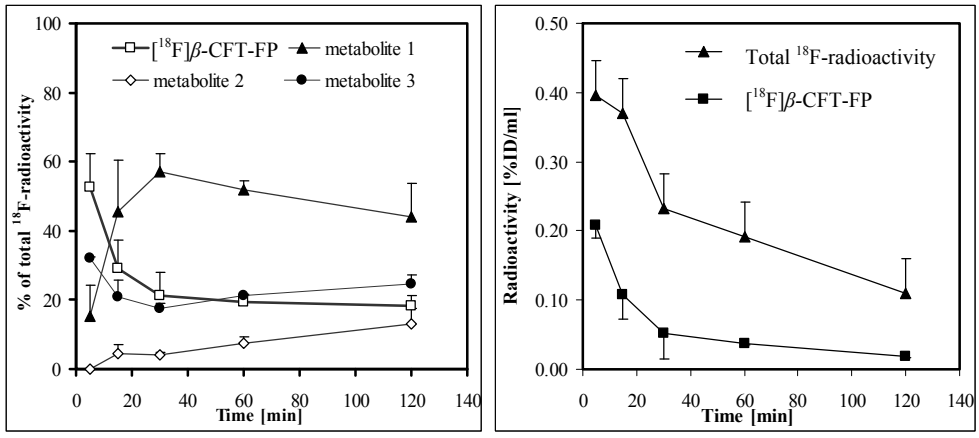

A. B.

Figure 5.18. The proportions (%, mean ± SD) of [^{18}F]β-CFT-FP and its radiometabolites (A) and the TACs for the total ^{18}F-radioactivity and unmetabolized [^{18}F]β-CFT-FP (B), data from TLC analyses and PSL autoradiography.

5.4.3. Radiometabolite analyses of [^{18}F]FMe-McN (V)

The proportions of unmetabolized [^{18}F]FMe-McN and its radiolabelled metabolites were analyzed from plasma samples of female and male rats sacrificed at 120 min *p.i.* (Figure 5.19.). [^{18}F]FMe-McN metabolized quickly; the proportion of the unmetabolized [^{18}F]FMe-McN at 120 min *p.i.* was low, but similar for both genders: 6.6 ± 3.6 % of the total ^{18}F-radioactivity for female rats, and 6.1 ± 1.3 % for male rats. The proportion of very polar metabolites was ~ 70% for both genders, but the proportion of a nonpolar metabolite was lower for females (~ 14%) than for males (~ 20%). Other metabolites with minor amounts were also detected by TLC analyses

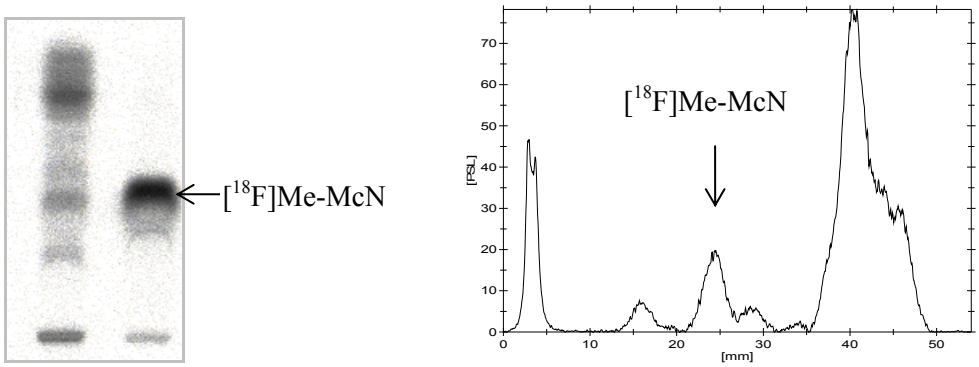

A. B.

Figure 5.19. A PSL autoradiogram of a TLC separation of a female rat plasma sample (A) and its analysis showing the peaks of [^{18}F]FMe-McN and its radiometabolites (B) at 120 min *p.i.*.

6. DISCUSSION

6.1. [^{18}F]FDOPA and [^{18}F]β-CFT as tracers for detection of dopaminergic hypofunction in a rat model of PD (I)

6.1.1. Characterization of the animal model of PD

The purpose of this study was to compare the usefulness of [^{18}F]β-CFT and [^{18}F]FDOPA to reflect the degree of dopaminergic neuronal loss in the SN of an animal model of PD. In this animal model (Ungerstedt and Arbuthnott 1970), the DA pathways in the midbrain of the rats are unilaterally destroyed by an intranigral injection of 6-OHDA, which provides the possibility for pharmacological characterisation of different degrees of nigrostriatal dopaminergic lesion as well as comparison of the findings between the lesioned and the intact side in the same animal.

The lesioned rats were divided into three groups according their behavioural responses to the dopaminergic drugs APO, AMPH and *L*-DOPA. More than 90% of the dopaminergic nerve terminals must be destroyed before animals exhibit contralateral rotations after a dose of APO has been administered (Sarre et al. 1992), whereas AMPH causes circling behaviour in animals with a 70% lesion (Hudson et al. 1993). All lesioned animals showed AMPH responses. Group 2 also showed APO responses and group 3 demonstrated responses for all drugs that accorded well with a decrease of over 90% in the numbers of TH-immunopositive neurons in the left SN. However, animals in group 1 with only AMPH responses had only a 50% lesion, somewhat lower than the 70% lesion reported for AMPH responses. The lesion in the SN also affects the *L*-DOPA responses (Robertson and Robertson 1989). However, the rats with over 90% nigral cell loss did not necessarily have a *L*-DOPA response reflecting the compensatory factors that normally affect *L*-DOPA responses.

As a direct dopaminergic agonist, APO induces contralateral (in the direction opposite to the lesion) circling behaviour that is related to the development of supersensitivity of DA receptors in the lesioned side. The indirect DA agonist, AMPH, causes ipsilateral circling due to its indirect presynaptic effect. AMPH releases DA only from the intact nerve endings on the unlesioned side, causing an imbalance in the activity between DA systems of left and right side that results in circling away from the side of higher DA activity (*i.e.* towards the lesioned side). Thus, the behavioural consequences of the direct (postsynaptic) and indirect (presynaptic) dopaminergic stimulation are diametrically opposed (Kaakkola and Teräväinen 1990, Rudnick and Clark 1993).

The degree of unilateral lesion for each animal was confirmed by counting nigral TH positive cell bodies. In humans, the content of TH mRNA has been shown to decline in a more linear manner with increasing age than the content of DAT mRNA (Bannon et al. 1992, Ito et al. 1999). In PD, the amount of mRNA for DAT per DA neuron is decreased, while TH mRNA levels are increased suggesting compensatory mechanisms

in surviving DA cells (Joyce et a. 1997). Because mRNAs for DAT and TH are collocated in the same cells of the SN and VTA (Augood et al. 1993), the TH immunopositivity can be used as a suitable marker for dopaminergic cell bodies.

6.1.2. Comparison of [^{18}F]FDOPA and [^{18}F]β-CFT uptakes in the STR and SN

[^{18}F]FDOPA is a fluorinated positron-emitting analogue of *L*-DOPA, a precursor of DA (Firnau et al. 1973). Accumulation of [^{18}F]FDOPA in the dopaminergic terminals reflects [^{18}F]FDOPA transport, decarboxylation to DA, and its storage in the presynaptic vesicles, and determines thereby the number of functioning nerve terminals (Cumming et al. 1987, Firnau et al. 1987, Sawle et al. 1990, Snow et al. 1993). The uptake of a DAT tracer, [^{18}F]β-CFT, reflects the levels of DA and DAT protein on the cell membranes (Wilson et al. 1996, b). Thus, the uptake of [^{18}F]FDOPA and [^{18}F]β-CFT reflects different aspects of the dopaminergic function.

In the present rat model of unilateral PD, the striatal uptake of both [^{18}F]FDOPA and [^{18}F]β-CFT was sufficiently sensitive to detect nigrostriatal hypofunction, and identify the loss of nigral neurons. When comparing the tracer uptakes with the behavioural responses and the nigral cell loss, the reduction in the [^{18}F]FDOPA or [^{18}F]β-CFT uptake was greatest in animals with the strongest responses to APO, *i.e.* in the rats with over 90% nigral lesions, and smaller in animals with only AMPH responses, *i.e.* in the rats with 50% nigral lesions. The striatal uptake of both tracers was not dependent on responses to *L*-DOPA. However, all animal groups showed significantly greater declines in the striatal and nigral uptake of [^{18}F]β-CFT than in the uptake of [^{18}F]FDOPA. When the nigral neurons were reduced to about half, the striatal [^{18}F]FDOPA uptake was reduced by ~ 14 %, whereas the [^{18}F]β-CFT uptake reduced by ~ 56 %. In the rats with over 90% nigral lesion, striatal [^{18}F]FDOPA and [^{18}F]β-CFT uptakes reduced by ~ 26% and ~ 87%, respectively.

In accordance with our results, DAT ligands [^{125}I]PE2I and [^{125}I]β- CIT, reflected the decrease of dopaminergic neurons more precisely than did [^{14}C]*L*-DOPA or a D2 receptor ligand [^{125}I]iodobenzamine in a similar rat model of PD (Chalon et al. 1999, Ito et al. 1999). In a PET study of both healthy and MPTP lesioned C57Bl/6 mice, [^{18}F]FDOPA and 6-[^{18}F]fluoro-*L*-*m*-tyrosine (precursors of DA) failed to visualize clearly the mouse STR, whereas [^{18}F]FECNT (a DAT tracer) was able to delineate the striatal degeneration in lesioned mice. Despite the pre-treatment of animals with entacapone and carbidopa, [^{18}F]FDOPA metabolized to radioactive metabolites that could enter the brain and contribute to non-specific radioactivity accumulation (Honer et al. 2006). [^{18}F]β-CFT was also more sensitive in detecting the dopaminergic hypofunction in clinical PET studies (Rinne et al. 1999a,b, 2001). However, the [^{18}F]FDOPA-PET in humans has been shown to be useful in the diagnosis of PD and the assessment of individual disease progression, but the evidence is not conclusive with respect to its utility in the differential diagnosis between PD and other

parkinsonian syndromes, or in the differentiation between grades of PD (Puñal-Riobóo et al. 2009). It has been suggested that the [^{18}F]FDOPA uptake overestimates the level of DA innervation in the STR of patients with PD (Lee et al. 2000) and in the STR of lesioned rats (Ito et al. 1999). In PD, the remaining dopaminergic neurons increase their turnover rate and thereby compensate for the loss of neurons (Bernheimer et al. 1973). Compensatory changes in receptors, in DOPA decarboxylase activity and in the function of presynaptic dopaminergic terminals may also be involved. In conclusion, the uptake of [^{18}F]FDOPA seems to be more affected by compensatory metabolic changes than the uptake of DAT tracers, like [^{18}F]*β*-CFT, and consequently is less sensitive in detecting mild dopaminergic lesions.

6.2. [^{18}F]*β*-CFT-FP and [^{18}F]*β*-CFT as tracers for DAT in the rat (II, III)

6.2.1. [^{18}F]β-CFT-FP as a DAT tracer in rat brains

Based on the promising properties of [^{11}C]*β*-CFT (Wong et al. 1993), Firnau et al. (1995) synthesized its ^{18}F-labelled *N*-fluoropropyl analogue ([^{18}F]*β*-CFT-FP). The specificity and selectivity of its carbon-11 labelled analogue [^{11}C]*β*-CFT-FP for DAT were demonstrated in post-mortem human brain sections (Kämäräinen et al. 2000a,b), and the synthesis procedures for [^{18}F]*β*-CFT-FP were further developed and optimized (Kämäräinen et al. 1999, Koivula et al. 2005). In study II we determined the biodistribution of [^{18}F]*β*-CFT-FP as a function of time in the rat brain and peripheral tissues, and the specificity of the tracer to DAT.

[^{18}F]*β*-CFT-FP showed very fast and high accumulation in the STR that contains the highest densities of DAT sites in the rat brain (Nirenberg et al. 1996, 1997a, 1997b), reflecting a good blood-brain barrier penetration. The maximum STR-to-CE ratio of 3.1 was reached at 5 min *p.i.*. Firnau et al. (1995) determined this uptake ratio in their initial *ex vivo* study of rats at one time point, at 60 min *p.i.*, and it was higher (3.2) than our value of 1.9 at 60 min, which was calculated from biodistribution data that generally give slightly lower values as compared with autoradiographic data. The rapid washout (poor retention) of [^{18}F]*β*-CFT-FP from the brain reflects reversible binding kinetics and only a moderate DAT affinity that is in accordance with the reported affinity (K_i) of 47.9 nM (Harada et al. 2004).

GBR 12909 significantly decreased the uptake of [^{18}F]*β*-CFT-FP in the STR, indicating that [^{18}F]*β*-CFT-FP binding reflects specific DAT labelling. No significant [^{18}F]*β*-CFT-FP binding was observed in the HY, THA and DR brain regions of high SERT densities (D'Amato et al. 1987), or in the LC, where the NET is located (Burchett and Bannon 1997). The STR contains only intermediate levels of SERT, and NET is virtually absent in the STR (Hoffman et al. 1998). Thus, [^{18}F]*β*-CFT-FP was DAT selective, which is in line with the affinities (K_i) of 318 nM for SERT and 9910 nM for NET reported by Harada et al. (2004).

6.2.2. Pharmacokinetic properties of [^{18}F]β-CFT and [^{18}F]β-CFT-FP

In study III, the biological properties of the tropane compounds, [^{18}F]*β*-CFT-FP and [^{18}F]*β*-CFT, were compared in rats (Table 6.1.). [^{18}F]*β*-CFT-FP showed fast, reversible binding kinetics with a moderate STR-to-CE ratio of 3.1 at 5 min *p.i.*, whereas [^{18}F]*β*-CFT showed slow, "irreversible-like" binding kinetics with a high STR-to-CE ratio of 9.2 at 120 min. A high STR-to-CE ratio and slow kinetics for [^{18}F]*β*-CFT have also been reported in a preliminary rat study (Haaparanta et al. 1996) and in human PET studies (Laakso et al. 1998, Rinne et al. 1999a, 1999b). The fast, reversible kinetics of [^{18}F]*β*-CFT-FP are a consequence of its lower DAT affinity and rapid washout from target sites. The "irreversible-like" binding kinetics of [^{18}F]*β*-CFT would suggest that it was due to the binding to the high affinity sites on DAT (Mach et al. 2000). High affinity leads to longer-lasting binding and slower washout of the ligand, resulting in slower kinetics. Among *β*-CIT and *β*-CFT derivatives, the substitution of the *N*-methyl group by a fluoropropyl or fluoroethyl group gives analogues with lower DAT affinity (Okada et al. 1998, Goodman et al. 1997, Harada et al. 2004, Torres et al. 2003, Neumeyer et al. 1994) and faster kinetics, as shown by [^{18}F]*β*-CIT-FP (Lundkvist et al. 1997), [^{18}F]*β*-CFT-FE (Harada et al. 2004), and [^{18}F]*β*-CFT-FP in the present study.

For both tracers, a high ^{18}F-radioactivity accumulation was seen in the excretory organs and in the pancreas, thereby demonstrating specific DAT binding. In addition to the brain expression, DAT immunoreactivity has been detected in the stomach, pancreas and kidneys (Torres et al.2003, Eisenhofer 2001). The liver showed a very high, increasing accumulation of [^{18}F]*β*-CFT-radioactivity (8.3 %ID/g at 120 min *p.i.*) contrary to the accumulation of [^{18}F]*β*-CFT-FP, which was rather high at 5 min (1.8 %ID/g), but decreased thereafter (0.15 %ID/g at 120 min). This reflects the rate of the hepatic metabolism; [^{18}F]*β*-CFT metabolized slowly, while [^{18}F]*β*-CFT-FP was metabolized and excreted rapidly. Organs or tissues with early peak uptakes usually reflect the binding of the tracers themselves, while those that slowly accumulate radioactivity may reflect more the accumulation of radiolabelled metabolites. In subcutaneous fat, the [^{18}F]*β*-CFT-radioactivity content showed a maximum of 0.08 %ID/g at 40 min, whereas the [^{18}F]*β*-CFT-FP-derived radioactivity content reached the highest value of 0.29 %ID/g later, at 60 min, and was high still at 120 min, which may reflect the accumulation of lipophilic radiometabolites. [^{18}F]*β*-CFT-derived radioactivity in the bone was relatively low, even at 120 min *p.i.* (0.20 %ID/g) reflecting good stability of the carbon-fluorine bond of the phenyl ring, whereas [^{18}F]*β*-CFT-FP exhibited an increasing accumulation of ^{18}F-radioactivity in the bone (1.38 %ID/g at 120 min), and thereby higher defluorination.

6.2.3. Specificity, selectivity and affinity of [^{18}F]β-CFT and [^{18}F]β-CFT-FP

GBR 12909 significantly decreased the uptake of both tracers in the STR, which indicates that the binding of both tracers was specific to DAT. Fluoxetine had no effects on the [^{18}F]*β*-CFT uptake in the brain regions with high SERT densities

(D´Amato et al 1987, Hoffman et al. 1998) thereby proving the high selectivity of [^{18}F]*β*-CFT to DAT over SERT. On the contrary, nisoxetine significantly decreased the [^{18}F]*β*-CFT uptake in the brain regions rich in NET sites (Burchett and Bannon 1997, Lorang, et al. 1994), also clearly indicating that [^{18}F]*β*-CFT specifically binds to NET sites.

Harada et al. (2004) determined the affinities of several tropane analogues to human monoamine transporters *in vitro*. *β*-CFT had a moderate DAT affinity (K_i 25.8 nM), but to some extent higher compared to that of *β*-CFT-FP (K_i 47.9 nM). The affinities (K_i) of *β*-CFT and *β*-CFT-FP for SERT were low: 157 nM and 318 nM, respectively, and the affinities for NET were in the μM range, suggesting a negligible NET binding. However, the unexpected high NET binding of [^{18}F]*β*-CFT in our studies suggests that [^{18}F]*β*-CFT has a significantly higher NET affinity. Therefore, affinities (K_i) of *β*-CFT reported by Torres et al. (2003) that are similar to those reported by Harada for DAT (26.1 nM), and SERT (127 nM), but different for NET (31.9 nM), are in line with our results. These differences in affinities determined *in vitro* may be caused by different experimental procedures and species' differences. In addition, binding studies *in vitro* may not be adequate to describe the characteristics of *in vivo* binding to an intact system (Farde et al. 1994).

6.2.4. Metabolism of phenyltropanes

[^{18}F]*β*-CFT was more resistant to metabolism than [^{18}F]*β*-CFT-FP (Figures 5.16.A. and 5.18.A). The proportion of unmetabolized [^{18}F]*β*-CFT was ~ 65% of the total ^{18}F-radioactivity during the whole MD study of 120 min (Haaparanta et al. 2004), whereas [^{18}F]*β*-CFT-FP metabolized quickly, within 30 min, and thereafter the proportion of unmetabolized tracer in plasma was ~ 20%. Time activity curves (Figures 5.16.B. and 5.18.B) show that the amount of unmetabolized [^{18}F]*β*-CFT in the first MD-fraction (0-15 min) was 0.04 %ID/ml, the corresponding value for [^{18}F]*β*-CFT-FP in plasma was higher, 0.20 %ID/ml (5 min), but, as a consequence of the rapid metabolism of [^{18}F]*β*-CFT-FP, the amounts of both unmetabolized tracers were ~ 0.015 %ID/ml at 120 min. Low [^{18}F]*β*-CFT-radioactivity levels in plasma result from its retention in tissues due to its high affinity binding. High plasma levels of [^{18}F]*β*-CFT-FP-derived radioactivity are caused by its fast washout from tissues due to its lower affinity and to high metabolite concentrations. In human PET studies, this means that the input function for [^{18}F]*β*-CFT-FP has to be corrected for ^{18}F-radiolabelled metabolites, in contrast to PET studies using [^{18}F]*β*-CFT (Laakso et al. 1998, Rinne et al. 1999a, 1999b).

An undesired property of PET tracers is their rapid metabolism, especially to nonpolar, lipophilic, radiolabelled metabolites. Radiotracers should be as resistant as possible to rapid peripheral metabolism, because target availability of the radioligand will significantly decrease as a consequence of rapid metabolism. Moreover, metabolites should be either polar, *i.e.* hydrophilic, so that they do not enter the brain, or, if

nonpolar, should be unlabelled because radiometabolites can often bind to targets with altered affinity and selectivity and contribute to radioactivity accumulation in tissues. For example, a DAT tracer [^{11}C]β-CIT-FP generates [^{11}C]nor-β-CIT with high SERT affinity and is capable of brain access (Lundkvist et al. 1997). Slow metabolism is also favourable, because PET scanners, isotope calibrators and well counters measure radioactivity concentrations without being able to distinguish between the unmetabolized parent tracer and its metabolites.

The labelling sites in the radioligands have been reported to influence their susceptibility to metabolism and the formation of active radiolabelled metabolites. A ^{18}F-label can be introduced in tropane derivatives as a fluoroalkyl group for *N*-substitution, as an alcohol portion of the carboxylate ester, or by electrophilic substitution of a trimethyltin group on the phenyl ring. Phenyltropanes radiolabelled in the methyl ester position metabolized slower than the ones with a radiolabel in the *N*-group position; *e.g.* ~ 80% of unmetabolized [*O*-methyl-^{11}C]β-CIT-FP ([^{11}C]β-CIT-FP) was detected in monkey plasma compared to 30% of [^{11}C]β-CIT at ~ 25 min (Lundkvist et al. 1995). The most resistant ^{18}F-labelling site against metabolism may be the 4'-position in the phenyl ring, as shown by the 4-[^{18}F]fluorine moiety of [^{18}F]β-CFT.

Cocaine can metabolize in several ways, by an ester hydrolysis, *N*-demethylation, *N*-oxidation, aryl hydroxylation and/or epoxidation and dehydrobenzoylation (Stehouwer and Goodman 2009). Cocaine analogues, like phenyltropanes, in which the 3β-benzoyl group has been replaced by a 3β-(4-substituted phenyl) group, lack one of the ester groups of cocaine, and are therefore more resistant to metabolic degradation (Wong et al. 1993). The initial steps in the oxidative metabolism of phenyltropanes are the *N*-dealkylation catalyzed by cytochrome P-450-oxidases to yield norphenyltropanes and carbon residues, like formaldehyde, and the hydrolysis of the 2β-carbomethoxy group by carboxyl esterases to yield a 2β-carboxylic acid (Neumeyer et al. 1994, Zoghbi et al. 2006). [^{18}F]FECNT, which has a *N*-2-[^{18}F]fluoroethyl group and a chloride instead of fluorine in [^{18}F]β-CFT-FE, metabolized quickly in rats, monkeys and humans to a polar compound identified as an unlabelled, *N*-dealkylated FECNT (nor-CCT); traces of β-carboxylic acid and three ^{18}F-labelled two-carbon residues; 2-[^{18}F]fluoroethanol; 2-[^{18}F]fluoroacetaldehyde; and 2-[^{18}F]fluoroacetic acid (Neumeyer et al. 1994), which were able to enter into the brain (Zoghbi et al. 2006). A fast metabolism to polar compounds was also seen in [^{18}F]FPCT, a 4-chlorophenyl analogue of [^{18}F]β-CFT-FP (Goodman et al. 1997) and [^{18}F]β-CFT-FE (Harada et al. 2004), and can also be expected for [^{18}F]β-CFT-FP. In our study, radiometabolites in the brain tissue were not measured, but their presence in the brain is possible due to the structural similarity of [^{18}F]β-CFT-FP with [^{18}F]FECNT, [^{18}F]FPCT and [^{18}F]β-CFT-FE. [^{18}F]fluorine moiety in the phenyl ring is more resistant against metabolism as seen by the low defluorination of [^{18}F]β-CFT, thus, radiolabelled nor-β-CFT and the 2β-carboxylic acid

may be the primary metabolites of [^{18}F]*β*-CFT. Because [^{18}F]*β*-CFT and [^{18}F]*β*-CFT-FP have their ^{18}F-radiolabels at different positions (4'-[^{18}F]fluorophenyl *vs*. *N*-3-[^{18}F]fluoropropyl), they generate different kinds of radiolabelled metabolites, such as [^{18}F]nor-*β*-CFT and the [^{18}F]*β*-CFT-carboxylic acid form or 3-[^{18}F]fluoropropanol and its aldehyde and acid forms, respectively.

Table 6.1. Comparison of some properties of [^{18}F]*β*-CFT and [^{18}F]*β*-CFT-FP in rats.

Compared properties	**[^{18}F]*β*-CFT**	**[^{18}F]*β*-CFT-FP**
Maximum STR-to-CE ratio	9.2 ± 2.0 (120 min)	3.1 ± 0.6 (5 min)
Liver uptake at 120 min (%ID/g)	8.3 ± 1.2	0.15 ± 0.06
Bone uptake at 120 min (%ID/g)	0.20 ± 0.15	1.38 ± 0.54
Subcutaneous fat uptake (%ID/g)	0.08 ± 0.03 (40 min)	0.29 ± 0.03 (60 min)
Selectivity	DAT, NET	DAT
Binding kinetics	slow	fast, reversible
Amount of unmetabolized tracer in plasma at 120 min *p.i.*	~ 65 %	~ 20 %
Probable primary ^{18}F-labelled metabolites	[^{18}F]nor-*β*-CFT and [^{18}F]*β*-CFT-carboxylic acid	3-[^{18}F]fluoropropanol 3-[^{18}F]fluoropropanal 3-[^{18}F]fluoropropionic acid

In summary, substitution of an *N*-methyl group in [^{18}F]*β*-CFT by a [^{18}F]fluoropropyl group significantly changed the properties of the tracer as shown in rats: [^{18}F]*β*-CFT showed binding to both DAT and NET, slow kinetics and metabolism, whereas [^{18}F]*β*-CFT-FP showed high selectivity to DAT, fast kinetics and metabolism. [^{18}F]*β*-CFT-FP may be a suitable PET tracer for imaging human striatal DAT sites due to its fast kinetics and good selectivity for DAT, although its fast metabolism and the possible entry of its radiometabolites into the brain as well as its fast defluorination may be problematic. PET imaging of the extrastriatal DAT sites that are expressed at lower densities, may require a tracer with a higher DAT affinity.

6.3. [^{18}F]FMe-McN as a tracer for SERT in the rat (IV, V)

6.3.1. Pharmacokinetic properties of [^{18}F]FMe-McN

Zessin et al. (1999, 2001) developed an efficient synthesis for enantiomerically pure thioester precursors from racemic McN5652 and synthesized the [^{18}F]fluoromethyl analogue of (+)McN5652 ([^{18}F]FMe-McN) using the methods described by Eskola et al. (1999) and Bergman et al. (2001). (+)McN5652 was shown to have a high SERT affinity (K_i 0.72 nM) *in vitro*, while the fluoromethyl analogue FMe-McN had a somewhat lower SERT affinity (K_i 2.3 nM) (Zessin et al. 2001).

[^{18}F]FMe-McN showed a high uptake in the brain regions with high densities of SERT sites (DR, HY, AMY, SN and LC), and low uptake in the CE. However, because serotonergic and noradrenergic neurons project to the CE, low levels of SERT and NET sites are also present in the CE. Some immunoreactivity for the DAT protein has also been demonstrated in certain lobules of the cerebellar vermis in monkeys (Melchitzky and Lewis 2000). Despite the expression of monoamine transporters, the cerebellar cortex was used as a reference region in studies II-V, since the uptake of all used tracers in this region was the lowest among all brain regions. As a result of the rapid uptake and slow clearance for [^{18}F]FMe-McN, the DR-to-CE ratio increased with time and reached a maximum value of 9 within 3.5 hours *p.i.*. For [^{11}C](+)McN5652, the HY-to-CE ratio was 6.2 in mouse brain at 90 min (Suehiro et al. 1993a), which is comparable to our values of 5.1 and 7.0 measured at 60 and 120 min *p.i.*, respectively. A significantly lower DR-to-CE ratio of 1.6 at 120 min was obtained using the fluoroethyl analogue [^{18}F]FEt-McN (Suehiro et al. 1996).

In study IV, high [^{18}F]FMe-McN uptakes were found in the adrenal glands, lungs, intestine, spleen, kidneys, and liver (Figure 5.10.). In addition to neuronal expression, SERT sites have been identified in many peripheral organs and tissues, such as the adrenal glands, intestinal mucosa, kidneys, thyroids, pancreas, pulmonary endothelium (lung), spleen, stomach and platelets (Blakely et al. 1994, Hoffman et al. 1991, 1998, Kitayama and Dohi 1996, Lin et al. 2002, Meister et al. 1995, Mortensen et al. 1999, Schroeter et al. 1997). Particularly in the gastrointestinal tract, which contains the greatest amount (95%) of 5-HT in the body, the 5-HT activity is regulated by SERT. The increasing accumulation of the ^{18}F-radioactivity in bone over time indicated some defluorination of [^{18}F]FMe-McN.

The PET data obtained by Brust et al. (2003a) from female pigs demonstrated that [^{18}F]FMe-McN reached transient equilibrium between specific and non-specific uptake during a PET scan of 120 min, suggesting faster kinetics than that of [^{11}C](+)McN5652 (Suehiro et al. 1993a, 1993b, Szabo et al. 1995a,b). [^{18}F]FMe-McN showed higher specific binding in pig brain than the ^{11}C-labelled analogue and thereby raises possibilities for imaging and quantification of human SERT sites. Due to the longer half-life of fluorine-18, [^{18}F]FMe-McN allows prolonged studies and imaging periods and may provide transient equilibrium in human PET studies.

6.3.2. Specificity and selectivity of [^{18}F]FMe-McN

Pharmacological studies with fluoxetine, GBR 12909 and nisoxetine *ex vivo* and *in vitro* indicated that the binding of [^{18}F]FMe-McN was specific and selective for SERT. The ^{11}C-labelled analogue [^{11}C](±)McN5652 was also shown to be SERT selective in mice *ex vivo* (Suehiro et al. 1993a). In addition, [^{3}H]citalopram, a selective SERT ligand, and [^{18}F]FMe-McN showed good correlation in the SERT binding *in vitro*

(Kretzschmar et al. 2003). In peripheral organs, fluoxetine only significantly decreased [^{18}F]FMe-McN uptake in the intestine, although a tendency towards lower uptake values was also seen in the adrenal glands, lungs and spleen (Figure 5.10.).

6.3.3. Effect of gender on the SERT binding

The gonadal hormones, estrogen, progesterone and testosterone, exert differentiating actions on the neuronal system during brain development, leading to sexual dimorphism (Segovia et al. 1999), *i.e.* sex differences in the number of neurons, neuronal volume, and extent of dendritic extension and branching in several brain regions (McEwen 2001). These differences persist in adult life, although the brain has the ability to change reversibly in response to circulating hormones (McEwen 1999). Sexual dimorphism and the effects of gonadal hormones on the serotonergic neural system, including SERT functions, have also been reported (Bethea et al. 2002, Pecins-Thompson et al. 1998, Rubinow et al. 1998, McQueen et al. 1997, Zhang et al. 2002). *E.g.* the extracellular 5-HT in the HY is regulated in a manner that is gender and estrous cycle dependent; during estrous, when female rats are responding to high levels of estrogen and progesterone, the extracellular 5-HT has been reported to decrease by ~ 20% in female rats (Gundlah et al. 1998). The high response of estrous females to fluoxetine suggests that the low extracellular 5-HT content during estrous may result from the increased SERT activity (Maswood et al. 1999).

Although we expected that SERT levels in the HY of estrous female rats might be increased and detected using [^{18}F]FMe-McN *ex vivo*, we did not find any significant differences between males and estrous females in the [^{18}F]FMe-McN uptake. In line with our results, Choi et al. (2000) reported that male and female rats showed similar and comparable regional brain uptakes of [^{123}I]ADAM, a selective SPECT tracer for SERT. Many of the reported effects of gonadal hormones on SERT activity *in vitro* and *in situ* have been inconsistent, suggesting that SERT regulation occurs via transient changes in a single day of the estrous cycle. The densities of SERT sites measured by radioligands *in vitro* and the content of mRNA measured using *in situ* hybridization usually reflect the total number of transporters in the cell, while the *in vivo* or *ex vivo* experiments measure the number of functional transporters on the cell surface. The apparently conflicting observations may also be related to differences in species, to the treatments of the animals or to dependence on experimental procedures (Attali et al. 1997, Bethea et al. 2002, Rubinow et al. 1998).

The 5-HT levels fluctuate in some brain regions with the light/dark cycle of the day along with the estrous cycle phases. Proestrous females have the highest 5-HT levels during the light portion and diestrous females during the dark portion of the light/dark cycle. Males and estrous females show relatively constant extracellular 5-HT levels between light and dark portions of the cycle (Maswood et al. 1999). With respect to the light/dark cycle, all rats in study V were studied at the same time of the day, at noon.

In peripheral organs and tissues, male rats exhibited higher tissue-to-blood ^{18}F-radioactivity ratios in the adrenal glands, lungs, kidneys and spleen, all of which show specific SERT binding. This may indicate a higher peripheral SERT activity in males. Females had significantly higher tissue-to-blood ratios in the heart, liver, muscle and fat; rat tissues lacking SERT sites (Ramamoorthy et al. 1993). A high accumulation of ^{18}F-radioactivity in fat may indicate a formation of lipophilic metabolites or a high lipophilicity for the tracer. On the other hand, differences in the uptake ratios, especially in excretory organs, may suggest differences in the kinetics of [^{18}F]FMe-McN between genders. Because study V was performed only at one time point (120 min *p.i.*), the true nature of these differences remains unknown.

6.3.4. Effect of animal body mass and age on the SERT binding

In animal studies, males of the same body mass and age should normally be used to avoid the effects of the estrous cycle with fluctuating hormone levels in females. Thus, studies on the gender differences in animals are challenging; if males are of the same age, they are much bigger in size than females. The concentrations of radiotracers in tissue samples are usually expressed as %ID/g of tissue, when the animals are of the same body mass. However, this is not satisfactory for comparing data from animals of different body mass, especially in cases when the radioligands are uniformly distributed in all tissues without preferential or specific uptake. The uptake of a radioligand from animals of different sizes can be expressed as a % administered radioactivity per total organ (%ID/organ), but this is not suitable for all tissues, such as blood, bones, fat and muscles. Various expressions have been described that normalize tissue concentration data according to body mass, *e.g.* radioactivity concentration (% of total dose/g of tissue times g of body mass/100), relative concentration (RC, MBq found/g tissue divided by MBq administered/g body mass), the differential absorption ratio (DAR, %ID/g times g body mass/100) or the standardized uptake value (SUV, Bq/g tissue divided by injected Bq/g body mass).

In study V, we suggested that DAR or SUV values might overestimate the influence of the body mass, since [^{18}F]FMe-McN was not evenly distributed in the body, but bound with high affinity to SERT sites. As female rats were smaller in size, ^{18}F-radioactivity uptakes in tissues and organs were normalized to blood radioactivity and expressed as ratios of %ID/g $_{tissue}$ to %ID/g $_{blood}$. In study IV, 32 male rats with body masses of 367 ± 47 g, and 8 females with body masses of 265 ± 21 g, were used, and the uptake values were expressed as %ID/g. However, we suggest that since the female rats belong to different groups (30, 60, 120 or 240 min), the effect of their lower body masses and the gender differences on the uptake values may not be significant, although it may increase SD of the means. The brain uptake of [^{18}F]FMe-McN, expressed as an uptake ratio of a brain region to the CE, is not dependent on the body mass of the animal, and was not dependent on the gender in study V, and is therefore an appropriate way to express *ex vivo* results of brain experiments.

Aging has been reported to increase the amount of SERT mRNA (Meister et al. 1995) and the number of SERT sites in the rat brain till late adulthood (Moll et al. 2000). The expression of SERT mRNA in the bulbospinal system was increased by 20-30% in aged (30 months) male rats compared to 2 - 3-month-old rats (Meister et al. 1995). On the contrary, DAT sites in the STR, but not in the midbrain, were reported to increase till puberty and decline strain-specifically thereafter to about one-fourth of the pubertal values at old age in Wistar rats (Moll et al. 2000).

Aging also has effects on the SERT function in the course of the light/dark cycle; the SERT binding was highest in young animals in the morning and in older rats in the evening (Krajnak et al. 2003). In study V, the female rats were 4 - 5 months old and the males 6 months old, a difference which should not cause age-related effects on SERT binding.

6.3.5. Metabolites and lipophilicity of [^{18}F]FMe-McN

In study V, the amounts of the radiometabolites of [^{18}F]FMe-McN were determined only at one time point, at 120 min *p.i.*. The metabolism of [^{18}F]FMe-McN was rather fast; ~ 94% of the total ^{18}F-radioactivity at 120 min in plasma originated from radiometabolites. The proportions of unmetabolized tracer and its polar main metabolite were similar for both genders, but the amount of a nonpolar metabolite was lower for females (~ 14%) than for males (~ 20%). This might reflect either the accumulation of the nonpolar metabolite in greater amounts in the fat of female rats, since females showed higher ^{18}F-radioactivity uptakes in fat, or differences in the kinetics and excretion of the metabolites. Without metabolite profiles and biodistribution data as a function of time for both male and female rats, the true nature of this difference remains speculative.

High ^{18}F-radioactivity content in fat may also reflect high lipophilicity for [^{18}F]FMe-McN; a log D of 3.10 was reported for the unlabelled tracer (Brust et al. 2003b). High non-specific binding is generally attributed to protein or lipid adhesion. For brain radioligands, some lipophilicity is essential for penetration through the BBB by passive diffusion (Halldin et al. 2001). The logarithm of the partition coefficient between water and octanol (log P) is widely used to describe the lipophilicity of radioligands, *e.g.* the log P values for citalopram, fluvoxamine, McN5652, paroxetine and sertraline were between 3.5 and 4.5 indicating relatively high lipophilicity, while the log P for DASP was 1.9. ^{11}C-labelled compounds with log P values between 0.9 and 2.5 were reported to pass readily across the BBB. However, there was no firm relation between log P values and the degree of non-specific binding (Elfving et al. 2001). An appropriate log P value for brain imaging tracers is normally between 1 and 3 for good brain entry and low non-specific binding. However, there are differences between measured and calculated log P values, or when different softwares are used for calculation (Ding et

al. 2005, Mavel et al. 2008, Stehouwer and Goodman 2009). In the present study, the log P values for the radiotracers were not determined.

In summary, [^{18}F]FMe-McN showed high SERT binding and selectivity, high target-to-nontarget ratios, but relatively slow kinetics and fast metabolism in rats. No differences between genders were found in the binding of [^{18}F]FMe-McN *ex vivo* in the rat brain; differences in the ^{18}F-radioactivity contents in peripheral organs may indicate either higher SERT activity in male rats or differences in the kinetics of [^{18}F]FMe-McN between genders. We suggest that [^{18}F]FMe-McN has the potential for imaging and quantification of SERT sites.

6.4. Methods

6.4.1. Radioactivity measurements

Radioactivity measurements of tissue samples were done by gamma counting (annihilation gamma quanta) in a well counter or in an ionisation chamber, which were cross-calibrated for absolute measurements of ^{18}F-radioactivities. All the measured radioactivities were decay-corrected to the time of the injection of the tracer.

Digital PSL autoradiography using imaging plates is based on the detection of positrons (beta counting) and provides an excellent method for both localization and quantification of radioactivity concentrations in brain sections. The spatial resolution of PSL autoradiography, *i.e.* the minimum pixel size of 25 μm x 25 μm, is sufficient, but limited as compared to the resolution (< 20 μm) of conventional X-ray film autoradiography; on the other hand, imaging plates are more sensitive than X-ray films. The amount of radioactivity that can be stored using imaging plates is high providing a wide dynamic linear range of four decades. In addition, exposure times can be reduced to one-tenth of conventional X-ray film exposure times (Knol et al. 2008). PSL autoradiography combined with TLC has several advantages over radio high-performance liquid chromatography (radioHPLC) in radiometabolite analyses. By using the radioTLC method, several samples can be applied on the same TLC plate, and can be developed and analyzed simultaneously without decay corrections (Klebovich et al. 1997, Haaparanta et al. 2006). In addition, all the radioactive material is visible on TLC plate, while some compounds may retain on the column when using radioHPLC. On the other hand, by using radioHPLC a significantly better peak resolution can be achieved. In study III, for example, the peak resolution of [^{18}F]*β*-CFT-FP and one of its metabolites on HPTLC-RP-18 plates was poor. Similar poor peak resolution was seen in study V, where the peak of a very polar metabolite of [^{18}F]FMe-McN probably was comprised of more than one metabolite.

6.4.2. In vitro, ex vivo and in vivo methods

In vitro binding studies provide information regarding ligand affinity, selectivity and the density of binding sites, as well as the localization of the binding sites, if *in vitro* studies are performed using tissue sections. The binding step can be modified for a variety of purposes; *e.g.* by adding excess unlabelled ligand during the binding step the pharmacological specificity, selectivity and pharmacokinetics of the radioligand can be determined. Because chemically or physically inappropriate environments (concentrations, salts, fixatives, pH, temperature, etc.) in *in vitro* studies can significantly alter the binding affinity of a radioligand, the experimental procedures and methods should be carefully optimized. As a consequence, the results from *in vitro* studies in the literature are not necessarily comparable with each other. *In vitro* methods were used in study IV to estimate the relative displacing potencies of fluoxetine, GBR12909 and nisoxetine in the binding of [^{18}F]FMe-McN.

Biodistribution studies *ex vivo* provide the distribution of the total radioactivity including potential metabolites at a certain time point in different organs and tissues, usually as %ID/g of tissue. *Ex vivo* examination of animals pre-treated with selective and competing drugs prior to radioligand injection demonstrates the specificity and selectivity of a radioligand both in brain sections and tissue samples. The binding of radioligands and other drugs occurs *in vivo*, but the measurements of the radioactivity *ex vivo* offer a better spatial resolution with PSL autoradiography as compared to *in vivo* PET imaging, particularly in brain studies. Biodistribution data from animals can also be used for the computerized prediction of dosimetry for human PET studies.

Differences between *in vitro*, *ex vivo* and *in vivo* binding have been demonstrated for many ligands. The radioligand binding to membrane homogenates or tissue sections *in vitro*, reflecting both plasma membrane and intracellular binding sites, is usually less implicated than receptor binding *in vivo*, reflecting functional binding sites on the surface of plasma membranes. The discrepancy between mRNA or protein contents, determined by *in situ* or *in vitro* methods and binding activity *in vivo,* could be related to neural interactions in the intact, living organisms that are under a dynamic regulation including posttranslational modifications, compensatory changes, changes in conformational states of the receptors, trafficking, and recycling of the binding sites.

The greatest advantage of PET is its potential to non-invasively image and study biochemical processes *in vivo* without altering or affecting the homeostasis or the biochemical process under investigation in any way. Using the computed tomography (CT) or magnetic resonance imaging (MRI) together with PET imaging, the anatomical localization of the radioactivity accumulation can be verified and analysed. An advantage of animal PET imaging is that the same animal can be used several times, *e.g.* during a progression of a disease or for following up the curing process. However, animals are usually anaesthetized during a PET study and several anaesthetics,

including ketamine, have been reported to change the binding properties of radioligands. *E.g.* in a monkey PET study, ketamine increased the binding of both [^{11}C]*β*-CFT and [^{11}C]*β*-CIT-FE in a dose-dependent manner, and the binding equilibrium in the STR was also reached significantly faster as compared to the conscious state (Tsukada et al. 2001). Therefore, the effects of anaesthetics must be taken into account when comparing data from *ex vivo* (usually without anaesthetics) and *in vivo* studies.

6.5. Future directions

The main goal of this study was to evaluate two new radioligands, [^{18}F]*β*-CFT-FP and [^{18}F]FMe-McN, as PET tracers for DAT and SERT, respectively, in rats. Both of the novel tracers are suitable, but not ideal tracers for PET imaging. Therefore, although several suitable PET tracers for monoamine transporters have been developed, further improvement of the physical (*i.e.* SA), chemical as well as the biological properties of the tracer candidates is still needed.

Currently, a small animal PET/CT scanner (Siemens Inveon) is available at Turku PET Centre and in the future it will be a complementary and powerful tool for providing information, especially about the kinetics and biodistribution of the radioligands. Additionally, several knock-out animal models are now available for evaluation of novel radiotracers, *e.g.* for verification of the specificity and selectivity of tracers. They can also be used in studies of the physiological significance of monoamine transporters as well as in drug development using PET tracers. At present and maybe more in the future, a fruitful collaboration with pharmaceutical companies might provide promising lead molecules for radiolabelling at Turku PET Centre and thereby for development of novel PET tracers.

7. CONCLUSIONS

The major conclusions of the studies presented in this thesis are:

- In the rat model of unilateral PD, the striatal and nigral uptake of both [^{18}F]FDOPA and [^{18}F]*β*-CFT was sensitive in detecting nigrostriatal hypofunction, and in reflecting the number of nigral dopaminergic neurons. However, the uptake of [^{18}F]FDOPA may be more affected by compensatory changes than the uptake of [^{18}F]*β*-CFT, a DAT tracer. Thus, [^{18}F]*β*-CFT is more sensitive in detecting mild nigral lesions in rat brains.

- The substitution of a methyl group at the *N*-position of [^{18}F]*β*-CFT by an ^{18}F-labelled fluoropropyl group and the subsequent change in the position of the ^{18}F-label significantly affected the kinetics, selectivity and metabolism of the tracer. [^{18}F]*β*-CFT showed slow, irreversible-like kinetics, with a high target-to-non-target ratio, whereas [^{18}F]*β*-CFT-FP showed fast, reversible binding kinetics and a significantly lower target-to-non-target ratio. Both tracers showed specific binding to DAT sites, and [^{18}F]*β*-CFT also to NET sites. [^{18}F]*β*-CFT was more resistant to metabolic degradation, while [^{18}F]*β*-CFT-FP showed fast metabolism and was more vulnerable to *in vivo* defluorination. [^{18}F]*β*-CFT-FP is not an ideal DAT tracer, but it may be a suitable tracer for imaging human striatal DAT sites that are expressed at high densities. Although the binding kinetics of tracers is significantly faster in rats than in humans, [^{18}F]*β*-CFT-FP may reach the binding equilibrium in humans within a suitable imaging time. However, the fast metabolism and the possible entry of radiometabolites into the brain as well as its fast defluorination may be problematic. Despite its slow kinetics and ability to bind to NET sites, [^{18}F]*β*-CFT may be more suitable as a PET tracer for clinical PET imaging of DAT.

- [^{18}F]FMe-McN showed appropriate biodistribution in rats, a high SERT selectivity with negligible DAT and NET affinity, and high target-to-non-target ratios, but relatively slow kinetics and fast metabolism in rats. However, [^{18}F]FMe-McN shows potential for the imaging and quantification of SERT sites. Although the brain is a sexually dimorphic organ, no differences were found between genders in the binding of [^{18}F]FMe-McN *ex vivo* in the rat brain. Differences in the ^{18}F-radioactivity content in peripheral organs may indicate higher SERT activity in male rats or differences between genders in the kinetics of [^{18}F]FMe-McN.

8. ACKNOWLEDGEMENTS

This work was carried out at the MediCity Research Laboratory/PET Preclinical Imaging Laboratory of the Turku PET Centre, University of Turku.

I express my appreciation to Professor Jaakko Hartiala, Head of the Department of Clinical Physiology and Nuclear Medicine, for giving me the opportunity to undertake this work. I am most grateful to Professor Juhani Knuuti, Director of the Turku PET Centre, for providing me with the opportunity to perform these studies and for creating excellent working facilities and an inspiring atmosphere for scientific research at the Turku PET Centre. I also thank Professor Sirpa Jalkanen for providing excellent facilities and an atmosphere conducive to scientific work at the MediCity Research Laboratory.

I owe my deepest gratitude to my supervisors, Professor Olof Solin and Docent Merja Haaparanta-Solin. I warmly thank you, Olof, for introducing me to the special world of short-lived radionuclides and radiotracers. Your vast knowledge and enormous experience in the whole field of PET radiochemistry and molecular imaging, and your enthusiastic attitude towards research have inspired me in this work. I also want to warmly thank you, Merja, for teaching me in the "busy" working with short-lived radiotracers and in several theoretical and practical issues in the field of experimental animal science. I thank you also for sharing with me several other projects that have broadened my understanding of nuclear medicine.

Professor Jesper Ekelund and Dr. Anu Airaksinen, the official reviewers of this thesis, are warmly acknowledged for their valuable and constructive comments and criticism, which clearly improved the manuscript.

I would like to express my gratitude to my co-authors and collaborators for the pleasant and enthusiastic working atmosphere during these years; I especially wish to warmly thank Professor Juha Rinne for introducing me to the interesting world of brains at the Department of Neurology, University of Turku. I also want to thank Dr. Antti Haapalinna and Riitta Niemi from Orion Pharma, for providing the lesioned and pharmacologically characterized rats for study I. I wish to thank Professor Jörg Steinbach, Drs. Peter Brust, and Jörg Zessin for their excellent collaboration in the pre-clinical evaluation of [^{18}F]FMe-McN. I also want to thank Teija Koivula, Tiina Lipponen, Outi Perhola and Jouko Vepsäläinen for their collaboration in the pre-clinical evaluation of [^{18}F]β-CFT-FP. I express my warmest thanks to my co-authors at the Turku PET Centre: Jörgen Bergman, Olli Eskola, Veronica Fagerholm, Sarita Forsback, Tove Grönroos and Pertti Lehikoinen. Without your wealth of expertise in, and knowledge of, animal experiments and radiochemistry these studies could not have been performed. I am most grateful to Tarja Marttila and Marko Vehmanen for their

excellent assistance in the animal studies and to Nina Lauren, Margit Åhman-Kantola and Marja-Liisa Pakkanen for their assistance at the radiochemistry laboratory. I want to warmly thank Docent Sven-Johan Heselius, and Stefan Johansson, Per-Olof Eriksson, Erkki Stenvall and Johan Rajander for their expertise in radionuclide production.

I wish to thank Eveliina Arponen, Semi Helin, Anna Kirjavainen, Kjell Någren, Johanna Rokka, Nina Savisto, and Tapio Viljanen for sharing their experiences in the field of radiochemisty. Piritta Saipa, Riikka Purtanen, Juha and Hanna Seikkula, Miikka Lehtinen and all the personnel at the Laboratory of Radiochemistry are acknowledged for their expertise in laboratory functions, and Esa Kokkomäki, Timo Saarinen, and Simo Vauhkala for their expertise in automation and technical issues. I also warmly thank Gunilla Wikman and Pirjo Rautiainen for their excellent guidance in quality assurance issues. Marko Tättäläinen and Rami Mikkola are greatly acknowledged for their excellent support with computers, and Mirja Jyrkinen for her kind secretarial assistance. I also want to thank Docent Ulla-Marjut Jaakkola, Director of the Animal Facility of the University of Turku, and the personnel for their excellent services.

I wish to warmly thank Professor Pirjo Nuutila and Professor Heikki Minn for their enthusiasm and for providing an inspirational atmosphere for scientific research at the Turku PET Centre. I also want to thank Professors Jarmo Hietala and Anne Roivainen, and Iina Laitinen, Kirsi Virtanen and Helena Tuunanen for sharing other interesting scientific projects with me during these years. Especially, Hannu Sipilä, Pauliina Luoto, Vesa Oikonen, Chunlei Han, Mika Teräs, Tuula Tolvanen, Jarkko Johansson, all the medical laboratory technologists and radiographers, and other past and present personnel are acknowledged for the pleasant atmosphere within the TYKS-PET unit. I also want to thank all the personnel of the MediCity PET laboratories: Laura Haavisto, Tamiko Ishizu, Kirsi Mikkola, Anniina Pakkanen, Eliisa Riuttala, Jonna Sinkkonen, Leena Tokoi-Eklund and Marko Tirri, and also Elina Wiik, Pirjo Rantala, Svetlana Egutkina and Ioan Iagar. Turku Imanet, Marita Kailajärvi and Pertti Lehikoinen are acknowledged for the fruitful collaboration in several projects during the past years.

I want thank my godmother Esteri Kujansuu for her kind support during my whole life. I am most grateful to all my dear friends, especially to Kirsti, Riitta, Hellevi, Elina, Petri, Anna, Mira, Outi, Ulla, Marja-Liisa, Rita, Satu, Sirkka-Liisa, Pirkko and Sari for their friendship over many years and for sharing the good and bad days. I thank also Iiris, Liisa, Pentti, Matti and Jouko for sharing my interest in movies and all the friends in Turun Sunnuntaimaalarit ry, especially Laura, Kyllikki, Sirpa and Matti.

I owe my deepest thanks to my son Henri; you have always been the most important thing in my life. I also wish to thank your friends; young, talented musicians, especially Antti, Henri, and Vesa for innumerable enjoyable moments with jazz music.

Today, I feel myself extremely fortunate to be able to thank Henna, my daughter-in-law, for your kindness and friendship, and especially for “Jalonen”, my beloved grandchild.

This study was partly financially supported by grants from the University of Turku Foundation and the Finnish Society of Nuclear Medicine.

Turku, January 2011

Päivi Marjamäki

9. REFERENCES

Amara SG, Kuhar MJ. Neurotransmitter transporters: Recent progress. Annu Rev Neurosci 1993;16:73–93.

Andersen PH. The dopamine uptake inhibitor GBR 12909: selectivity and molecular mechanism of action. Eur J Pharmacol 1989;166:493–504.

Attali G, Weizman A, Gil-Ad I, Rehavi M. Opposite modulatory effects of ovarian hormones on rat brain dopamine and serotonin transporters. Brain Research 1997;756:153–159.

Augood SJ, Westmore K, McKenna PJ, Emson PC. Co-expression of dopamine transporter mRNA and tyrosine hydroxylase mRNA in ventral mesencephalic neurones. Mol Brain Res 1993;20:328–334.

Bannon MJ, Poosch MS, Xia Y, Goebel DJ, Cassin B, Kapatos G. Dopamine transporter mRNA content in human substantia nigra decreases precipitously with age. Proc Natl Acad Sci USA 1992;89:7095–7099.

Bannon MJ, Granneman JG, Kapatos G. The dopamine transporter. Potential involvement in neuropsychiatric disorders. In: Bloom FE, Kupfer DJ, editors. Psychopharmacology: The Fourth Generation of Progress. New York: Raven Press, Ltd., 1995;179–188.

Bannon MJ, Michelhaugh SK, Wang J, Sacchetti P. The human dopamine transporter gene: gene organisation, transcriptional regulation, and potential involvement in neuropsychiatric disorders. Eur Neuropsychopharmacol 2001;11: 449–455.

Bannon MJ. The dopamine transporter: role in neurotoxicity and human disease. Toxicol Appl Pharmacol 2005;204:355–60.

Bennett BA, Wichems CH, Hollingsworth CK, Davies HML, Thornley C, Sexton T, Childers SR. Novel 2-Substituted cocaine analogs: uptake and ligand binding studies at dopamine, serotonin and norepinephrine transport sites in the rat brain. J Pharmacol Exp Ther 1995;272:1176–1186.

Bergman J, Haaparanta M, Lehikoinen P, Solin O. Electrophilic synthesis of 6-[^{18}F]fluoro-L-DOPA starting from aqueous [^{18}F]fluoride. J Labelled Cpd Radiopharm 1994;35:476–477.

Bergman J, Lehikoinen P, Solin O. Specific radioactivity and radiochemical yield in electrophilic fluorination: Case study with [^{18}F]CFT. J Labelled Cpd Radiopharm 1997;40:38–39.

Bergman J, Solin O. Fluorine-18-labeled fluorine gas for synthesis of tracer molecules. Nucl Med Biol 1997;24:677–683.

Bergman J, Eskola O, Lehikoinen P, Solin O. Automated synthesis and purification of [^{18}F]bromofluoromethane at high specific radioactivity. Appl Radiat Isot 2001;54:927–933.

Bergström K, Halldin C, Hall H, Lundkvist C, Ginovart N, Swahn C-G, Farde L. In vitro and in vivo characterisation of nor-β-CIT: a potential radioligand for visualisation of the serotonin transporter in the brain. Eur J Nucl Med 1997;24:596–601.

Bernheimer H, Birkmayer W, Hornykiewicz O, Jellinger K, Scitelberger F. Brain dopamine and the syndromes of Parkinson and Huntington: clinical, morphological, and neurochemical correlations. J Neurol Sci 1973;20:415–455.

Berridge CW, Waterhouse BD. The locus coeruleus-noradrenergic system: modulation of behavioral state and state-dependent cognitive processes. Brain Res Rev 2003;42:33–84.

Bethea CL, Lu NZ, Gundlah C, Streicher JM. Diverse actions of ovarian steroids in the serotonin neural system. Front Neuroendocrinol 2002;23:41–100.

Blakely RD, Berson HE, Fremeau Jr RT, Caron MG, Peek MM, Prince HK, Bradley CC. Cloning and expression of a functional serotonin transporter from rat brain. Nature 1991;354:66–70.

Blakely RD, DeFelice LJ, Hartzell HC. Molecular physiology of norepinephrine and serotonin transporters. J Exp Biol 1994;196:263–281.

Blakely RD, Ramamoorthy S, Schroeter S, Qian Y, Apparsundaram S, Galli A, DeFelice LJ. Regulated phosphorylation and trafficking of antidepressant-sensitive serotonin transporter proteins. Biol Psychiatry 1998;44:169–178.

Blakely RD, Bauman AL. Biogenic amine transporters: regulation in flux. Curr Opin Neurobiol 2000;10:328–336.

Blakely RD, DeFelice LJ, Galli A. Biogenic amine neurotransmitter transporters: just when you thought you knew them. Physiology 2005;20:225–231.

Brust P, Zessin J, Kuwabara H, Pawelke B, Kretzschmar M, Hinz R, Bergman J, Eskola O, Solin O, Steinbach J, Johannsen B. Positron emission tomography imaging of the serotonin transporter in the pig brain using [^{11}C](+)-McN5652 and S-([^{18}F]fluoromethyl)-(+)-McN5652. Synapse 2003a;47:143–151.

Brust P, Hinz R, Kuwabara H, Hesse S, Zessin J, Pawelke B, Stephan H, Bergmann R, Steinbach J, Sabri O. In vivo measurement of the serotonin transporter with (S)-([^{18}F]fluoromethyl)-(+)-McN5652. Neurophychopharmacology 2003b; 28:2010–2019.

Burchett SA, Bannon MJ. Serotonin, dopamine and norepinephrine transporter mRNAs: heterogeneity of distribution and response to 'binge' cocaine administration. Mol Brain Res 1997;49:95–102.

Carroll FI, Lewin AH, Boja JW, Kuhar MJ. Cocaine receptor: biochemical characterization and structure-activity relationships of cocaine analogues at the dopamine transporter. J Med Chem 1992;35:969–981.

Carson RE, Breier A, de Bartolomeis A, Saunders RC, Su TP, Schmall B, Der MG, Pickar D, Eckelman WC. Quantification of amphetamine-induced changes in [^{11}C]raclopride binding with continuous infusion. J Cereb Blood Flow Metab 1997;17:437–447.

Chalon S, Emond P, Bodard S, Vilar M-P, Thiercelin C, Besnard J-C, Guilloteau D. Time course of changes in striatal dopamine transporters and D_2 receptors with specific iodinated markers in a rat model of Parkinson's disease. Synapse 1999;31:134–139.

Chalon S, Tarkiainen J, Garreau L, Hall H, Emond P, Vercouillie J, Farde L, Dasse P, Varnas K, Besnard J-C, Halldin C, Guilloteau D. Pharmacological characterization of *N,N*-dimethyl-2-(2-amino-4-methylphenylthio)benzylamine as a ligand of the serotonin transporter with high affinity and selectivity. J Pharmacol Exp Ther 2003;304:81–87.

Chalon S, Hall H, Saba W, Garreau L, Dollé F, Halldin C, Emond P, Bottlaender M, Deloye J-B, Helfenbein J, Madelmont J-C, Bodard S, Mincheva Z, Besnard J-C, Guilloteau D. Pharmacological characterization of (E)-N-(4-fluorobut-2-enyl)-2β-carbomethoxy-3β-(4'-tolyl) nortropane (LBT-999) as a highly promising fluorinated ligand for the dopamine transporter. J Pharmacol Exp Ther 2006;317:147–152.

Chaly T, Dhawan V, Kazumata K, Antonini A, Margouleff C, Dahl JR, Belakhlef A, Margouleff D, Yee A, Wang S, Tamagnan G, Neumeyer JL, Eidelberg D. Radiosynthesis of [^{18}F]N-3-fluoropropyl-2-β-carbomethoxy-3-β-(4-iodophenyl)nortropane and the first human study with positron emission tomography. Nucl Med Biol 1996;23:999–1004.

Chang AS, Starnes DM, Chang SM. Possible existence of quaternary structure in the high-affinity serotonin transport complex. Biochem Biophys Res Commun 1998;249:416–421.

Chitneni SK, Garreau L, Cleynhens B, Evens N, Bex M, Vermaelen P, Chalon S, Busson R, Guilloteau D, Van Laere K, Verbruggen A, Bormans G. Improved synthesis and metabolic stability analysis of the dopamine transporter ligand [^{18}F]FECT. Nucl Med Biol 2008;35:75–82.

Choi S-R, Hou C, Oya S, Mu M, Kung M-P, Siciliano M, Acton PD, Kung HF. Selective in vitro and in vivo binding of [^{123}I]ADAM to serotonin transporters in rat brain. Synapse 2000;38:403–412.

Clarke RL, Daum SJ, Gambino AJ, Aceto MD, Pearl J, Levitt M, Cumiskey WR, Bogado EF. Compounds affecting the central nervous system. 4. 3β-Phenyltropane-2-carboxylic esters and analogs. J Med Chem 1973;16:1260–1267.

Cumming P, Boyes BE, Martin WR, Adam M, Grierson J, Ruth T, McGeer EG. The metabolism of [^{18}F]6-Fluoro-L-3,4-dihydroxyphenylalanine in the hooded rat. J Neurochem 1987;48:601–608.

D´Amato RJ, Largent BL, Snowman AM, Snyder SH. Selective labeling of serotonin uptake sites in rat brain by [^{3}H]citalopram contrasted to labeling of multiple sites by [^{3}H]imipramine. J Pharmacol Exp Ther 1987;242:364–371.

Dannals RF, Ravert HT, Wilson AA, Scheffel U, Frost JJ, Wagner HN Jr. Synthesis of a radiotracer for studying serotonin uptake sites: carbon-11 labeled N-methylparoxetine. J Labelled Cpd Radiopharm 1989;26(Suppl 1):205–206.

Das MK, Mukherjee J. Radiosynthesis of [F-18]fluoxetine as a potential radiotracer for serotonin reuptake sites. Appl Radiat Isot 1993;44:835–842.

Davis MR, Votaw JR, Bremner JD, Byas-Smith MG, Faber TL, Voll RJ, Hoffman JM, Grafton ST, Kilts CD, Goodman MM. Initial human PET imaging studies with the dopamine transporter ligand ^{18}F-FECNT. J Nucl Med 2003;44:855–861.

Ding Y-S, Lin K-S, Logan J, Benveniste H, Carter P. Comparative evaluation of positron emission tomography radiotracers for imaging the norepinephrine transporter: (S,S) and (R,R) enantiomers of reboxetine analogs ([^{11}C]-methylreboxetine, 3-Cl-[^{11}C]methylreboxetine and [^{18}F]fluororeboxetine), (R)-[^{11}C]nisoxetine, [^{11}C]oxaprotiline and [^{11}C]lortalamine. J Neurochem 2005;94:337–351.

Ding Y-S, Singhal T, Planeta-Wilson B, Gallezot J-D, Nabulsi N, Labaree D, Ropchan J, Henry S, Williams W, Carson RE, Neumeister A, Malison RT. PET imaging of the effects of age and cocaine on the norepinephrine transporter in the human brain using (S,S)-[^{11}C]O-methylreboxetine and HRRT. Synapse 2010;64:30–38.

Dollé F, Emond P, Hinnen F, Mavel S, Mincheva Z, Saba S, Valette H, Chalon S, Halldin C, Legailliard J, Madelmont J-C, Deloye J-B, Bottlaender M, Guilloteau D. Radiosynthesis of [^{18}F]LBT-999, a selective radioligand for the visualisation of the dopamine transporter with PET. J Labelled Cpd Radiopharm 2005;48(Suppl 1):S180.

Drewes B, Sihver W, Willbold S, Olsson RA, Coenen HH. New 2α-tropane amides as potential PET ligands for the dopamine transporter. Nucl Med Biol 2007;34:531–539.

Duncan GE, Little KY, Kirkman JA, Kaldas RS, Stumpf WE, Breese GR. Autoradiographic characterization of [^{3}H]imipramine and [^{3}H]citalopram binding in rat and human brain: species differences and relationships to serotonin innervation patterns. Brain Res 1992;591:181–197.

Eisenhofer G. The role of neuronal and extraneuronal plasma membrane transporters in the inactivation of peripheral catecholamines. Pharmacol Therapeutics 2001;91:35–62.

Eisenhofer G, Kopin IJ, Goldstein DS. Catecholamine metabolism: a contemporary view with implications for physiology and medicine. Pharmacol Rev 2004;56:331–349.

Elfving B, Bjørnholm B, Ebert B, Knudsen GM. Binding characteristics of selective serotonin reuptake inhibitors with relation to emission tomography studies. Synapse 2001;41:203–211.

Emond P, Garreau L, Chalon S, Boazi M, Caillet M, Bricard J, Frangin Y, Mauclaire L, Besnard J-L, Guilloteau D. Synthesis and ligand binding of nortropane derivatives: N-substituted 2β-carbomethoxy-3β-(4′-iodophenyl)nortropane and N-(3-iodoprop-(2E)-enyl)-2β-carbomethoxy-3β-(3′,4′-disubstituted phenyl)nortropane. New high-affinity and selective compounds for the dopamine transporter. J Med Chem 1997;40:1366–1372.

Emond P, Vercouillie J, Innis R, Chalon S, Mavel S, Frangin Y, Halldin C, Besnard J-C, Guilloteau D. Substituted diphenyl sulfides as selective serotonin transporter ligands: synthesis and *in vitro* evaluation. J Med Chem 2002;45:1253–1258.

Endres CJ, Carson RE. Assessment of dynamic neurotransmitter changes with bolus or infusion delivery of neuroreceptor ligands. J Cereb Flow Metab 1998;18:1196–1210.

Eskola O, Bergman J, Lehikoinen P, Ögren M, Långström B, Solin O. Synthesis of ^{18}F-bromofluoromethane [^{18}F]FCH_2Br; Fluoromethylation reagent with high specific radioactivity. J Labelled Cpd Radiopharm 1999;42(Suppl 1):S543–545.

Ettlinger DE, Häusler D, Wadsak W, Girschele F, Sindelar KM, Mien L-K, Ungersböck J, Viernstein H, Kletter K, Dudczak R, Mitterhauser M. Metabolism and autoradiographic evaluation of [^{18}F]FE@CIT: a comparison with [^{123}I]β-CIT and [^{123}I]FP-CIT. Nucl Med Biol 2008;35:475–479.

Farde L, Eriksson L, Blomquist G, Halldin C. Kinetic analysis of central [^{11}C]raclopride binding to D_2-dopamine receptors studied by PET – a comparison to the equilibrium analysis. J Cereb Blood Flow Metab 1989;9:696–708.

Farde L, Halldin C, Müller L, Suhara T, Karlsson P, Hall H. PET study of [^{11}C]β-CIT binding to monoamine transporters in the monkey and human brain. Synapse 1994;16:93–103.

Firnau G, Nahmias C, Garnett S. The preparation of [^{18}F]5-fluoro-DOPA with reactor-produced fluorine-18. Int J Appl Radiat Isot 1973; 24:182–184.

Firnau G, Sood S, Chirakal R, Nahmias C, Garnett ES. Cerebral metabolism of 6-[^{18}F]fluoro-L-3,4-dihydroxyphenylalanine in the primate. J Neurochem 1987;48:1077–1082.

Firnau G, Chen JJ, Murthy D. N-[^{18}F]fluoroalkyl-CFT: synthesis and cerebral distribution. J Labelled Cpd Radiopharm 1995;37(Suppl 1):55–57.

Fischman AJ, Bonab AA, Babich JW, Livni E, Alpert NM, Meltzer PC, Madras BK. [^{11}C/^{127}I]Altropane: a highly selective ligand for PET imaging of dopamine transporter sites. Synapse 2001;39:332–342.

Frankle WG, Huang Y, Hwang D-R, Talbot PS, Slifstein M, Van Heertum R, Abi-Dargham A, Laruelle M. Comparative evaluation of serotonin transporter radioligands ^{11}C-DASB and ^{11}C-McN 5652 in healthy humans. J Nucl Med 2004;45: 682–694.

Frazer A, Hensler JG. Serotonin. In GJ Siegel (editor), Basic neurochemistry: Molecular, cellular and medical aspects, 6th ed. Philadelphia: Lippincott-Raven Publishers, 1999, pp 263–292.

Gether U, Andersen PH, Larsson OM, Schousboe A. Neurotransmitter transporters: molecular function of important drug targets. Trends Pharmacol Sci 2006;27:375–383.

Gifford AN, Gatley SJ, Volkow ND. Evaluation of the importance of rebinding to receptors in slowing the approach to equilibrium of high-affinity PET and SPECT radiotracers. Synapse 1998;28:167–175.

Goodman MM, Keil R, Shoup TM, Eshima D, Eshima L, Kilts C, Votaw J, Camp VM, Votaw D, Smith E, Kung M-P, Malveaux E, Watts R, Huerkamp M, Wu D, Garcia E, Hoffman JM. Fluorine-18-FPCT: a PET radiotracer for imaging

dopamine transporters. J Nucl Med 1997;38:119–126.

Goodman MM, Kilts CD, Keil R, Shi B, Martarello L, Xing D, Votaw J, Ely TD, Lambert P, Owens MJ, Camp VM, Malveaux E, Hoffman JM. ^{18}F-Labeled FECNT: a selective radioligand for PET imaging of brain dopamine transporters. Nucl Med Biol 2000;27:1–12.

Gundlah C, Simon LD, Auerbach SB. Differences in hypothalamic serotonin between estrous phases and gender: an in vivo microdialysis study. Brain Res 1998;785:91–96.

Haaparanta M, Bergman J, Laakso A, Hietala J, Solin O. [^{18}F]CFT ([^{18}F]WIN 35,428), a radioligand to study the dopamine transporter with PET: biodistribution in rats. Synapse 1996; 23:321–327.

Haaparanta M, Grönroos T, Marjamäki P, Eskola O, Bergman J, Paul R, Solin O. In vivo sampling for pharmacokinetic studies in small experimental animals: a combination of microdialysis, planar chromatography and digital autoradiography. Mol Imag Biol 2004;6:27–33.

Haaparanta M, Grönroos T, Eskola O, Bergman J, Solin O. Planar chromatographic analysis and quantification of short-lived radioactive metabolites from microdialysis fractions. J Chromatogr A 2006;1108:136–139.

Hahn MK, Blakely RD. Monoamine transporter gene structure and polymorphisms in relation to psychiatric and other complex disorders. Pharmacogenomics J 2002;2:217–253.

Hahn MK, Robertson D, Blakely RD. A mutation in the human norepinephrine transporter gene (SLC6A2) associated with orthostatic intolerance disrupts surface expression of mutant and wild-type transporters. J Neurosci 2003;23:4470–4478.

Haka MS, Kilbourn MR. Synthesis and regional mouse brain distribution of [^{11}C]nisoxetine, a norepinephrine uptake inhibitor. Int J Rad Appl Instrum B 1989;16:771–774.

Halldin C, Farde L, Lundkvist C, Ginovart N, Nakashima Y, Karlsson P, Swahn C-G. [^{11}C]β-CIT-FE, a radioligand for quantitation of the dopamine transporter in the living brain using positron emission tomography. Synapse 1996;22:386–390.

Halldin C, Gulyás B, Langer O, Farde L. Brain radioligands – state of the art and new trends. Q J Nucl Med 2001;45:139–152.

Halldin C, Erixon-Lindroth N, Pauli S, Chou Y-H, Okubo Y, Karlsson P, Lundkvist C, Olsson H, Guilloteau D, Emond P, Farde L. [^{11}C]PE2I: a highly selective radioligand for PET examination of the dopamine transporter in monkey and human brain. Eur J Nucl Med Mol Imaging 2003; 30:1220–1230.

Halldin C, Lundberg J, Sóvágó J, Gulyás B, Guilloteau D, Vercouillie J, Emond P, Chalon S, Tarkiainen J, Hiltunen J, Farde L. [^{11}C]MADAM, a new serotonin transporter radioligand characterized in the monkey brain by PET. Synapse 2005;58:173–183.

Hallikainen T, Saito T, Lachman HM, Volavka J, Pohjalainen T, Ryynänen O-P, Kauhanen J, Syvälahti E, Hietala J, Tiihonen J. Association between low activity serotonin transporter promoter genotype and early onset alcoholism with habitual impulsive violent behavior. Mol Psychiatry 1999;4:385–388.

Hansson SR, Mezey É, Hoffman BJ. Serotonin transporter messenger RNA in the developing rat brain: early expression in the serotonergic neurons and transient expression in non-serotonergic neurons. Neurosci 1998;83:1185–1201.

Harada N, Ohba H, Fukumoto D, Kakiuchi T, Tsukada H. Potential of [^{18}F]β-CFT-FE (2β-carbomethoxy-3β-(4-fluorophenyl)-8-(2-[^{18}F]fluoroethyl)nortropane) as a dopamine transporter ligand: a PET study in the conscious monkey brain. Synapse 2004;54:37–45.

Heikkila RE, Manzino L. Behavioral properties of GBR 12909, GBR 13069 and GBR 13098: specific inhibitors of dopamine uptake. Eur J Pharmacol 1984;103:241–248.

Helfenbein J, Sandell J, Halldin C, Chalon S, Emond P, Okubo Y, Chou Y-H, Frangin Y, Douziech L, Gareau L, Swahn C-G, Besnard J-C, Farde L, Guilloteau D. PET examination of three potent cocaine derivatives as specific radioligands for the serotonin transporter. Nucl Med Biol 1999;26:491–499.

Hirschfeld RM. History and evolution of the monoamine hypothesis of depression. J Clin Psychiatry 2000;61, Suppl 6:4-6.

Hirvonen J, Johansson J, Teräs M, Oikonen V, Lumme V, Virsu P, Roivainen A, Någren K, Halldin C, Farde L, Hietala J. Measurement of striatal and extrastriatal dopamine transporter binding with high-resolution PET and [^{11}C]PE2I: quantitative modeling and test-retest reproducibility. J Cereb Blood Flow Metab 2008;1:1–11.

Ho H-P, Olsson M, Westberg L, Melke J, Eriksson E. The serotonin reuptake inhibitor fluoxetine reduces sex steroid-related aggression in female rats: An animal model of premenstrual irritability? Neuropsychopharmacology 2001;24:502–510.

Hoffman BJ, Mezey E, Brownstein MJ. Cloning of a serotonin transporter affected by antidepressants. Science 1991;254:579–580.

Hoffman BJ, Hansson SR, Mezey É, Palkovits M. Localization and dynamic regulation of biogenic amine transporters in the mammalian central nervous system. Front Neuroendocrinol 1998;19:187–231.

Honer M, Hengerer B, Blagoev M, Hintermann S, Waldmeier P, Schubiger PA, Ametamey SM. Comparison of [^{18}F]FDOPA, [^{18}F]FMT and [^{18}F]FECNT for imaging dopaminergic neurotransmission in mice. Nucl Med Biol 2006;33:607–614.

Houle S, Ginovart N, Hussey D, Meyer JH, Wilson AA. Imaging the serotonin transporter with positron emission tomography: initial human studies with [^{11}C]DAPP and [^{11}C]DASB. Eur J Nucl Med 2000;27:1719–1722.

Hrdina PD, Foy B, Hepner A, Summers RJ. Antidepressant binding sites in brain: Autoradiographic comparison of [^{3}H]paroxetine and [^{3}H]imipramine localization and relationship to serotonin transporter. J Pharmacol Exp Ther 1990;252:410–418.

Hsu SM, Raine L. Protein A, avidin and biotin in immunohistochemistry. J Histochem Cytochem 1981;29:349–353.

Hsu SM, Raine L, Fanger H. Use of avidin-biotin-peroxidase complex (ABC) in immunoperoxidase techniques: a comparison between ABC and unlabeled antibody (PAP) procedures. J Histochem Cytochem 1981;29:577–580.

Huang Y, Hwang D-R, Narendran R, Sudo Y, Chatterjee R, Bae S-A, Mawlawi O, Kegeles LS, Wilson AA, Kung HF, Laruelle M. Comparative evaluation in nonhuman primates of five PET radiotracers for imaging the serotonin transporters: [^{11}C]McN5652, [^{11}C]ADAM, [^{11}C]DASB, [^{11}C]DAPA, and [^{11}C]AFM. J Cereb Blood Flow Metab 2002;22:1377–1398.

Huang Y, Narendran R, Bae S-A, Erritzoe D, Guo N, Zhu Z, Hwang D-R, Laruelle D. A PET imaging agent with fast kinetics: synthesis and *in vivo* evaluation of the serotonin transporter ligand [^{11}C]2-[2-dimethylaminomethylphenylthio)]-5-fluorophenylamine ([^{11}C]AFA). Nucl Med Biol 2004;31:727–738.

Hudson JL, van Horne CG, Strömberg I, Brock S, Clayton J, Masserano J, Hoffer BJ, Gerhardt GA. Correlation of apomorphine- and amphetamine-induced turning with nigrostriatal dopamine content in unilateral 6-hydroxydopamine lesioned rats. Brain Res 1993;626:167–174.

Hume SP, Pascali C, Pike VW, Turton DR, Ahier RG, Myers R, Bateman DM, Cremer JE, Manjil LG, Dolan R. Citalopram: labelling with carbon-11 and evaluation in rat as a potential radioligand for in vivo studies of 5-HT re-uptake sites. Nucl Med Biol 1991;18:339–351.

Ito Y, Fujita M, Shimada S, Watanabe Y, Okada T, Kusuoka H, Tohyama M, Nishimura T. Comparison between the decrease of dopamine transporter and that of L-DOPA uptake for detection of early to advanced stage of Parkinson's disease in animal models. Synapse 1999;31:178–185.

Iversen L. Neurotransmitter transporters and their impact on the development of psychopharmacology. Br J Pharm 2006;147:S82–S88.

Jacobs BL, Azmitia EC. Structure and function of the brain serotonin system. Physiol Rev 1992;72:165–229.

Jarkas N, Votaw JR, Voll RJ, Williams L, Camp VM, Owens MJ, Purselle DC, Bremner JD, Kilts CD, Nemeroff CB, Goodman MM. Carbon-11 HOMADAM: A novel PET radiotracer for imaging serotonin transporters. Nucl Med Biol 2005; 32:211–224.

Jarkas N, Voll RJ, Williams L, Votaw JR, Owens M, Goodman MM. Synthesis and *in vivo* evaluation of halogenated *N,N*-dimethyl-2-(2'-amino-4'-hydroxymethylphenylthio)benzylamine derivatives as PET serotonin transporter ligands. J Med Chem 2008;51:271–281.

Jayanthi LD, Ramamoorthy S. Regulation of monoamine transporters: influence of psychostimulants and therapeutic antidepressants. AAPS J 2005;7:E728–738.

Jin C, Navarro HA, Page K, Carroll FI. Synthesis and monoamine transporter binding properties of 2β-[3'-(substituted benzyl)isoxazol-5-yl]- and 2β-[3'-methyl-4'-(substituted phenyl)isoxazol-5-yl]-3β-(substituted phenyl)tropanes. Bioorg Med Chem 2008a;16:6682–6688.

Jin C, Navarro HA, Carroll FI. Development of 3-phenyltropane analogues with high affinity for the dopamine and serotonin transporters and low affinity for the norepinephrine transporter. J Med Chem 2008b;51:8048–8056.

Joyce JN, Smutzer G, Whitty CJ, Myers A, Bannon MJ. Differential modification of dopamine transporter and tyrosine hydroxylase mRNAs in midbrain of subjects with Parkinson's, Alzheimer's with parkinsonism, and Alzheimer's disease. Mov Disord 1997;12:885–897.

Kaakkola S, Teräväinen H. Animal models of Parkinsonism. Pharmacol Toxicol 1990;67:95–100.

Kazumata K, Dhawan V, Chaly T, Antonini A, Margouleff C, Belakhlef A, Neumeyer J, Eidelberg D. Dopamine transporter imaging with fluorine-18-FPCIT and PET. J Nucl Med 1998;39:1521–1530.

Kilbourn MR, Haka MS, Mulholland GK, Jewett DM, Kuhl DE. Synthesis of radiolabeled inhibitors of presynaptic monoamine uptake systems: [^{18}F]GBR-13119 (DA), [^{11}C]nisoxetine (NE) and [^{11}C]fluoxetine (5-HT). J Labelled Cpd Radiopharm 1989;26:412–414.

Kilbourn MR. Fluorine-I8 labeling of radiopharmaceuticals. Nuclear Science Series no. NAS-NS-3203. National Academy Press, Washington, DC, USA, 1990.

Kitayama S, Dohi T. Cellular and molecular aspects of monoamine neurotransmitter transporters. Jpn J Pharmacol 1996;72:195–208.

Klebovich I, Szúnyog J, Hazai I. TLC-DAR for the analysis of biological samples. A newly developed rapid tool for studying drug metabolism. J Planar Chromatogr 1997;10:399–405.

Knol RJJ, de Bruin K, de Jong J, van Eck-Smit BLF, Booij J. In vitro and ex vivo storage phosphor imaging of short-living radioisotopes. J Neurosci Meth 2008;168:341–357.

Kocabas AM, Rudnick G, Kilic F. Functional consequences of homo- but not hetero-oligomerization between transporters for the biogenic amine neurotransmitters. J Neurochem 2003;85:1513–1520.

Koivula T, Perhola O, Kämäräinen E-L, Lipponen T, Vepsäläinen J, Solin O. Simplified synthesis of N-(3-[^{18}F]fluoropropyl)-2β-carbomethoxy-3β-(4-fluorophenyl)nortropane ([^{18}F]β-CFT-FP) using [^{18}F]fluoropropyl tosylate as the labelling reagent. J Labelled Cpd Radiopharm 2005;48:463–471.

Krajnak K, Rosewell KL, Duncan MJ, Wise PM. Aging, estradiol and time of day differentially affect serotonin transporter binding in the central nervous system of female rats. Brain Res 2003;990:87–94.

Kretzschmar M, Brust P, Zessin J, Cumming P, Bergmann R, Johannsen B. Autoradiographic imaging of the serotonin transporter in the brain of rats and pigs using S-([^{18}F]fluoromethyl)-(+)-McN5652. European Neuropsychopharmacology 2003;13:387–397.

Kuhar MJ, Couceyro PR, Lambert PD. Catecholamines. In: Siegel GJ, Agranoff BW, Albers RW, et al., editors. Basic neurochemistry: Molecular, cellular and medical aspects, 6th edition. Philadelphia: Lippincott-Raven Publishers, 1999, pp 243–262.

Kämäräinen E-L, Kyllönen T, Lundkvist C, Hall H, Bergström K, Yu M, Någren K, Sandell J, Airaksinen A, Vepsäläinen J, Hiltunen J, Jaakkola T, Halldin C. Labeling of the dopamine transporter ligand β-CFT-FP with^{18}F or ^{11}C. J Labelled Cpd Radiopharm 1999:42(Suppl.1):S414-416.

Kämäräinen E-L, Kyllönen T, Airaksinen A, Lundkvist C, Yu M, Någren K, Sandell J, Langer O, Vepsäläinen J, Hiltunen J, Bergström K, Lötjönen S, Jaakkola T, Halldin C. Preparation of [^{18}F]β-CFT-FP and [^{11}C]β-CFT-FP, selective radioligands for visualisation of the dopamine transporter using positron emission tomography (PET). J Labelled Cpd Radiopharm 2000a; 43:1235–1244.

Kämäräinen E-L, Kyllönen T, Hall H, Lundkvist C, Bergström K, Yu M, Någren K, Sandell J, Airaksinen A, Vepsäläinen J, Tuomisto L, Hiltunen J, Jaakkola T, Halldin C. Autoradiographic examination of a new dopamine transporter radioligand, carbon-11 β-CFT-FP, in the post mortem human brain. Eur J Nucl Med 2000b;27:S1221.

Laakso A, Bergman J, Haaparanta M, Vilkman H, Solin O, Hietala J. [^{18}F]CFT ([^{18}F]WIN 35,428), a radioligand to study the dopamine transporter with PET: characterization in human subjects. Synapse 1998;28:244–250.

Laruelle M, Slifstein M, Huang Y. Relationships between radiotracer properties and image quality in molecular imaging of the brain with positron emission tomography. Mol Imaging Biol 2003;5:363–375.

Lasne M-C, Pike VW, Turton DR. The radiosynthesis of [N-methyl-^{11}C]-sertraline. Appl Radiat Isot 1989;40:147–151.

Lau T, Horschitz S, Berger S, Bartsch D, Schloss P. Antidepressant-induced internalization of the serotonin transporter in serotonergic neurons. FASEB J 2008;22:1702–1714.

Lee C, Samii A, Sossi V, Ruth T, Schulzer M, Holden J, Wudel J, Pal P, Fuente-Fernandez R, Calne D, Stoessl A. In vivo positron emission tomographic evidence for compensatory changes in presynaptic dopaminergic nerve terminals in Parkinson's disease. Ann Neurol 2000;47:493–503.

Lee BS, Chu S, Lee KC, Lee B-S, Chi DY, Choe YS, Kim SE, Song YS, Jin C. Syntheses and binding affinities of 6-nitroquipazine analogues for serotonin transporter: Part 3. A potential 5-HT transporter imaging agent, 3-(3-[^{18}F]fluoropropyl)-6-nitroquipazine. Bioorg Med Chem 2003;11: 4949–4958.

Lesch KP, Aulakh CS, Wolozin BL, Tolliver TJ, Hill JL, Murphy DL. Regional brain expression of serotonin transporter mRNA and its regulation by

reuptake inhibiting antidepressants. Mol Brain Res 1993;17:31–35.

Li Q, Ma L, Innis RB, Seneca N, Ichise M, Huang H, Laruelle M, Murphy DL. Pharmacological and genetic characterization of two selective serotonin transporter ligands: 2-[2-(dimethylaminomethylphenylthio)]-5-fluoromethylphenylamine (AFM) and 3-amino-4-[2-(dimethylaminomethylphenylthio)]benzonitrile (DASB). J Pharmacol Exp Ther 2004;308:481–486.

Lin K-J, Ye X-X, Yen T-C, Wey S-P, Tzen K-Y, Ting G, Hwang J-J. Biodistribution study of [^{123}I] ADAM in mice: correlation with whole body autoradiography. Nucl Med Biol 2002;29:643–650.

Lorang D, Amara SG, Simerly RB. Cell-type-specific expression of catecholamine transporters in the rat brain. J Neurosci 1994;14:4903–4914.

Lundkvist C, Halldin C, Swahn C-G, Hall H, Karlsson P, Nakashima Y, Wang S, Milius RA, Neumeyer JL, Farde L. [O-Methyl-^{11}C]β-CIT-FP, a potential radioligand for quantitation of the dopamine transporter: preparation, autoradiography, metabolite studies, and positron emission tomography examinations. Nucl Med Biol 1995;22:905–913.

Lundkvist C, Halldin C, Ginovart N, Swahn C-G, Farde L. [^{18}F]β-CIT-FP is superior to [^{11}C]β-CIT-FP for quantitation of the dopamine transporter. Nucl Med Biol 1997;24:621–627.

Lundkvist C, Loc´h C, Halldin C, Bottlaender M, Ottaviani M, Coulon C, Fuseau C, Mathis C, Farde L, Mazierè B. Characterization of bromine-76-labelled 5-bromo-6-nitroquipazine for PET studies of the serotonin transporter. Nucl Med Biol 1999; 26:501–507.

Mach RH, Nader MA, Ehrenkaufer RL, Gage HD, Childers SR, Hodges LM, Hodges MM, Davies HML. Fluorine-18-labeled tropane analogs for PET imaging studies of the dopamine transporter. Synapse 2000;37:109–117.

Mamounas LA, Mullen CA, O'Hearn E, Molliver ME. Dual serotoninergic projections to forebrain in the rat: morphologically distinct 5-HT axon terminals exhibit differential vulnerability to neurotoxic amphetamine derivatives. J Comp Neurol 1991;314:558–586.

Maryanoff BE, McComsey DF, Constanzo MJ, Setler PE, Gardocki JF, Shank RP, Schneider CR. Pyrroloisoquinoline antidepressants: enantioselective inhibition of tetrabenazine-induced ptosis and neuronal uptake of norepinephrine, dopamine and serotonin. J Med Chem 1984;27:943–946.

Masson J, Sagné C, Hamon M, El Mestikawy S. Neurotransmitter transporters in the central nervous system. Pharmacol Rev 1999;51:439–464.

Maswood S, Truitt W, Hotema M, Caldaroda-Pastuszka M, Uphouse L. Estrous cycle modulation of extracellular serotonin in mediobasal hypothalamus: role of the serotonin transporter and terminal autoreceptors. Brain Res 1999;831:146–154.

Mavel S, Vercouillie J, Garreau L, Raguza T, Rawna AW, Chalon S, Guilloteau D, Emond P. Docking study, synthesis, and in vitro evaluation of fluoro-MADAM derivatives as SERT ligands for PET imaging. Bioorg Med Chem 2008; 16:9050–9055.

McEwen BS. Permanence of brain sex differences and structural plasticity of the adult brain. Proc Natl Acad Sci 1999;96:7128–7130.

McEwen BS. Genome and hormones: gender differences in physiology. Invited review: Estrogens effects on the brain: multiple sites and molecular mechanisms. J Appl Physiol 2001;91:2785–2801.

McQueen JK, Wilson H, Fink G. Estradiol-17β increases serotonin transporter (SERT) mRNA levels and the density of SERT-binding sites in female rat brain. Mol Brain Res 1997;45:13–23.

Meister B, Johnson H, Ulfhake B. Increased expression of serotonin transporter messenger RNA in raphe neurons of the aged rat. Mol Brain Res 1995;33:87–96.

Melchitzky DS, Lewis DA. Tyrosine hydroxylase- and dopamine transporter-immunoreactive axons in the primate cerebellum. Evidence for a lobular- and laminar-specific dopamine innervation. Neuropsychopharmacology 2000;22:466–472.

Meltzer PC, Liang AY, Brownell A-L, Elmaleh DR, Madras BK. Substituted 3-phenyltropane analogs of cocaine: synthesis, inhibition of binding at cocaine recognition sites, and positron emission tomography imaging. J Med Chem 1993;36:855–862.

Miller GM, Yatin SM, De La Garza II R, Goulet M, Madras BK. Cloning of dopamine, norepinephrine and serotonin transporters from monkey brain: relevance to cocaine sensitivity. Mol Brain Res 2001;87:124–143.

Mitterhauser M, Wadsak W, Mien L-K, Hoepping A, Viernstein H, Dudczak R, Kletter K. Synthesis and biodistribution of [^{18}F]FE@CIT, a new potential tracer for the dopamine transporter. Synapse 2005;55:73–79.

Moll GH, Mehnert C, Wicker M, Bock N, Rothenberger A, Rűther E, Huether G. Age-associated changes in the densities of presynaptic monoamine transporters in different regions of the

rat brain from early juvenile life to late adulthood. Dev Brain Res 2000;119:251–257.

Morón JA, Brockington A, Wise RA, Rocha BA, Hope BT. Dopamine uptake through the norepinephrine transporter in brain regions with low levels of the dopamine transporter: evidence from knock-out mouse lines. J Neurosci 2002;22:389–395.

Mortensen OV, Kristensen AS, Rudnick G, Wiborg O. Molecular cloning, expression and characterization of a bovine serotonin transporter. Brain Res Mol Brain Res 1999;71:120–126.

Mortensen OV, Larsen MB, Prasad BM, Amara SG. Genetic complementation screen identifies a mitogen-activated protein kinase phosphatase, MKP3, as a regulator of dopamine transporter trafficking. Mol Biol Cell 2008;19:2818–2829.

Murphy DL, Lerner A, Rudnick G, Lesch K-P. Serotonin transporter: gene, genetic disorders and pharmacogenetics. Molecular Interventions 2004;4:109–123.

Müller L, Halldin C, Farde L, Karlsson P, Hall H, Swahn C-G, Neumeyer J, Gao Y, Milius R. [^{11}C]β-CIT, a cocaine analogue. Preparation, autoradiography and preliminary PET investigations. Nucl Med Biol 1993;20:249–255.

Namavari M, Bishop A, Satyamurthy N, Bida G, Barrio JR. Regioselective radiofluorodestannylation with [^{18}F]F_2 and [^{18}F]CH_3COOF: a high yield synthesis of 6-[^{18}F]Fluoro-L-dopa. Int J Rad Appl Instrum A 1992;43:989–996.

Neumeyer JL, Wang S, Gao Y, Milius RA, Kula NS, Campbell A, Baldessarini RJ, Zea-Ponce Y, Baldwin RM, Innis RB. N-ω-fluoroalkyl analogs of (1R)-2β-carbomethoxy-3β-(4-iodophenyl)-tropane (β-CIT): radiotracers for positron emission tomography and single photon emission computed tomography imaging of dopamine transporters. J Med Chem 1994;37:1558–1561.

Nickels RJ, Hichwa RD, Daube ME. An ^{18}O target for the high yield production of ^{18}F fluoride. Int J Appl Rad Isotop 1983;34:625–629.

Nirenberg MJ, Vaughan RA, Uhl GR, Kuhar MJ, Pickel VM. The dopamine transporter is localized to dendritic and axonal plasma membranes of nigrostriatal dopaminergic neurons. J Neurosci 1996;16:436–447.

Nirenberg MJ, Chan J, Pohorille A, Vaughan RA, Uhl GR, Kuhar MJ, Pickel VM. The dopamine transporter: comparative ultrastructure of dopaminergic axons in limbic and motor compartments of the nucleus accumbens. J Neurosci 1997a;17:6899–6907.

Nirenberg MJ, Chan J, Vaughan RA, Uhl GR, Kuhar MJ, Pickel VM. Immunogold localization of the dopamine transporter: an ultrastructural study of the rat ventral tegmental area. J Neurosci 1997b;17:5255–5262.

Okada T, Fujita M, Shimada S, Sato K, Schloss P, Watanabe Y, Itoh Y, Tohyama M, Nishimura T. Assessment of affinities of beta-CIT, beta-CIT-FE, and beta-CIT-FP for monoamine transporters permanently expressed in cell lines. Nucl Med Biol 1998;25:53–58.

Oya S, Choi S-R, Hou C, Mu M, Kung M-P, Acton PD, Siciliano M, Kung HF. 2-((2-((dimethylamino)methyl)phenyl)thio)-5-iodophenylamine (ADAM): an improved serotonin transporter ligand. Nucl Med Biol 2000;27:249–254.

Oya S, Choi SR, Coenen H, Kung HF. New PET imaging agent for the serotonin transporter: [^{18}F]ACF (2-[(2-amino-4-chloro-5-fluorophenyl)-thio]-*N,N*-dimethylbenzenmethanamine). J Med Chem 2002;45:4716–4723.

Ozaki N, Goldman D, Kaye WH, Plotnicov K, Greenberg BD, Lappalainen J, Rudnik G, Murphy DL. Serotonin transporter missense mutation associated with a complex neuropsychiatric phenotype. Mol Psychiatry 2003;8:933–936.

Parhi AK, Wang JL, Oya S, Choi S-R, Kung M-P, Kung HF. 2-(2'-((dimethylamino)methyl)-4'-(2-fluoroalkoxy)phenylthio)benzenamine derivatives as serotonin transporter imaging agents. J Med Chem 2007;50:6673–6684.

Paxinos G, Watson C. The rat brain in stereotaxic coordinates. Academic Press, Inc, New York, 1986.

Pecins-Thompson M, Brown NA, Bethea CL. Regulation of serotonin re-uptake transporter mRNA expression by ovarian steroids in rhesus macaques. Mol Brain Res 1998;53:120–129.

Piñeyro G, Blier P. Autoregulation of serotonin neurons: role in antidepressant drug action. Pharmacol Rev 1999; 51:533–591.

Plisson C, McConathy J, Martarello L, Malveaux EJ, Camp VM, Williams L, Votaw JR, Goodman MM. Synthesis, radiosynthesis, and biological evaluation of carbon-11 and iodine-123 labeled 2β-carbomethoxy-3β-[4'-((Z)-2-haloethenyl)phenyl]tropanes: candidate radioligands for in vivo imaging of the serotonin transporter. J Med Chem 2004;47:1122–1135.

Puñal-Riobóo J, Serena-Puig A, Varela-Lema L, Álvarez-Páez AM, Ruano-Ravina A. Clinical utility of 18F-DOPA-PET in movement disorders. A systematic review. Rev Esp Med Nucl 2009; 28:106–113.

Ramamoorthy S, Bauman AL, Moore KR, Han H, Yang-Feng T, Chang AS, Ganapathy V, Blakely RD. Antidepressant- and cocaine-sensitive human

serotonin transporter: Molecular cloning, expression, and chromosomal localozation. Proc Natl Acad Sci 1993;90:2542–2546.

Ravna AW, Sylte I, Dahl SG. Molecular mechanism of citalopram and cocaine interactions with neurotransmitter transporters. J Pharmacol Exp Ther 2003; 307:34–41.

Rinne JO, Bergman J, Ruottinen H, Haaparanta M, Eronen E, Oikonen V, Sonninen P, Solin O. Striatal uptake of a novel PET ligand [^{18}F]beta-CFT, is reduced in early Parkinson's disease. Synapse 1999a;31:119–124.

Rinne JO, Ruottinen H, Bergman J, Haaparanta M, Sonninen P, Solin O. Usefulness of a dopamine transporter PET ligand [^{18}F]β-CFT in assessing disability in Parkinson's disease. J Neurol Neurosurg Psychiatry 1999b;67:737–741.

Rinne J, Nurmi E, Ruottinen HM, Eskola O, Bergman J and Solin O. [^{18}F]FDOPA and [^{18}F]CFT are both sensitive PET markers to detect presynaptic dopaminergic hypofunction in early Parkinson's disease. Synapse 2001:40:193–200.

Robertson GS, Robertson HA. Evidence that L-DOPA-induced rotational behavior is dependent on both striatal and nigral mechanisms. J Neurosci 1989;9:3326–3331.

Robertson SD, Matthies HJ, Galli A. A closer look at amphetamine induced reverse transport and trafficking of the dopamine and norepinephrine transporters. Mol Neurobiol 2009;39:73–80.

Rubinow DR, Schmidt PJ, Roca CA. Estrogen-serotonin interactions: Implications for affective regulation. Biol Psychiatry 1998;44:839–850.

Rudnick G, Clark J. From synapse to vesicle: the reuptake and storage of biogenic amine neurotransmitters. Biochim Biophys Acta 1993; 1144:249–263.

Ruth TJ, Wolf AP. Absolute cross section for the production of ^{18}F via the ^{18}O(p,n)^{18}F reaction. Radiochimica Acta 1979;26:21–24.

Saba W, Valette H, Schöllhorn-Peyronneau M-A, Coulon C, Ottaviani M, Chalon S, Dollé F, Emond P, Halldin C, Helfenbein J, Madelmont J-C, Deloye J-B, Guilloteau D, Bottlaender M. [^{11}C]LBT-999: A suitable radioligand for investigation of extra-striatal dopamine transporter with PET. Synapse 2007;61:17–23.

Sarre S, Herregodts P, Deleu D, Devrieze A, De Klippel N, Ebinger G, Michotte Y. Biotransformation of L-DOPA in striatum and substantia nigra of rats with a unilateral, nigrostriatal lesion: a microdialysis study. Naunyn-Schmiedeberg´s Arch Pharmacol 1992; 346:277–285.

Sawle GV, Colebatch JG, Shah A, Brooks DJ, Marsden CD, Frackowiak RSJ. Striatal function in normal aging: implications for Parkinson's disease. Ann Neurol 1990;28:799–804.

Schou M, Halldin C, Sóvágó J, Pike VW, Gulyás B, Mozley PD, Johnson DP, Hall H, Innis RB, Farde L. Specific in vivo binding to the norepinephrine transporter demonstrated with the PET radioligand, (S,S)-[^{11}C]MeNER. Nucl Med Biol 2003;30:707–714.

Schou M, Halldin C, Sóvágó J, Pike VW, Hall H, Gulyás B, Mozley PD, Dobson D, Shchukin E, Innis RB, Farde L. PET evaluation of novel radiofluorinated reboxetine analogs as norepinephrine transporter probes in the monkey brain. Synapse 2004;53:57–67.

Schou M, Sóvágó J, Pike VW, Gulyás B, Bøgesø KP, Farde L, Halldin C. Synthesis and positron emission tomography evaluation of three norepinephrine transporter radioligands: [C-11]desipramine, [C-11]talopram and [C-11]talsupram. Mol Imaging Biol 2006;8:1–8.

Schou M, Zoghbi SS, Shetty HU, Shchukin E, Liow J-S, Hong J, Andrée BA, Gulyás B, Farde L, Innis RB, Pike VW, Halldin C. Investigation of the metabolites of (S,S)-[^{11}C]MeNER in humans, monkeys and rats. Mol Imaging Biol 2009;11:23–30.

Schroeter S, Levey AI, Blakely RD. Polarized expression of the antidepressant-sensitive serotonin transporter in epinephrine-synthesizing chromaffin cells of the rat adrenal gland. Mol Cell Neurosci 1997;9:170–184.

Schwartz JW, Blakely RD, DeFelice LJ. Binding and transport in norepinephrine transporters. J Biol Chem 2003;278:9768–9777.

Seeman P, Guan HC, Niznik HB. Endogenous dopamine lowers the dopamine D2 receptor density as measured by [^{3}H]raclopride: implications for positron emission tomography of the human brain. Synapse 1989;3:96-97.

Segovia S, Guillamón A, del Cerro MCR, Ortega E, Pérez-Laso C, Rodriguez-Zafra M, Beyer C. The development of brain sex differences: a multisignaling process. Behav Brain Res 1999;105:69–80.

Shank RP, Vaught JL, Pelley KA, Setler PE, McComsey DF, Maryanoff BE. McN-5652: a highly potent inhibitor of serotonin uptake. J Pharmacol Exp Ther 1988;247:1032-1038.

Shetty HU, Zoghbi SS, Liow J-S, Ichise M, Hong J, Musachio JL, Halldin C, Seidel J, Innis RB, Pike VW. Identification and regional distribution in rat brain of radiometabolites of the dopamine transporter PET radioligand [^{11}C]PE2I. Eur J Nucl Med Mol Imaging 2007;34:667–678.

Shiue GG, Choi S-R, Fang P, Hou C, Acton PD, Cardi C, Saffer JR, Greenberg JH, Karp JS, Kung HF, Shiue C-Y. *N,N*-Dimethyl-2-(2-amino-4-^{18}F-fluorophenylthio)benzylamine (4-^{18}F-ADAM): An improved PET radioligand for serotonin transporters. J Nucl Med 2003;44:1890–1897.

Singh S. Chemistry, design, and structure-activity relationship of cocaine antagonists. Chem Rew 2000;100:925–1024.

Snow BJ, Tooyama I, McGeer EG, Yamada T, Calne DB, Takahashi H, Kimura H. Human positron emission tomographic [^{18}F]fluorodopa studies correlate with dopamine cell counts and levels. Ann Neurol 1993;34:324–330.

Stehouwer JS, Jarkas N, Zeng F, Voll RJ, Williams L, Camp VM, Malveaux EJ, Votaw JR, Howell L, Owens MJ, Goodman MM. Synthesis, radiosynthesis, and biological evaluation of fluorine-18 labeled 2β-carbo(fluoroalkoxy)-3β-(3'-((Z)-2-haloethenyl)phenyl)nortropanes: Candidate radioligands for in vivo imaging of the serotonin transporter with positron emission tomography. J Med Chem 2008;51:7788–7799.

Stehouwer JS, Goodman MM. Fluorine-18 radiolabeled PET tracers for imaging monoamine transporters: dopamine, serotonin, and norepinephrine. PET Clin 2009;4:101–128.

Stout D, Petric A, Satyamurthy N, Nguyen Q, Huang S-C, Namavari M, Barrio JR. 2β-Carbomethoxy-3β-(4- and 2-[^{18}F]fluoromethyl-phenyl)tropanes: Specific probes for in vivo quantification of central dopamine transporter sites. Nucl Med Biol 1999;26:897–903.

Suehiro M, Wilson AA, Scheffel U, Dannals RF, Ravert HT, Wagner HN Jr. Radiosynthesis and evaluation of N-(3-[^{18}F]fluoropropyl)paroxetine as a radiotracer for in vivo labeling of serotonin uptake sites by PET. Nucl Med Biol 1991;18:791–796.

Suehiro M, Scheffel U, Dannals RF, Wilson AA, Ravert HT, Wagner HN Jr. Synthesis and biodistribution of a new radiotracer for in vivo labeling of serotonin uptake sites by PET, *cis-N,N*-[^{11}C]dimethyl-3-(2´,4´-dichlorophenyl)indanamine (*cis*-[^{11}C]DDPI).Nucl Med Biol 1992;19:549–553.

Suehiro M, Scheffel U, Dannals RF, Ravert HT, Ricaurte GA, Wagner HN Jr. A PET radiotracer for studying serotonin uptake sites: Carbon-11-McN-5652Z. J Nucl Med 1993a;34:120–127.

Suehiro M, Scheffel U, Ravert HT, Dannals RF, Wagner HN Jr. [^{11}C](+)McN5652 as a radiotracer for imaging serotonin uptake sites with PET. Life Sci 1993b;53:883–892.

Suehiro M, Greenberg JH, Shiue C-Y, Gonzalez C, Dembowski B, Reivich M. Radiosynthesis and biodistribution of the S-[^{18}F]Fluoroethyl analog of McN5652. Nucl Med Biol 1996;23:407–412.

Sulzer D, Chen T-K, Lau YY, Kristensen H, Rayport S, Ewing A. Amphetamine redistributes dopamine from synaptic vesicles to the cytosol and promotes reverse transport. J Neurosci 1995;15:4102–4108.

Sur C, Betz H, Schloss P. Immunocytochemical detection of the serotonin transporter in rat brain. Neuroscience 1996;73:217–231.

Surratt CK, Ukairo OT, Ramanujapuram S. Recognition of psychostimulants, antidepressants, and other inhibitors of synaptic neurotransmitter uptake by the plasma membrane monoamine transporters. AAPS J 2005;7:E739–E751.

Szabo Z, Kao PF, Scheffel U, Suehiro M, Mathews WB, Ravert HT, Musachio JL, Marenco S, Kim SE, Ricaurte GA, Wong DF, Wagner HN Jr, Dannals RF. Positron emission tomography imaging of serotonin transporters in the human brain using [^{11}C](+)McN5652. Synapse 1995a;20:37–43.

Szabo Z, Scheffel U, Suehiro M, Dannals RF, Kim SE, Ravert HT, Ricaurte GA, Wagner HN Jr. Positron emission tomography of 5-HT transporter sites in the baboon brain with [^{11}C]McN5652. J Cereb Blood Flow Metab 1995b;15:798–805.

Szabo Z, McCann UD, Wilson AA, Scheffel U, Owonikoko T, Mathews WB, Ravert HT, Hilton J, Dannals RF, Ricaurte GA. Comparison of (+)-^{11}C-McN5652 and ^{11}C-DASB as serotonin transporter radioligands under various experimental conditions. J Nucl Med 2002;43:678–692.

Takano A, Suhara T, Sudo Y, Inoue M, Hashimoto K, Zhang M-R, Ichimiya T, Yasuno F, Suzuki K. Comparative evaluation of two serotonin transporter ligands in the human brain: [^{11}C](+)McN5652 and [^{11}C]cyanoimipramine. Eur J Nucl Med 2002;29:1289–1297.

Takano A, Gulyás B, Varrone A, Halldin C. Comparative evaluations of norepinephrine transporter radioligands with reference tissue models in rhesus monkeys: (*S,S*)-[^{18}F]FMeNER-D_2 and (*S,S*)-[^{11}C]MeNER. Eur J Nucl Med Mol Imaging 2009;36:1885–1891.

Tejani-Butt SM, Brunswick DJ, Frazer A. [^{3}H]Nisoxetine: a new radioligand for norepinephrine uptake sites in brain. Eur J Pharm 1990;191:239–243.

Tejani-Butt SM. [^{3}H]Nisoxetine: a radioligand for quantitation of norepinephrine uptake sites by autoradiography or by homogenate binding. J Pharmacol Exp Ther 1992; 260:427–436.

Torres GE, Gainetdinov RR, Caron MG. Plasma membrane monoamine transporters: structure,

regulation and function. Nature Rev Neurosci 2003;4:13–25.

Tsukada H, Nishiyama S, Kakiuchi T, Ohba H, Sato K, Harada N. Ketamine alters the availability of striatal dopamine transporter as measured by [^{11}C]β-CFT and [^{11}C]β-CIT-FE in the monkey brain. Synapse 2001;42:273–280.

Uhl GR, Hall FS, Sora I. Cocaine, reward, movement and monoamine transporters. Mol Psychiatry 2002;7:21–26.

Ungerstedt U, Arbuthnott GW. Quantitative recording of rotational behavior in rats after 6-hydroxydopamine lesions of the nigrostriatal dopamine system. Brain Res 1970;24:485–493.

Van Dort ME, Kim J-H, Tluczek L, Wieland DM. Synthesis of ^{11}C-labeled desipramine and its metabolite 2-hydroxydesipramine: potential radiotracers for PET studies of the norepinephrine transporter. Nucl Med Biol 1997;24:707–711.

Van Ness SH, Owens MJ, Kilts CD. The variable number of tandem repeats element in DAT I regulates in vitro dopamine transporter density. BMC Genetics 2005;6:55–65.

Vaughan RA. Phosphorylation and regulation of psychostimulant-sensitive neurotransmitter transporters. J Pharmacol Exp Ther 2004;310:1–7.

Wang JL, Parhi AK, Oya S, Lieberman B, Kung M-P, Kung HF. 2-(2'-((Dimethylamino)methyl)-4'-(3-[^{18}F]fluoropropoxy)phenylthio)benzenamine for PET imaging of serotonin transporters. Nucl Med Biol 2008;35:447–458.

White KJ, Walline CC, Barker EL. Serotonin transporters: implications for antidepressant drug development. AAPS J 2005;7:E421–E433.

Wilson AA, DaSilva JN, Houle S. In vivo evaluation of [^{11}C]- and [^{18}F]-labelled cocaine analogues as potential dopamine transporter ligands for positron emission tomography. Nucl Med Biol 1996a;23:141–146.

Wilson AA, Ginovart N, Schmidt M, Meyer JH, Threlkeld PG, Houle S. Novel radiotracers for imaging the serotonin transporter by positron emission tomography: synthesis, radiosynthesis, and in vitro and ex vivo evaluation of ^{11}C-labeled 2-(phenylthio)araalkylamines. J Med Chem 2000; 43:3103–3110.

Wilson AA, Johnson DP, Mozley D, Hussey D, Ginovart N, Nobrega J, Garcia A, Meyer J, Houle S. Synthesis and in vivo evaluation of novel radiotracers for the in vivo imaging of the norepinephrine transporter. Nucl Med Biol 2003;30:85–92.

Wilson JM, Levey AI, Rajput A, Ang L, Guttman M, Shannak K, Niznik HB, Hornykiewicz O, Pifl C, Kish SJ. Differential changes in neurochemical markers of striatal dopamine nerve terminals in idiopathic Parkinson's disease. Neurology 1996b;47:718–726.

Wong DF, Yung B, Dannals RF, Shaya EK, Ravert HT, Chen CA, Chan B, Folio T, Scheffel U, Ricaurte GA, Neumeyer JL, Wagner HN Jr, Kuhar MJ. In vivo imaging of baboon and human dopamine transporters by positron emission tomography using [^{11}C]WIN 35,428. Synapse 1993:15:130–142.

Wong DT, Bymaster FP, Engleman EA. Prozac (fluoxetine, Lilly 110140), the first selective serotonin uptake inhibitor and an antidepressant drug: Twenty years since its first publication. Life Sci 1995;57:411–441.

Wuest F, Berndt M, Strobel K, van den Hoff J, Peng X, Neumeyer JL, Bergmann R. Synthesis and radiopharmacological characterization of 2β-carbo-2'-[^{18}F]fluoroethoxy-3β-(4-bromo-phenyl)-tropane ([^{18}F]MCL-322) as a PET radiotracer for imaging the dopamine transporter (DAT). Bioorg Med Chem 2007;15:4511–4519.

Xing D, Chen P, Keil R, Kilts CD, Shi B, Camp VM, Malveaux G, Ely T, Owens MJ, Votaw J, Davis M, Hoffman JM, BaKay RAE, Subramanian T, Watts RL, Goodman MM. Synthesis, biodistribution, and primate imaging of fluorine-18 labeled 2β-carbo-1′-fluoro-2-propoxy-3β-(4-chlorophenyl) tropanes. Ligands for the imaging of dopamine transporters by positron emission tomography. J Med Chem 2000;43:639–648.

Zahniser NR, Doolen S. Chronic and acute regulation of Na^+/Cl^--dependent neurotransmitter transporters: drugs, substrates, presynaptic receptors, and signaling systems. Pharmacology and Therapeutics 2001;92:21–55.

Zeng F, Mun J, Jarkas N, Stehouver JS, Voll RJ, Tamagnan GD, Howell L, Votaw JR, Kilts CD, Nemeroff CB, Goodman MM. Synthesis, radiosynthesis, and biological evaluation of carbon-11 and fluorine-18 labeled reboxetine analogs: Potential positron emission tomography radioligands for in vivo imaging of the norepinephrine transporter. J Med Chem 2009; 52:62–73.

Zessin J, Gucker P, Ametamey SM, Steinbach J, Brust P, Vollenweider FX, Johannsen B, Schubiger PA. Efficient synthesis of enantio-merically pure thioester precursors of [^{11}C]McN-5652 from racemic McN-5652. J Labelled Cpd Radiopharm 1999;42:1301–1312.

Zessin J, Eskola O, Brust P, Bergman J, Steinbach J, Lehikoinen P, Solin O, Johannsen B. Synthesis of S-([^{18}F]fluoromethyl)-(+)-McN5652 as a potential

PET radioligand for the serotonin transporter. Nucl Med Biol 2001;28:857–863.

Zessin J, Deuther-Conrad W, Kretzschmar M, Wüst F, Pawelke B, Brust P, Steinbach J, Bergmann R. [^{11}C]SMe-ADAM, an imaging agent for the brain serotonin transporter: synthesis, pharmacological characterization and microPET studies in rats. Nucl Med Biol 2006;33:53–63.

Zhang J-Q, Cai W-Q, Zhou D-S, Su B-Y. Distribution and differences of estrogen receptor beta immunoreactivity in the brain of adult male and female rats. Brain Res 2002;935:73–80.

Zhou FC, Tao-Cheng J-H, Segu L, Patel T, Wang Y. Serotonin transporters are located on the axons beyond the synaptic junctions: anatomical and functional evidence. Brain Res 1998;805:241–254.

Zoghbi SS, Shetty HU, Ichise M, Fujita M, Imaizumi M, Liow J-S, Shah J, Musachio JL, Pike VW, Innis RB. PET imaging of the dopamine transporter with ^{18}F-FECNT: a polar radiometabolite confounds brain radioligand measurements. J Nucl Med 2006;47:520–527.